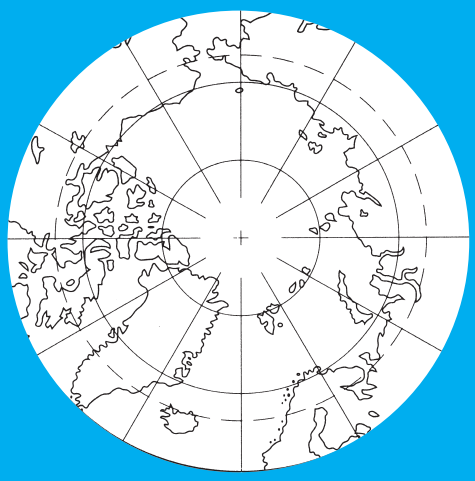

Polarforschung

84. Jahrgang • Nr. 1 • 2014

ISSN (print) 0032-2490
ISSN (online) 2190-1090

POLARFORSCHUNG

herausgegeben vom
Alfred-Wegener-Institut Helmholtz-Zentrum
für Polar- und Meeresforschung
und der
Deutschen Gesellschaft für Polarforschung e. V.

published by the
Alfred Wegener Institute Helmholtz Centre
for Polar Polar and Marine Research
and the
German Society of Polar Research

POLARFORSCHUNG – published by the Deutsche Gesellschaft für Polarforschung (DGP) and the Alfred Wegener Institute Helmholtz Centre for Polar Polar and Marine Research (AWI) – is a peer-reviewed, multidisciplinary research journal that publishes the results of scientific research related to the Arctic and Antarctic realm, as well as to mountain regions associated with polar climate. The POLARFORSCHUNG editors welcome original papers and scientific review articles from all disciplines of natural as well as from social and historical sciences dealing with polar and subpolar regions. Manuscripts may be submitted in English (preferred) or German. In addition POLARFORSCHUNG publishes Notes (mostly in German), which include book reviews, general commentaries, reports as well as communications broadly associated with DGP issues.

Contents / Inhalt

Cover illustration: Midnight on 17 January 2010 in the 2135 m high Mesa Range base camp of the expedition GANOVEX X of the German Federal Institute for Geosciences and Natural Resources (BGR) on the Rennick Glacier of northern Victoria Land in Antarctica. The approximately 700 m high cliff of Tobin Mesa in the background consists of layers of c. 180 Million years old Kirkpatrick lava flows of the Ferrar Supergroup. These flood basalts are related to the initial break-up of the supercontinent Gondwana in Jurassic times. Detailed aerogeophysial and geological studies in the Mesa Range region was one of the main research task of GANOVEX X.

Umschlagbild: Mitternacht am 17. Januar 2010 im 2135 m hoch gelegenen Mesa Range Basislager der Expedition GANOVEX X der deutschen Bundesanstalt für Geowissenschaften und Rohstoffe (BGR) auf dem Rennick-Gletscher im nördlichen Victoria Land der Antarktis. Im Hintergrund befindet sich die etwa 700 m hohe Wand der Tobin Mesa mit ihren Lagen aus etwa 180 Millionen Jahre alten Kirkpatrick-Laven der Ferrar Supergroup. Diese Flutbasalte sind ein Produkt des in der Jurazeit einsetzenden Aufbrechens des Superkontinentes Gondwana. Detaillierte aerogeophysikalische und geologische Untersuchungen in der Mesa Range bildeten einen der Schwerpunkte von GANOVEX X.

 – Satz und Druck: Müller Ditzen AG, Bremerhaven. Erscheinungsort: Bremerhaven.

Polarforschung 84 (1), 1–13, 2014

A High Resolution Aeromagnetic Survey over the Mesa Range, Northern Victoria Land, Antarctica

by Detlef Damaske[1], Bernd Schreckenberger[1] and Felix Goldmann[1]

Abstract: During the GANOVEX X campaign in 2009/10, an aeromagnetic survey was carried out over the Mesa Range in northern Victoria Land. The survey was aiming to resolve the fine structure of the magnetic anomalies over the Jurassic volcanic rocks of the Mesa Range known from previous surveys by reducing the flight line separation and flying in a terrain-following mode. The survey was laid out to prove or disprove the existence of feeder dikes in the Mesa Range. It also targeted the surrounding areas of the upper Rennick Glacier and Aeronaut Glacier to detect whether the volcanics are restricted to the outcropping areas or extend underneath the ice as well as to follow postulated fault lines across and connect them to structures at the fringe of the postulated pull-apart basin, in which the Mesa Range resides centrally.
The outcome of the survey is a high-resolution map, which supports the interpretation of the Mesa Range to be the remnant of an elsewhere eroded plane of flood basalts or sills. No evidence was found for feeder dykes, which were thought to exist in some places and to be detectable through singular, round magnetic anomalies. Thus, it is likely that the sources for the volcanics are not local, but stem from regions a certain distance away from the area investigated.
The volcanics are restricted to the outcrops and there was no indication of fault lines across the neighbouring glaciers.

Zusammenfassung: Im Rahmen von GANOVEX X 2009/10 wurde eine Befliegung im Bereich der Mesa Range im zentralen North Victoria Land durchgeführt. Ziel der Vermessung war die Erfassung der Feinstruktur der bekannten magnetischen Anomalien über den jurassischen Vulkaniten der Mesa Range. Dazu wurden die Messlinien in engem Abstand angelegt und in einem möglichst konstanten Abstand über Grund geflogen. Die Anlage der Vermessung sollte ermöglichen, die Existenz von vulkanischen Zufuhrschloten in der Mesa Range nachzuweisen. Das Messgebiet erstreckte sich über die benachbarten Regionen des oberen Rennick Glaciers und Aeronaut Glaciers hinaus, um zu überprüfen ob und wie weit sich die Vulkanite über den aufgeschlossenen Bereich hinaus unter dem Eis fortsetzen. Störungszonen in den Randgebirgen, die das vermutete Pull-apart-Becken, in dessen Zentrum die Mesa Range aufragt, umfassen, sollten durch den eisbedeckten Bereich verfolgt werden.
Das Ergebnis dieser Befliegung ist eine hochauflösende Karte des magnetischen Feldes. Das magnetische Muster unterstützt die Annahme, dass es sich bei der Mesa Range um die Reste einer Flutbasalt-Ebene handelt. Es konnten keinerlei Hinweise auf vulkanische Zufuhrschlote gefunden werden, die nach der älteren Befliegung aufgrund zirkularer Anomalien an einigen Stellen vermutet worden waren. Danach sind die Quellen der Vulkanite nicht lokal zu suchen, sondern weiter außerhalb des Untersuchungsgebietes.
Die Vulkanite sind auf den aufgeschlossenen Bereich beschränkt und Störungszonen unter den benachbarten Gletschern konnten nicht nachgewiesen werden.

INTRODUCTION

During the GANOVEX IV campaign in 1984/85, an aeromagnetic survey was carried out over parts of northern Victoria Land (Bosum et al. 1989, Bachem et al. 1989a, Bosum et al. 1991, Damaske 1988). The resulting map of the anomalies of the total magnetic field showed a clear signature of the volcanics of the Mesa Range with positive amplitudes of up to 500 nT directly above the outcrops, flanked by negative amplitudes of about -100 nT on both sides of the range (Fig. 1). Small circular high-amplitude anomalies were observed over the Deep Freeze Range (just north if the edge of the Priestley Glacier, see Behrendt et. al 1991) interpreted as caused by exposures of Kirkpatrick basalt. Singular, round-shaped anomalies over some parts of the Mesa Range were often discussed as being the magnetic expressions of feeder dykes for the Jurassic Ferrar dolerites and Kirkpatrick basalts (e.g. Bosum et al. 1989). On the other hand, the relatively wide separation of the survey lines (of 4.4 km) together with the relatively short distance to the magnetic sources – i.e., the volcanics of the Mesa Range – could have led to this effect. In this case, the small round-shaped anomalies (Fig. 1) would have nothing to do with any feeder dykes and are just an effect of insufficient density of survey lines in this area. An unambiguous answer can only be found in a survey with sufficiently small line separation, which is flown in a terrain-following mode. Such a survey would also address the extent of the volcanics underneath the surrounding glaciers and their "thickness", i.e. is there more volcanic material in the Mesa Range area than that of the exposed rocks?

During GANOVEX IX in 2005/06, massive dolerite dykes have been found at the eastern edge of the Aeronaut Glacier (area Mt. Carson-Runaway Hills), which could be interpreted as such feeder dykes for the basalt sheets (Viereck-Götte pers. comm. 2007). They could also relate to the postulated feeder dykes in the Mesa Range. It is also possible that the dykes follow NW-SE orientated fault lines which seem to be constituted as gaps between the Mesa Range sections such as the Pinnacle Gap between Tobin and Pain Mesa (Fig. 2).

The still unanswered major question is whether the basalt sheets in the upper Rennick Glacier area formed by local fissure eruptions or had their source outside the outcrops in the survey area (i.e. outside the Mesa Range itself). To clarify whether feeder dykes can really be observed within the basalt sheets of the Mesa Range and whether the observed fault systems can be traced through the glaciers flanking the Mesa Range, a densely spaced aeromagnetic survey was proposed for the GANOVEX X expedition.

Closely spaced surveys are still an exception in Antarctic airborne research, but their usefulness has been demonstrated in e.g. studies of the Jutulstraumen rift at 1 km line spacing by (Ferraccioli et al. (2005a, b) or in the detailed structural interpretations enabled by high resolution aeromagnetic data (Ferraccioli & Bozzo 2003).

[1] Bundesanstalt für Geowissenschaften und Rohstoffe (BGR), Stilleweg 2, Postfach 30655 Hannover, Germany.

Manuscript received 08 February 2014; accepted in revised form 07 May 2014

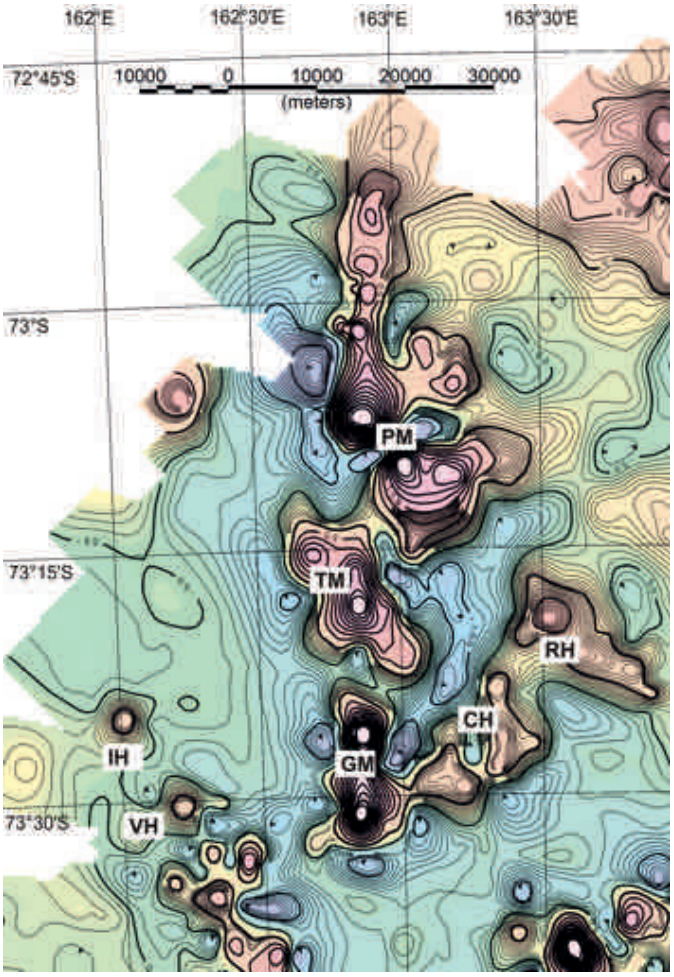

Fig. 1: Results from the GANOVEX IV survey (1984/85) show singular round magnetic anomalies over the Mesa Range (Pain Mesa PM, Tobin Mesa TM, Gair Mesa GM) and over neighbouring Chisholm (CH) and Runaway Hills (RH) and Deep Freeze Range (Illusion Hills IH, Vantage Hills VH).

Abb. 1: Die Ergebnisse der GANOVEX IV Befliegung (1984/85) zeigen einzelne runde magnetische Anomalien über der Mesa Range (Pain Mesa PM, Tobin Mesa TM, Gair Mesa GM) und den benachbarten Chrisholm Hills (CH) und Runaway Hills (RH) und der Deep Freeze Range (Illusion Hills IH, Vantage Hills VH).

LAYOUT OF THE SURVEY

To meet the above stated requirements, i.e. closely spaced and terrain following, a helicopter is the most suitable platform to perform the survey. As in earlier high resolution surveys meeting similar requirements (e.g. BOZZO et al. 1997, WILSON et al. 2007), a line spacing of 500 m is considered to be sufficient with tie lines perpendicular to the survey lines every 5 km (ratio 1:10). An envisaged ground clearance of 500 m allows a complete coverage of the anomalies.

The survey area (Fig. 2) covers the central and southern Mesa Range completely. It includes also the Aeronaut Glacier, Runaway and Chisholm Hills in the east and the negative anomalies (mapped in the GANOVEX IV survey) over the upper Rennick Glacier in the west. The survey line orientation is the same as for GANOVEX IV (BACHEM et al. 1989b) to allow direct comparison along individual lines. However, one must bear in mind that navigation in 1984/85 was less accurate and that the fixed-wing survey was flown at a constant barometric elevation.

As base for flight planning the USGS Antarctica 1:250 000 Reconnaissance Series topographic maps "Mt. Murchison" and "Sequence Hills" (Lambert conformal conic projection with standard parallels 72°40' S and 75°20' S) were used. The central meridian of 179° E (which determines the survey grid orientation) as well as the reference latitude of 74° 01' 05.2263" S, the false easting of 1123000 m, and false northing of 1444000 m were identical with projection parameters used for GANOVEX IV (BACHEM et al. 1989b). Using the geodetic reference system WGS 84 (World Geodetic System) instead of WGS 72 does not make a significant difference when directly comparing the new data along a line with those of the GANOVEX IV survey lines.

INSTRUMENTATION

An AS350B2 helicopter, owned and operated by Helicopters New Zealand (HNZ), was contracted to serve as the platform for the aeromagnetic survey. The helicopter was also used for logistic operations between the expedition's main base Gondwana Station and the survey camp in the Mesa Range. An extra fuel tank was installed to increase the range of the helicopter.

A Scintrex CS-3 caesium vapour magnetometer was utilised for the survey consisting of sensor head, cable and the sensor electronics. The sensor head was housed in a towed bird assembly and was connected to the bird's BNC connector. The bird was towed on an approximately 30 m long Kevlar reinforced coaxial cable that provided both the input DC power and the output signal at the Larmor frequency which is proportional to the magnetic field signal.

Measurements were made at a sampling rate of 10 Hz, corresponding to a ground interval of about 4 to 6 m, depending on the helicopter speed. All magnetic data were recorded in real-time to the PicoEnvirotec AGIS data acquisition system and then copied from the AGIS-XP computer to the field processing computers for quality control examination.

Position and precise time were recorded using a Novatel DL-V3 receiver with the antenna placed at the front window. At the base camp a GPS (Global Positioning System) base station was installed to obtain corrections for differential GPS post-processing.

Flight information was entered into the GPS database allowing the pilot to accurately navigate between waypoints. When flying in drape mode the elevation was controlled manually by the pilots using the helicopter's radar system and by the navigator aligning with the elevation on the neighbouring lines and tie lines.

MAGNETIC BASESTATION

Geomagnetic activity on ground (Fig. 3) was monitored with the GEM Systems GSM-19T instrument at the Mesa Range Camp, placed about 100 m from the camp installations (Fig. 4). The station operated nearly continuously from 3 to 19 January 2010. The total magnetic field was recorded every 10 seconds. As known from earlier observations in the northern Victoria Land region (DAMASKE 1989, 1993) the pattern of the

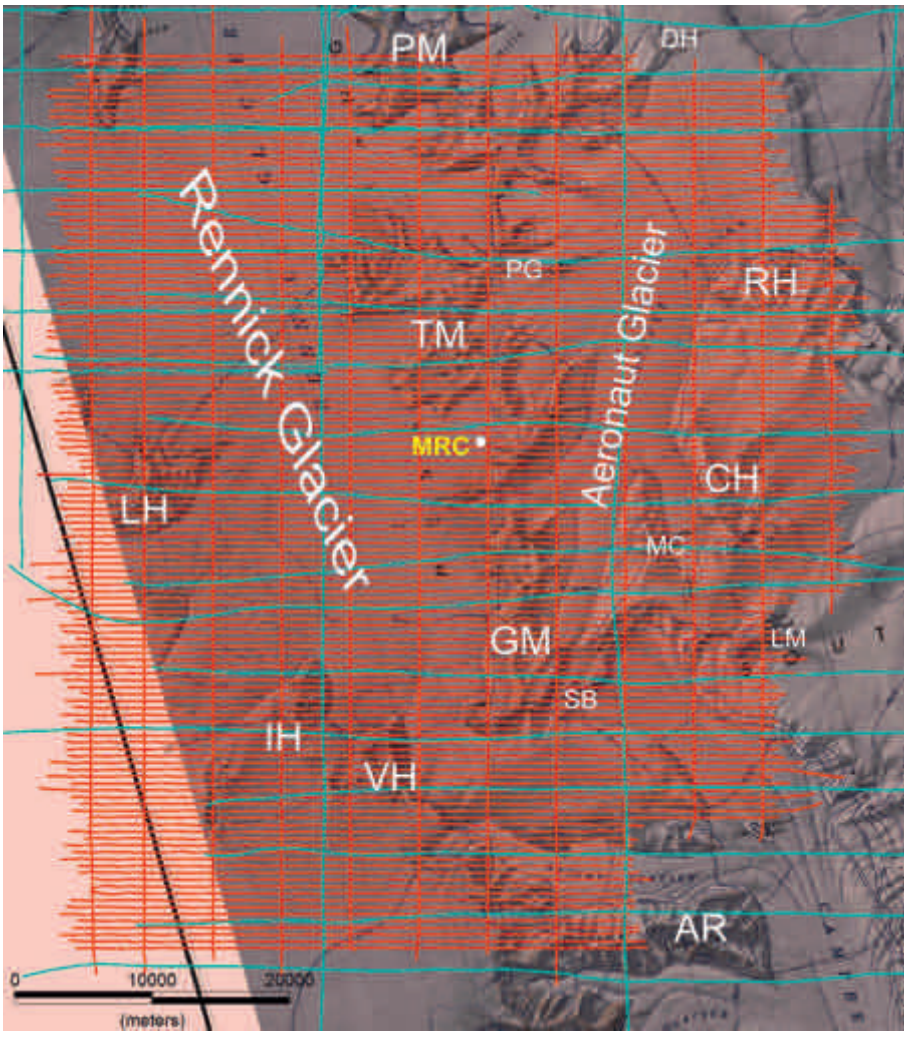

Fig. 2: Survey area GANOVEX X including all new survey lines (red) as well as lines flown during the surveys GANOVEX IV and GITARA V (Bozzo et al. 1998, 1999) (both light blue). All GANOVEX X survey flights were operated from the Mesa Range Camp (MRC). Feature names: Pain Mesa = PM, Tobin Mesa = TM, Gair Mesa = GM, Lichen Hills = LH, Illusion Hills = IH, Vantage Hills = VH, Runaway Hills = RH, Chisholm Hills = CH, Archambault Ridge = AR, Mt Carson = MC, Diversion Hills = DH, Pinnacle Gap = PG, Suture Bench = SB, Linn Mesa = LM. Topographic base: USGS Topographic Reconnaissance Map (250K) Mount Murchison).

Abb. 2: Das Befliegungsgebiet GANOVEX X mit den neuen Profillinien (rot) wie auch den Linien, die während GANOVEX IV und GITARA V geflogen wurden (beide in hellblau). Alle GANOVEX X -Messflüge wurden vom Mesa Range Camp (MRC) durchgeführt. Geländebezeichnungen: Pain Mesa = PM, Tobin Mesa = TM, Gair Mesa = GM, Lichen Hills = LH, Illusion Hills = IH, Vantage Hills = VH, Runaway Hills = RH, Chisholm Hills = CH, Archambault Ridge = AR, Mt Carson = MC, Diversion Hills = DH, Pinnacle Gap = PG, Suture Bench = SB, Linn Mesa = LM. Kartenbasis: USGS Topographic Reconnaissance Map (250K) Mount Murchison).

daily variations is characterized by a high level of magnetic activity in the local morning hours until after midday. The less disturbed period and thus the most favourable time of the day to perform survey flights ranges from 19 to 4 h (6 to 15 h UT) "local" time LT (i.e. the time stations in the western Ross Sea and Victoria Land use, corresponding to New Zealand summer time). A period of 3 hours on either side of this interval still appears to be acceptable for survey flights.

Also, the daily pattern of the magnetic activity exhibits a clear diurnal variation with a maximum around 15 h UT. This long wave daily trend, however, is of no concern with regard to the selection of survey times since it can be easily accounted for in the process of correcting the flight data with the base station data.

FIELD OPERATIONS AND SURVEY FLIGHTS

After completion of the major logistic tasks at the beginning of the expedition and prior to moving to the Mesa Range area one of the expedition's helicopters was equipped with the aeromagnetic survey system and flight tested in the vicinity of Gondwana Station. The equipment was installed at the Italian Mario Zucchelli Station where a helicopter hangar provided optimal conditions. The helicopter and the aeromagnetic survey team moved to the Mesa Range Camp (Fig. 5) on 31 December 2009. There, a fuel depot had been previously established with the help of a Twin Otter chartered by the Italian Antarctic Programme.

Unfavourable weather conditions delayed the first survey flight until 3 January 2010. Altogether 26 survey flights were carried out until 19 January 2010. There were 6 days with 3 flights, 2 days with 2 flights and 4 days with only one survey flight, each flight lasting about 2 hours. It was mostly due to adverse weather conditions that restricted survey flights. Not only cloud coverage, but also strong winds, in particular over the western section of the survey area with frequent katabatic winds or turbulences close to the steep flanks of the Mesa Range tabular mountains (Fig. 6) made survey flights difficult on some days.

The majority of the survey flights took place within the "magnetic window" when a relatively "quiet" magnetic field could be expected. However, due the necessity to compromise with the working times of other groups based in the Mesa Range Camp, some flights started as early as 13 h LT. The survey helicopter was also partially used for other tasks, i.e. moving other groups to and from their sample sites and to support moving the remote geological field camps in the lower Rennick Glacier area.

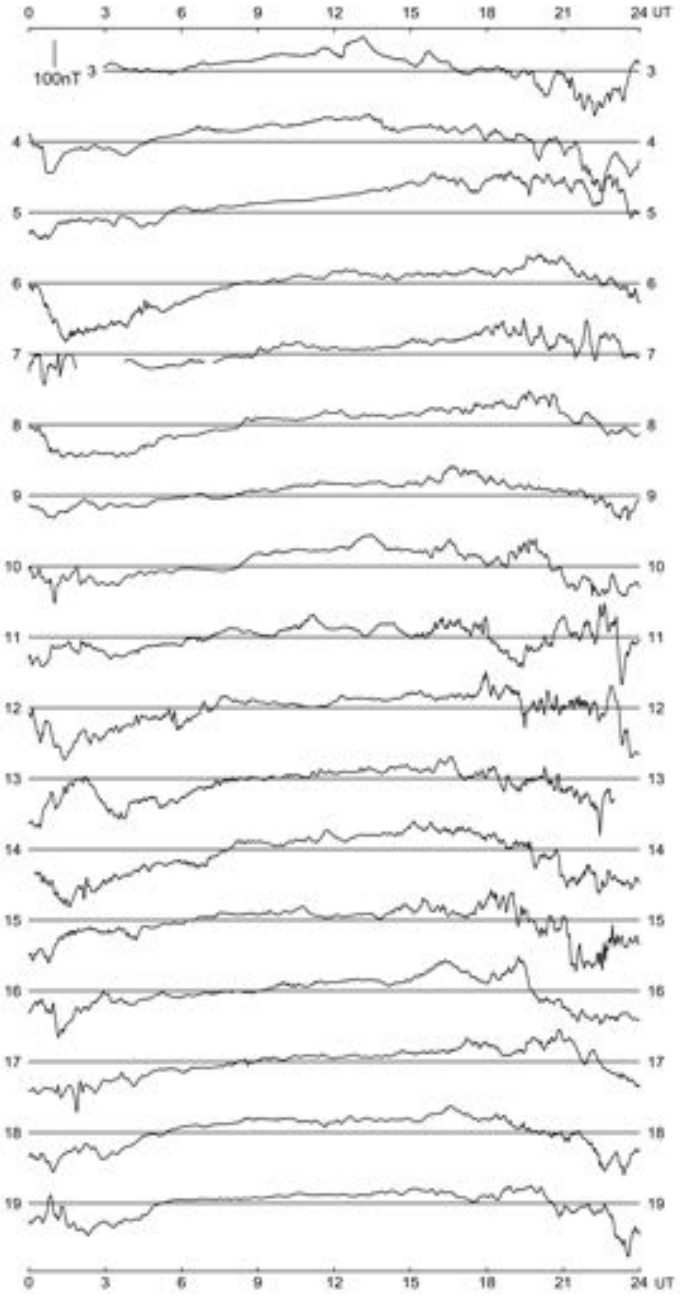

Fig. 3: Diurnal variations at Mesa Range Camp for the survey period from 3 to 19 January. Baseline value for all 24 hour UT-days is 64 000 nT.

Abb. 3: Magnetischer Tagesgang am Mesa Range Camp während der Befliegungen vom 3. bis 19. Januar. Die Basislinie an allen 24 UT-Tagen entspricht einem Wert von 64 000 nT.

A total of 7,400 km survey lines over an area of 3,300 km² were flown, using 56 ½ hours helicopter-time. After a final quality control of the data the survey was concluded on 20 January. Still in camp the aeromagnetic equipment was removed from the survey helicopter to return it to other logistic tasks of the expedition.

DATA PRE-PROCESSING AND QUALITY CONTROL

Preliminary processing for every survey flight took place immediately or at least after the last flight of the day. Using the

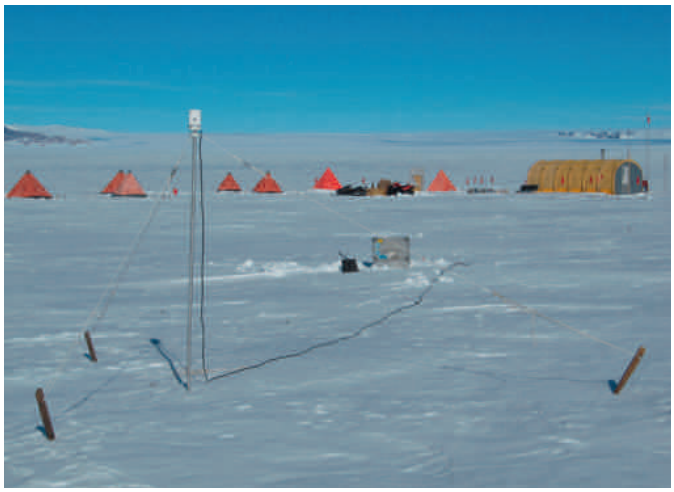

Fig. 4: Base station for the recording of the diurnal variations at Mesa Range Camp.

Abb. 4: Basisstation am Mesa Range Camp zur Aufzeichnung der täglichen Schwankungen des Erdmagnetfeldes.

Fig 5: Mesa Range Camp (elevation 2137 m) in front of the 3099 m high Mt Frustrum. Note the black layer of high magnetic basalts on top of the mountain.

Abb. 5: Das Mesa Range Camp (Höhe 2137 m) vor dem 3099 m hohen Mt. Frustrum. Die schwarze Auflage auf dem Gipfel besteht aus stark magnetischem Basalt.

PicoEnvirontec PEIView program the original PicoEnvirontec binary flight data files were converted into the binary Geosoft GBN format for use with OasisMontaj data processing software.

For each flight separately, the GBN formatted data were read into a new database of Geosoft GDB format in which a line header was edited and the flight number assigned to all lines of the flight. If necessary lines were renamed, empty or faulty rows eliminated. Also new projected x,y-channels, calculated from the geographic coordinates using the projection chosen for the survey (see above), were needed since the AGIS PEI-convert program used for navigation apparently calculated slightly different coordinates for the Lambert conformal projection, thus leading to slightly shifted lines. To reduce the amount of data only the most important data base columns, i.e., latitude, longitude, (GPS-)altitude, the new x,y coordi-

Fig. 6: Survey flights occasionally suffered from air turbulences occurring at the steep flanks of Mesa Range (Gair Mesa western side facing towards Exposure Hill).

Abb. 6: Die Messflüge wurden gelegentlich von Turbulenzen an den Steilhängen der Mesa Range (Gair Mesa westlich Richtung Exposure Hill) beeinflusst.

nates, (GPS-)time and the raw value of the recorded total magnetic field were exported to an ASCII-file forming the base for further quality control.

The ASCII-files from each survey flight were now imported into a single Geosoft GDB database to hand-edit (shorten) every single line and tie line at both ends to avoid multiple crossings for single lines. If possible only straight-line ends were kept. A preliminary IGRF processing was performed using IGRF2005, line date, and GPS altitude. The resulting magnetic anomaly was processed for a preliminary anomaly plot for each flight and also for the entire survey to obtain a first overview of the magnetic field pattern. After completion of the tie-line flights a preliminary analysis of crossover errors (altitude and magnetic anomaly values) was carried out to judge whether lines or sections of lines need to be re-flown (which was not the case).

Some sections in a number of lines show regular "wiggles" (Fig. 7). They are typically of 10 to 12 seconds width. The amplitude (peak-to-peak) varies from 1 nT to 5 nT, in most cases the amplitude is within the 2-3 nT range with a few exceptions of up to 10 nT amplitude. They are visually detectable only in the relatively "flat, quiet" sections of a line. They seem to be of higher amplitude at the beginning of lines and sometimes also at the end of lines. If they occur in the middle of lines they seem to be of lower amplitude and more regularly. This suggests an effect of sensor orientation: In the beginning of a line, the pilot often struggled to keep elevation or the helicopter was not perfectly aligned, yet. Thus, helicopter manoeuvres forced the bird to swing around and this may account for strong wiggles close to the start of a line, dying out when the flight was stabilized. Wind during the flight may have triggered swinging of the bird producing the wiggles also in middle sections of a line. It should be noted, that the wiggles seem to start during the fourth flight, but there were no wiggles detected before that flight. Since we do not have proof observations of the environmental conditions during the flights, we cannot further judge on this effect.

DATA PROCESSING

Removal of diurnal variations

The original 10-second recordings of the Mesa Range Camp magnetic base station were low-pass-filtered to remove the short period variations, which may not be representative over the whole survey area. In contrast to previous surveys in Victoria Land stretching over more than 100 km away from a base, the Mesa Range survey covered a relatively close area with a maximum distance of a survey point from the location of the magnetic base station of less than 60 km. Thus it was possible to use a relatively short filter as compared with the older surveys (see MASLANYJ & DAMASKE 1986). Different filter lengths have been tested and compared directly along single survey lines as well as in form of an anomaly map over the whole survey area: Applying a 5-minute filter or applying no filter at all showed best results. To smooth any artificial noise at the camp and the high frequency natural noise at the base station we decided to apply the 5-minute filter. These base values were then interpolated to 10 Hz intervals (T_{base}) and subtracted from the flight data (T_{air}) as follows:
$T_{cor} = T_{air} - T_{base} + BASE$ where BASE = 64 000 nT (mean base value over all days).

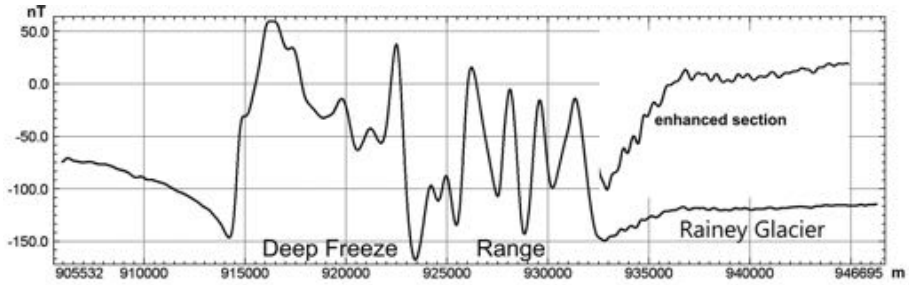

Fig. 7: Typical example for "wiggles" along a flight line. This line L990 runs west – east from the Deep Freeze Range (DFR) across outcrops south of the Vantage Hills to the upper Rainey Glacier, which runs along the Archambault Ridge on its northern side. The anomaly pattern typical for the dolerites of the DFR runs into a "flat" magnetic pattern over the Rainey Glacier. The appearance of "wiggles" at exactly this point (to better demonstrate the "wiggles" this section has been enhanced) can – in this case – clearly be attributed to strong katabatic winds dropping from the high plateau of the DFR to the low lying Rainey Glacier causing oscillations of the bird.

Abb. 7: Typisches Beispiel für Störungen entlang einer Fluglinie. Die Linie L990 verläuft in West-Ost-Richtung von der Deep Freeze Range (DFR) über Aufschlüsse südlich der Vantage Hills bis zum oberen Rainey Glacier, der nördlich längs zur Archambault Ridge verläuft. Das für die Dolerite der DFR typische Anomaliemuster schwächt sich über dem Rainey Glacier ab. Die gerade hier auftretenden Störungen (zur Verdeutlichung wurde dieser Bereich hervorgehoben) sind eindeutig auf starke katabatische Winde vom Plateau zurückzuführen, die den Flugköper in seitliche Schwingungen versetzten.

A possible dependence on flight direction

After base station correction the magnetic anomaly map shows artefacts that seem to be related to flight direction (Fig. 8a). The distinct step-wise appearance of steep gradients can be removed by the introduction of a lag correction. A series of different lag corrections were tried over 05, 10, 15, 20, 25 and 30 fiducials (one fiducial corresponds to 1/10 of a second and thus approximately 5 m with a survey speed of close to 100 knots). Applying this correction considerably improves the data (Fig. 8b). Since a 15-fiducial lag is definitely not sufficient to remove the effects at some edges and a 30-fiducial overcompensates the effect at some places, a 20-fiducial lag corresponding to about 90 m was chosen as the optimal shift to account for this flight direction dependent effect.

Another small "heading" effect was accounted for by removing the mean over all lines in W-E lines (90° course) from the individual W-E lines and the mean over all E-W lines (270° course) from the individual E-W lines. A small improvement in the anomaly map justifies the correction.

Removal of a reference field

Before obtaining a map of the anomalies of the crustal magnetic field, regional and global components of earth' magnetic field need to be removed. It is also advisable to remove these components before "levelling" the data since it makes it easier to judge on this processing step. Removal was done by first computing the International Geomagnetic Reference Field (IGRF) at all survey points at the respective survey altitude and then subtracting these values from the survey's total magnetic values. The IGRF 2005 coefficients were used to calculate the reference field values for a mean date (11 January 2010). Since these values are independent of the measured (and corrected) data they can later be added again and subsequently replaced with a more suitable reference model (e.g. the IGRF 2010, which was not available at the time of data processing).

Levelling

To remove effects of diurnal variations not accounted for by the base station correction, a "levelling" procedure, in which the differences at intersections of profile and tie lines are minimized, was carried out. Smoothing the data is necessary due to noise on some lines. To do this prior to levelling reduces also the effect of wrong values at intersections being used as discrepancies.

Low pass filters of 18 sec, 12 sec, and 6 sec lengths have been tested. Clearly an 18 sec filter significantly modifies shape and position of real anomalies. It does remove some of the artificial wiggles mentioned above and observed in parts of a number of lines, but not all. The 12 sec filter (corresponding to about 500 m (at 80 knots), thus the spacing of the lines) removes or at least reduces the wiggles to some part. However, there are a number of real anomalies for which the amplitudes are altered (their position is changed by less than 25 m which would be considered within positioning error), but more seriously, there are cases where obviously the shape of the anomaly has been

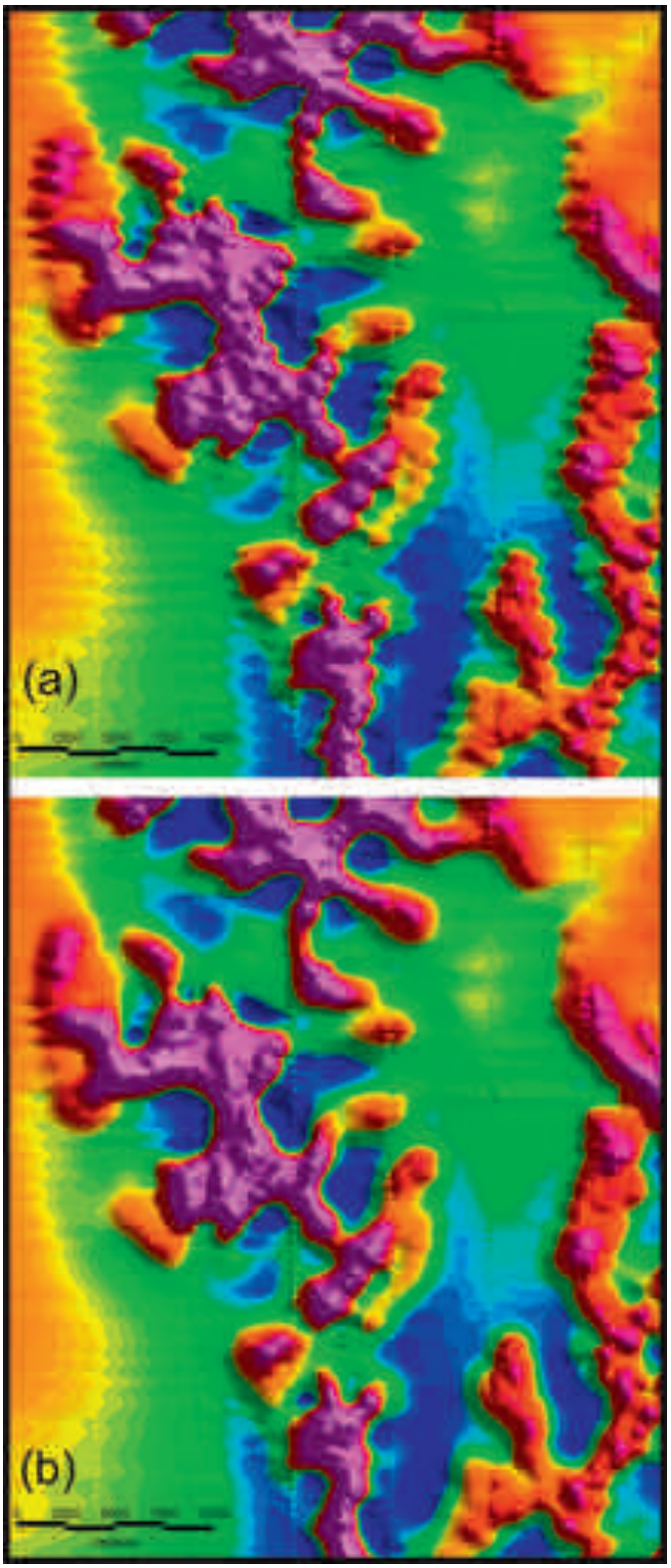

Fig. 8: (a) Section of the anomaly map after correcting for diurnal variations. Apparent over all lines is a possible dependence on the flight direction; (b) after applying a lag correction of 2 sec the "line-effects" are greatly reduced, especially in high gradient areas. Colour scale and shadowing as in Figure 9.

Abb. 8: (a) Ausschnitt aus der Anomalienkarte nach Abzug der täglichen Schwankungen des Erdmagnetfeldes. Sichtbar wird auch eine mögliche Abhängigkeit von der Flugrichtung; (b) nach „lag"-Korrektur von 2 sec sind die Linieneffekte weitestgehend reduziert, insbesondere in Gebieten mit großem Gradienten. Farbskala und Schatteneffekte wie in Abbildung 9.

modified. A 6 sec filter corresponds to about half the line spacing. Using this filter hardly changes the positioning of the anomaly peaks and changes in their amplitude are within an acceptable limit of less than 5 nT or less than 1.5 % of the peak-to-peak amplitude. Most important, there are no changes in the shape of the anomalies any more.

Applying the 6 sec filter does not remove the artificial wiggles at all, but a lot of very high frequency, low amplitude (<1 nT) noise including small spikes are removed. During levelling special attention was given to intersections lying in sections with "wiggles".

Levelling was done in two steps. First, a normal statistical levelling was applied. This involved an initial constant shift of each tieline with respect to the mean crossover difference with the profile lines, followed by the same procedure now reversed, i.e. lines shifted against the mean crossover difference of the tie lines. Since very large discrepancies in places of steep gradients of anomalies occur, a relatively large number of intersections had to be excluded. The result is an improvement in areas of "flat" magnetic field, but not in parts of high gradients. Taking these results now as a base and removing a linear trend in the tie lines and subsequently applying higher order trends along profile lines lead to a definite improvement in all the areas of a "flat" magnetic field. In the areas of high amplitudes, line effects are still very obvious. The normal "statistical levelling" approach cannot be continued there.

As a second step, a "pseudo-tie-line" method was developed (since the standard levelling methods and also a microlevelling approach (FERRACCIOLI et al. 1998) did not prove to be successful), in which only the profile lines are considered. Instead of the 5 km spaced original tie lines artificial tie lines spaced only 1 km are calculated and intersected with the profiles. Along these new tie lines a 4 point (i.e., over 4 profile lines) low pass filter (after experimenting with a number of different filters and filter lengths) was run. Calculating now differences at the intersections and using these for a correction (using the "careful levelling" option of the OasisMontaj levelling package with a tensioned spline) of the profiles – adjusts neighbouring profiles in such a way that line effects are greatly reduced. Again, this works best in "flat" (i.e. low gradient) areas. As before, large intersection differences have been excluded when applying this step over the whole survey. High gradient areas have been treated individually in separate steps in a similar way but now using also larger intersection differences.

The result of this second levelling step is a map which shows only a very few small line effects remaining. To include also the original, measured tie-lines in the final data-base, we used the "careful level" OasisMontaj application to adjust these now to the – per definition – perfect lines.

FIRST RESULTS

Anomaly description

The most distinct features in the anomaly map (Fig. 9) are strong positive amplitudes over the mesas. In most cases, the anomalies mimic almost exactly the topographically visible expression of the table mountains and ridges that rise above the ice (Fig. 10). The magnitude of the anomalies over flat mountain tops is about 400-700 nT but locally amplitudes up to 1200 nT and more occur. The other areas as there are the Runaway Hills, the Chisholm Hills, the Suture Bench, the Linn Mesa and the Lichen Hills – Illusion Hills – Vantage Hills as well as a plateau west of Archambault Ridge have lower positive amplitudes (mostly less than 250 nT).

The large glacier areas and particularly the Rennick Glacier appear nearly everywhere magnetically quiet. There are only a few exceptions from this observation. At the eastern end of Pain Mesa south of Diversion Hills, a 5 km long anomaly extends under the Aeronaut Glacier in SE direction and might be connected to a similar anomaly extending NW from the Runaway Hills under the glacier. The western part of Archambault Ridge seems to cause no magnetic anomaly but the flight altitude was higher than over the unnamed plateau west of it.

There is one area where weak to intermediate amplitude anomalies (up to 250 nT) occur over a wide ice and snow surface. This is west of Illusion Hills, Vantage Hills and the south-western continuation of these outcrops to Archambault Ridge. Flight altitude was low over this smooth surface and the snow and ice cover might be thin.

Modelling

Nearly all structures and particularly the mesas have a very irregular shape and can hardly be represented with two-dimensional models. Nevertheless, we tried to model one cross-section by a two-dimensional geometry with bodies limited in y-direction ($2^1/_2$ and $2^3/_4$ dimensional, GM-SYS modelling program) to get a first impression of the relationship between possible source bodies and magnetic anomalies. True 3D models will later be necessary to explore the data in more detail. Modelling was done for the original survey line L1110.

We used the ASTER Global Digital Elevation Model (GDEM) (https://wist.echo.nasa.gov) to describe the topography for the modelled cross section. The GDEM seems to be correct over most parts of the survey area but also contains areas with large errors over the ice and snow surface. By comparison with the topographic map (Fig. 2) we hand-edited the altitude values for the model line. Errors in that procedure are mostly not very important because nearly always the surface of the glaciers is concerned that does not represent a magnetic model surface.

Line L1110 (Figs. 10, 11) crosses the Gair Mesa at its greatest width. The western part of the line runs from just north of the Illusion Hills (IH) over the magnetically quiet ice surface in the southernmost part of the Rennick Glacier (Figs. 9, 10). To the east, Suture Bench (SB) is crossed while Linn Mesa (LM; see also Fig. 2) is just touched at its southern tip. The first simple model in Fig. 12a uses only model bodies for the topographically visible parts of Gair Mesa and Suture Bench. The bodies are restricted in their width (y-direction perpendicular to the line direction) to only 1 to 3 km simulating coarsely the irregular shape of the table mountain. Magnetization values were chosen to fit the anomaly at the given topography but are

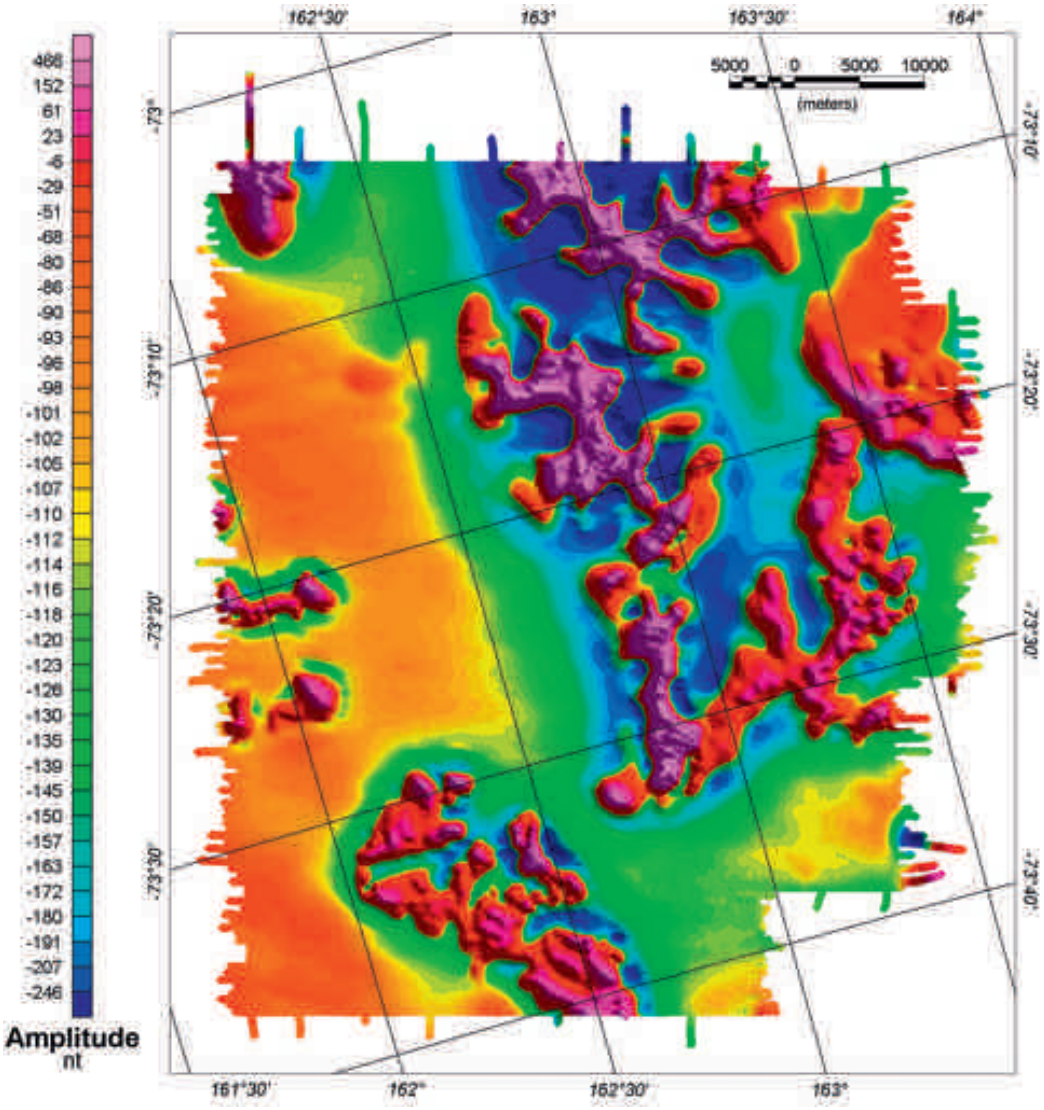

Fig. 9: Map of the anomalies of the total magnetic field after levelling. Colour scale is equal-area and shadowing direction from 45°.

Abb. 9: Anomalienkarte des Magnetfeldes nach dem Levelling. Farbskala ist „equal-area", Schattenwurf hier aus Richtung 45°.

in agreement with paleomagnetic investigations in the Mesa Range by McIntosh et al. (1986). Total magnetization values that combine remanent with induced magnetization at the inclination of the present field (-84°) are used as no information about the Königsberger ratio and magnetization directions are available. The Gair Mesa was subdivided into a lower part of about 700 m thickness with 3 A/m and an approximately 200 m thick cap with 5 A/m. These values seem to be reasonable for extrusive basalt flows from which the mesas in the survey area are built up. McIntosh et al. (1986) report NRM values for 15 samples from the Mesa Range that range from below 1 A/m to more than 10 A/m with an overall average of 4.1 A/m.

Fig. 12a shows that the magnetic anomaly can easily be modelled when only the topographically visible parts of Gair Mesa are regarded as magnetic bodies.

In Fig. 12b we tried to introduce a 500 m thick "root" below the higher parts of Gair Mesa on the expense of a reduced magnetization value for nearly the entire body. This is also in agreement with McIntosh et al. (1986) who report many samples with NRM values around 2 A/m. However, a very deep root with a much lower magnetization would necessarily reduce the steepness of the anomaly flanks. Thus we conclude that by far most of the anomaly is caused by the visible parts of Gair Mesa.

In order to investigate the question whether more magnetic bodies can be hidden under the ice in the glaciated areas Fig. 12b also contains two purely hypothetical source bodies below the surface of the Rennick Glacier. One of them may represent a 1 km wide dike ending about 500 m below the surface of the ice. The other body is a 5 km wide and 1 km thick block covered by 3 km thick ice. Their magnetization is assumed to be as strong as that of the main Gair Mesa body (2 A/m). The presence of these bodies causes distinct positive anomalies, which should be detectable in the smooth magnetic field over the glaciers. They therefore establish a minimum depth and maximum volume for significant basaltic source bodies under the glaciated areas.

Figs. 12c-e show the Gair Mesa in more detail. In Fig. 12c it is modelled with a uniform magnetization value for the whole body. It was chosen to fit the main part of the anomaly includeing its 'edge' anomalies which are typical for this and all other mesas (Fig. 9). The additional "peak" anomaly on top of the Gair Mesa needs special consideration because it is not adequately modelled. Fig. 12d uses a hypothetical 1 km wide

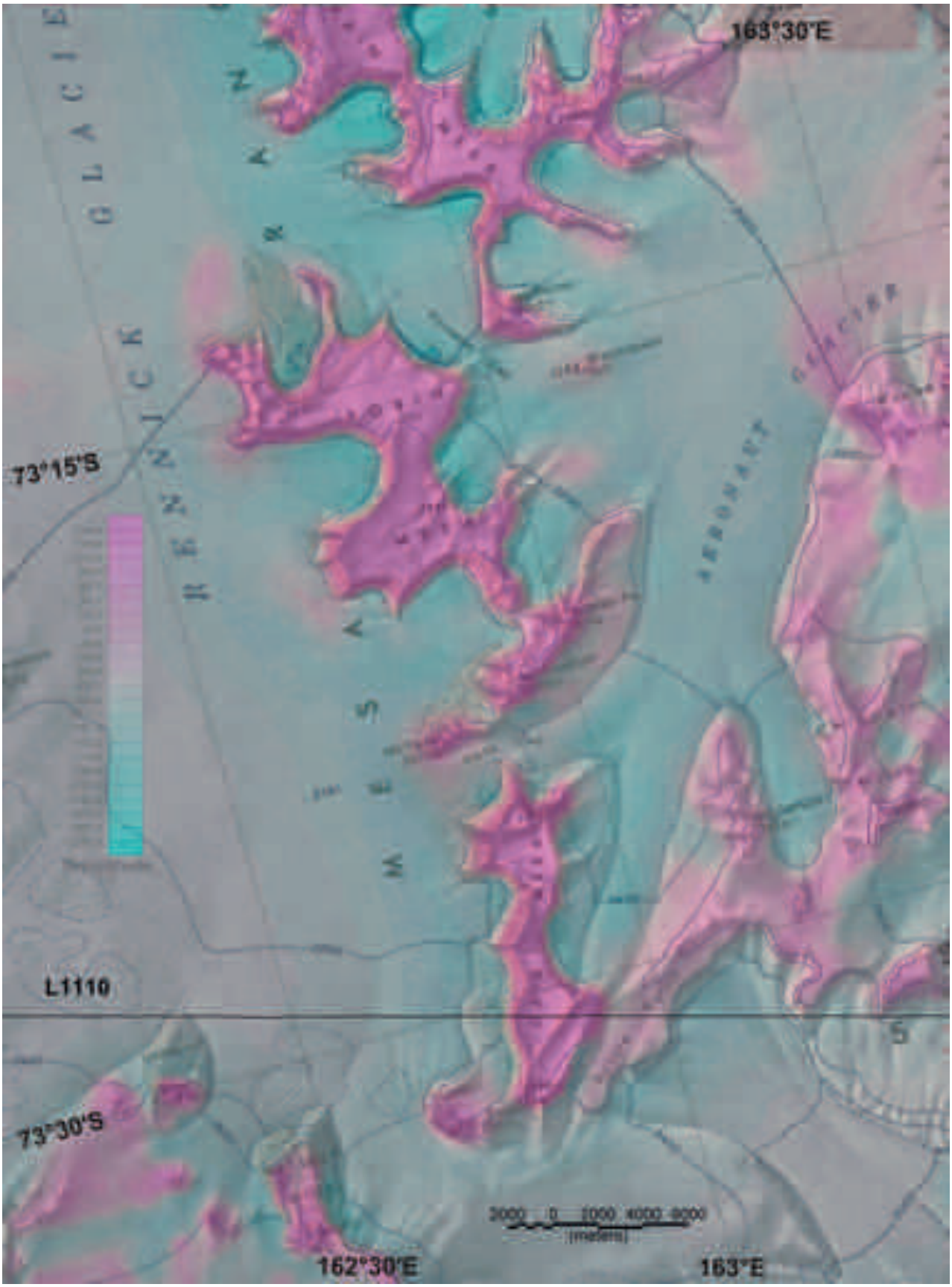

Fig. 10: The anomalies of the total magnetic field superimposed on the topographic map (section of the USGS Topographic Reconnaissance Map (250K) Mount Murchison). Colour scale is equal-area. The flight path for line L1110 is marked.

Abb. 10: Anomalienkarte des Magnetfeldes über topographischer Karte (Ausschnitt der USGS Topographic Reconnaissance Map (250K) Mount Murchison). Farbskala ist „equal-area". Der Flugweg für Linie L1110 ist markiert.

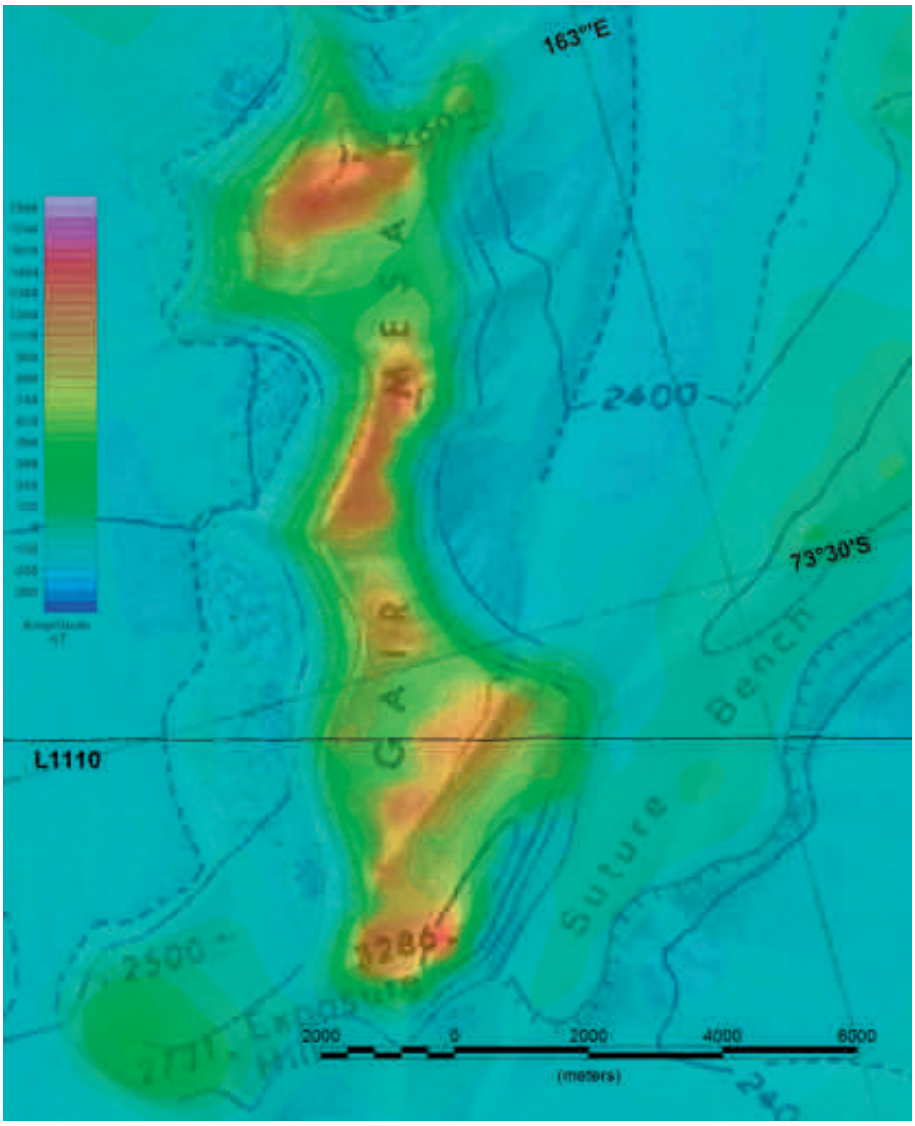

Fig. 11: Magnetic anomalies of the Gair Mesa. A linear colour scale was chosen to illustrate the magnetic pattern directly over the top of the mesa. The flight path for line L1110 is marked.

Abb. 11: Magnetische Anomalien der Gair Mesa. Eine lineare Farbskala wurde zur Verdeutlichung des magnetischen Musters direkt über dem Mesa Plateau gewählt. Der Flugweg für Linie L1110 ist markiert.

"feeder channel" and a slightly higher magnetization value to fit the observed anomaly. Another possibility is shown in Fig. 12e where the "peak" anomaly is caused by a small topographic ridge on top of the Gair Mesa combined with a higher magnetization value for the top of the Mesa. The ridge and the magnetic "peak" anomaly seem to be related to each other everywhere across the southern Gair Mesa plateau (Fig. 11). Therefore, we favour this model over that in Fig. 12d because the visible ridge and its connected anomaly provide a more natural explanation for the "peak" anomaly making a hypothetical "feeder dike" unnecessary. Consequently, this modelling approach was used in our preferred interpretation in Fig. 12a.

Fig. 12: Magnetic model calculation for flight line L1110 over the Rennick Glacier and the Gair Mesa. The anomalies are calculated for the draped flight path from GPS. Purple bodies are magnetized, yellow bodies denote non-magnetic rocks and ice. Their upper surface is defined by the ASTER Global Digital Elevation Model (GDEM) (https://wist.echo.nasa.govhttps://wist.echo.nasa.gov). Magnetic source bodies are limited in the y-direction perpendicular to the profile line (2 ½ dim). (a): Preferred model that explains the anomalies by topographically visible parts of the Mesas. (b): Alternative model using an additional "root" body for the Gair Mesa at reduced magnetizations. Two hypothetical bodies under the Rennick Glacier demonstrate that the presence of volcanic sources below most parts of the glacier areas are unlikely. (c)–(e): Detailed view of the Gair Mesa area. (c): Uniform magnetization of the Gair Mesa reproduces the "edge" anomaly of the main Gair Mesa body but fails to explain the peak on its top. (d): A feeder dike (1 km wide) below the Mesa may explain the "peak" anomaly. (e): "Peak" anomaly modelled by a topographic ridge on top of the Gair Mesa using a higher magnetization (approximately equivalent to (a)).

Abb. 12: Magnetische Modellrechnung für Linie L1110 über dem Rennick Gletscher und der Gair Mesa. Die Anomalien wurden für die mit GPS gemessene Flughöhe berechnet. Lila stellt magnetisches, Gelb nicht-magnetisches Gestein und Eis dar. Die Topographie stammt aus einem ASTER-Geländemodell (ASTER Global Digital Elevation Model (GDEM) (https://wist.echo.nasa.govhttps://wist.echo.nasa.gov)). Magnetische Quellen senkrecht zu den Profillinien (2 ½ dim) in y-Richtung begrenzt. (a): bevorzugtes Modell, das die Anomalien durch die sichtbare Topographie der Mesas erklärt. (b): alternatives Modell mit einem zusätzlichen „Wurzelkörper" für die Gair Mesa bei geringerer Magnetisierung. Zwei angenommene Quellkörper unter dem Rennick Gletscher machen deutlich, dass solche Körper unter den Gletschergebieten praktisch ausgeschlossen werden können. (c)–(e): Detailansichten der Gair Mesa. (c): Gleichförmige Magnetisierung der Gair Mesa reproduziert die Randanomalien der Gair Mesa aber nicht das zusätzliche magnetische Hoch. (e): Mit einer stärkeren Magnetisierung des obersten Teils der Gair Mesa kann das magnetische Hoch erklärt werden (entspricht mit leichten Abweichungen dem Model in (a)).

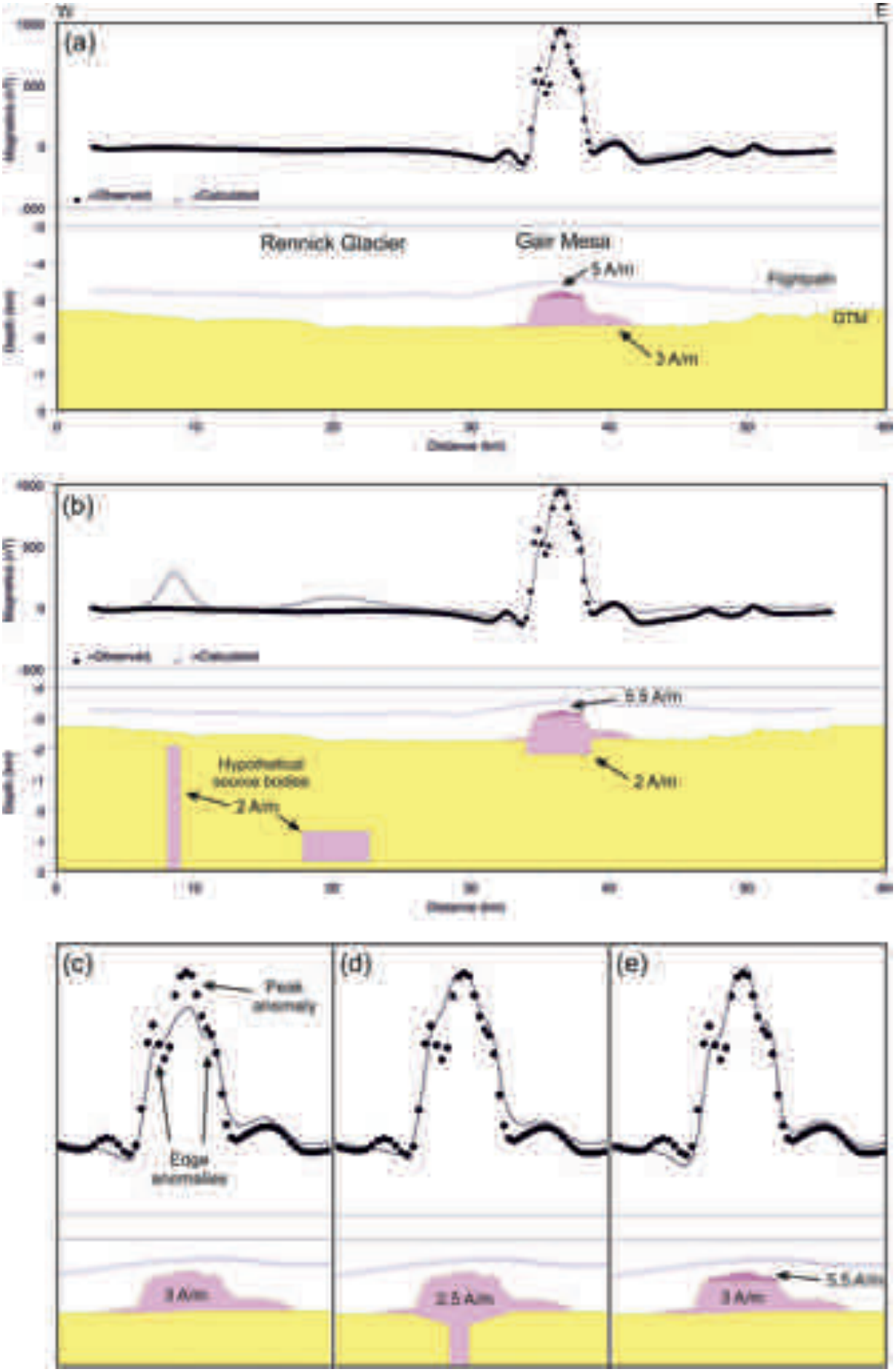
W
E
(a)
Renrick Glacier
Gair Mesa
5 A/m
3 A/m
DTM
(b)
6.5 A/m
2 A/m
Hypothetical source bodies
2 A/m
(c)
Peak anomaly
Edge anomalies
3 A/m
(d)
2.5 A/m
(e)
3 A/m

Indications for a highly magnetized top of the lava stack of the Mesa Range do exist. The more northerly Tobin Mesa near our Camp shows distinctively different darker basalt layers on the top, which were also recognized and sampled by McIntosh et al. (1986). They report for this "thick black, glassy flow" on the top of Pain Mesa a mean NRM intensity of 10.9 A/m (4 samples). These rocks seem also to be present on the northernmost edge of Gair Mesa but so far there are no indications for that flow variety on available photos from the usually snow-covered top of the southern Gair Mesa in the vicinity of our modelled line. The topographic ridge on top of the Gair Mesa is flanked on both sides with snow-covered depressions. If the snow cover in these depressions would have a significant thickness then the GDEM does not represent a magnetic surface and the true magnetic interface would have a more pronounced topography and the magnetic anomaly could be modelled using a lower magnetization value.

INTERPRETATION

The magnetic map in Fig. 9 shows that the anomalies can be subdivided into three main categories. (1) Areas with smooth, low amplitude appearance over glacier areas, (2) moderate anomaly amplitudes over some mountain areas and (3) distinct high amplitudes over the mesas.

(1) For the first category of the smooth magnetic field over the glaciers two possible explanations may apply: Either the lack of magnetic material in these areas or a greater source depth due to a thick ice cover in these areas or a combination of both. Unfortunately, ice thickness measurements are not available for the survey area. Ice thicknesses of more than one to two kilometres are unlikely but it cannot be excluded that the depth of the ice layer exceeds these values. Our hypothetical model (Fig. 12b provides arguments that any highly magnetized body like that of the Mesas must be located much deeper than it would be expected assuming a reasonable ice thickness. Thus any rocks, which might be present directly below the base of the ice are very likely not composed of Mesa Range basalts.

(2) The area with moderate anomalies seems to be underlain by weakly magnetized sedimentary, metamorphic and/or granitic rocks that sometimes may contain smaller amounts of intruded volcanic material (dikes and sills). It is also possible that this basement type underlies the glacier areas discussed above but due to the ice cover the magnetic pattern appears "flat".

(3) The high amplitudes over the mesas can obviously be explained by the topographically visual mesas if they have magnetization values that are typical for basalts. Deeper bodies are not necessary (see above).

CONCLUSION

One of the main questions, which this project was based on, was whether – in addition to the topographically visible expression of the basaltic mesas or the dolerite outcrops around – more volcanic material might be hidden under the ice. Clearly, only little volcanic material can be expected in the depressions of the Rennick Glacier and Aeronaut Glacier. It also appears that the gaps between the mesas and the areas directly adjacent to the mesa flanks do not contain volcanic material (at least not enough to produce a visible effect in the magnetic anomaly map). This supports the interpretation of the Mesa Range (and the Monument Nunataks further to the northwest) to be remnants of an elsewhere eroded plane of flood basalts or sills. The volcanic sequence of the mesas probably does not reach much below the present glacier level in agreement with earlier observations of outcropping Beacon sediments at the foot of some mesas.

The new magnetic map does not show any indications of circular anomalies, which might be associated with feeder dikes. Thus, we conclude that the previously discussed quasi-circular anomalies in the GANOVEX IV map were just artefacts of insufficient line spacing combined with low terrain clearance over the Mesa Range. It is thus likely that the basalt sheets forming the Mesas have their sources outside the upper Rennick area.

ACKNOWLEDGMENTS

The major part of this survey was conducted from a remote field camp in the Mesa Range. Without the help of many members of the expedition and the logistic support of the Italian Mario Zucchelli Station this camp – vital to our survey – would not have been established or functioning. In particular, we would like to express our thanks to the Helicopters New Zealand team and their constant support of this survey and to Maurice Conway who managed the camp during the entire field campaign in his professional and cheerful way. We would like to thank John C. Behrendt and Fausto Ferraccioli for their comments, which helped to improve the manuscript.

References

Bachem, H.-C., Boie, D.C. & Damaske, D. (1989a): Data Processing and Production of the Anomaly Maps of the Total Magnetic Field in the North Victoria Land/Ross Sea Area of the Antarctic.- Geol. Jb. E38: 81-89.

Bachem, H.-C., Bosum, W., Damaske, D. & Behrendt, J. (1989b): Planning and Execution of the GANOVEX IV Aeromagnetic Survey in North Victoria Land, Antarctica.- Geol. Jb. E38: 69-80.

Behrendt, J.C., LeMasurier, W.E., Cooper, A.K., Tessensohn, F., Tréhu, A. & Damaske, D. (1991): The west Antarctic Rift system: a review of geophysical investigations.- Contrib. Antarctic Research II, Antarctic Res. Ser. 53: 67-112.

Bosum, W., Damaske, D., Roland, N.W., Behrendt, J. & Saltus, R. (1989): The GANOVEX IV Victoria Land / Ross Sea Aeromagnetic Survey: Interpretation of Anomalies.- Geol. Jb. E38: 153-230.

Bosum, W., Damaske, D., Behrendt, J.C. & Saltus, R. (1991): The aeromagnetic survey of northern Victoria Land and the western Ross Sea during GANOVEX IV and a geophysical-geological interpretation.- In: M.R.A. THOMSON, J.A. CRAME, & J.W. THOMSON (eds), Geological Evolution of Antarctica, Proceedings of the Fifth International Symposium on Antarctic Earth Sciences, Cambridge University Press, 267-272.

Bozzo, E., Damaske, D., Caneva, G., Chiappini, M., Ferracioli, F., Gambetta, M. & Meloni, A. (1997): A High Resolution Aeromagnetic Survey over Proposed Drill Sites Off Shore of Cape Roberts in the Southwestern Ross Sea (Antarctica).- In: C.A. RICCI (ed), The Antarctic Region: Geological Evolution and Processes, 1129-1133.

Bozzo, E., Caneva, G., Gambetta, M. & Chiappini, M. (1998): Aeromagnetic survey (GITARA 5) on Lanterman-Evans Névé-Salamander Range. Terra Antarctica Rep. 2: 47-52.

Bozzo, E., Ferraccioli, F., Gambetta, M., Caneva, G., Spano, M., Chiappini, M. & Damaske, D. (1999): Recent progress in magnetic anomaly mapping over Victoria Land (Antarctica) and the GITARA 5 survey.- Antarctic Science 11: 209-216.

Damaske, D. (1988): Technical description of the 1:250,000 Maps of the Anomalies of the Total Magnetic Field Victoria Land/Ross Sea, Antarctica.- Aeromagnetic Survey During the Expedition GANOVEX IV 1984/85, pp.16, BGR, Hannover.

Damaske, D. (1989): Geomagnetic activity and its implications for the aeromagnetic survey in North Victoria Land.- Geol. Jb E38: 41-57.

Damaske, D. (1993): Geomagnetic activity in North Victoria Land during GANOVEX V.- Geolo. Jb. E47: 103-114.

Ferraccioli, F., Gambetta, M. & Bozzo, E. (1998): Microlevelling procedures applied to regional magnetic data: an example from the Transantarctic Mountains (Antarctica).- Geophys. Prospect. 46(2): 177-196.

Ferraccioli, F. & Bozzo, E. (2003): Cenozoic strike-slip faulting from the eastern margin of the Wilkes Subglacial Basin to the western margin of the Ross Sea Rift: an aeromagnetic connection.- Geol. Soc. London, Spec. Publ. 210(1): 109-133.

Ferraccioli, F., Jones, P.C., Curtis, M.L., Leat, P.T. & Riley, T.R. (2005a): Tectonic and magmatic patterns in the Jutulstraumen rift (?) region, East Antarctica, as imaged by high-resolution aeromagnetic data.- Earth Planets Space 57: 767-780.

Ferraccioli, F., Jones, P.C., Curtis, M.L. & Leat, P.T. (2005b): Subglacial imprints of early Gondwana break-up as identified from high resolution aerogeophysical data over western Dronning Maud Land, East Antarctica.- Terra Nova: 17(6): 573-579.

McIntosh, W.C., Kyle, P.R. & Sutter, J.F. (1986): Paleomagnetic results from the Kirkpatrick Basalt Group, Mesa Range, North Victoria Land, Antarctica.- In: E. STUMP (ed), Geological investigations in Northern Victoria Land, Antarctic Res. Ser. 46: 289-303.

Wilson, G., Damaske, D., Möller, H.D., Tinto, K. & Jordan, T. (2007): The geological evolution of southern McMurdo Sound – new evidence from a high-resolution aeromagnetic survey.- Geophys. J. Int. 170: 93-100. doi:10.1111/j.1365-246X.2007.03395x.

Polarforschung 84 (1), 15–21, 2014

Micro-Gravity Measurements in Northern Victoria Land, Antarctica, as Contribution to Geodynamic Investigations – a Feasibility Study

by Gerhard Jentzsch[1]

Abstract: This project comprises micro-gravity measurements in northern Victoria Land, Antarctica, using the existing Italian network with the basis Gondwana. The purpose was to add gravity data to the already collected deformation data. We used three gravimeters in parallel to increase the number of readings and – in parallel – to reduce the necessary flights to the points. With this project we could prove that such measurements are possible under the prevailing conditions (strong variations of temperature, air-pressure and elevation), and we could provide a first data set, which will serve as a reference for future work.

Zusammenfassung: Das hier vorgestellte Projekt umfasst Schwerediffe-renzmessungen im nördlichen Victoria Land an Punkten des italienischen Netzes für die Erfassung von Deformationen. Die Basisstation war Gond-wana. Ziel war, die von den Italienern beobachteten Deformationen durch Schwerediffe-renzen zu ergänzen. Dabei setzten wir drei Gravimeter gleich-zeitig ein, um einerseits die Anzahl der Beobachtungen zu vergrößern, um andererseits aber auch mit relativ wenigen Flügen auszukommen. Mit den Arbeiten konnten wir beweisen, dass derartige Messungen unter den vorherr-schenden Bedingungen (Temperaturänderungen, Luftdruckvariationen, große Höhendifferenzen) möglich sind. Es ist ein erster Datensatz erstellt worden, der als Referenz für zukünftige Untersuchungen dienen kann.

INTRODUCTION

The idea of performing micro-gravity measurements in northern Victoria Land (NVL) arose when we realized that within the Italian Antarctic programme in NVL repeated GPS-measurements are being carried out at well installed points in that area (VLNDEF: Victoria Land Network for Deformation Control; MANCINI 2000, MANCINI et al. 2004). Although the deformations obtained over a period of four years are quite small (seasons 1999-2000, 2000-2001, and 2002-2003; CAPRA et al. 2007), we expect from gravity observations additional information about on-going tectonic processes and/or mass changes caused by possible changes in the ice cover. Of course, such information will be available only by repeated measurements not before some years; but with our measurements we have now prepared the basis for such investigations.

Micro-gravity monitoring has been applied successfully in areas of active volcanism (see e.g. RYMER 1991; the results obtained by the author at three volcanoes are summarized in JENTZSCH et al. 2004). The advantage is that these measurements do not require a topographic reduction because the measurements are always carried out at the same points. Thus, the instrumental resolution and the measurement conditions, respectively, are the only limits for the resolution and accuracy of the measurements. In order to receive a reliable database we used three well-calibrated gravimeters together and repeated the measurements several times. Problems may occur due to snowfall, and – in this case – snow heights would have to be measured. But generally, the points are so exposed that local effects of the changing snow cover are not to be expected.

Using several gravimeters in parallel goes back to the procedures the colleagues in Fennoscandia applied: They used even more than three gravimeters during measurements along the so-called land-uplift lines which connected points in Norway, Sweden and Finland, and were repeatedly observed (MÄKINEN et al. 1985, EKMAN & MÄKINEN 1996) to determine the uplift after the ice retreat (GIA, glacial isostatic adjustment).

Actually, it was intended to get started with a small project to gain experiences before planning more comprehensive measurements. Since this was not possible because there was no Italian expedition in 2008/09, we decided to restrict ourselves to the vicinity of Terra Nova Bay under the possibilities offered by the Expedition GANOVEX X (Fig 1).

DIETRICH et al. (2001, 2004) have already carried out repeated GPS- and gravity observations in Antarctica, amongst others within the Chile-German expedition PATRIOT during the season 2004/2005 and in Dronning Maud Land (2003/2005). The aims of these works were similar, namely the determination of velocities of surface deformations as well as the variations of the gravity field and the detection of ice-induced mass changes and deformations of the crust (visco-elastic response).

But using only one gravimeter reduces the reliability and resolution of the observations. Therefore, we used three gravimeters in parallel. Our measurements were intended to prove if such measurements were even possible under the conditions of points at different elevations, helicopter transport, and strong temperature variations.

TECTONIC SETTING OF THE AREA OF NORTHERN VICTORIA LAND

The West Antarctic Rift System is the result of late Mesozoic and Cenozoic extension between East and West Antarctica, and represents one of the largest active continental rift systems

[1] Institute of Geosciences, University of Jena, Burgweg 11, D-07749 Jena, Germany.

Manuscript received 12 May 2014; accepted in revised form 08 September 2014.

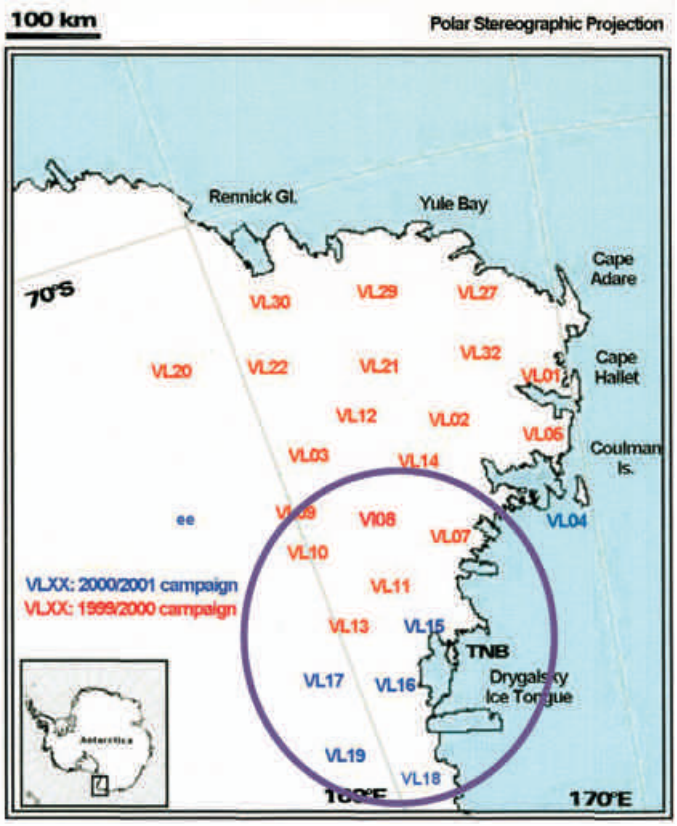

Fig. 1: Northern Victoria Land with the GPS-points of the Italian VLNDEF project (from Capra pers. comm.). The circle encompasses the points used for the gravity measurements. In this area we visited 13 points with three gravity meters, most of them more than twice, using the Gondwana Station as the reference. The North-South extension is about 250 km, West-East is about 100 km. TNB marks the Terra Nova Bight with station Gondwana (GOND).

Abb. 1: Nördliches Victoria Land mit den GPS-Punkten des italienischen VLNDEF-Projektes. Der Kreis umfasst die hier vermessenen Punkte. Es wurden insgesamt 13 Stationen aufgesucht mit drei Gravimetern, die meisten davon mehr als zweimal, mit Gondwana als Referenz. Die Nord-Süd-Ausdehnung liegt bei 250 km, in Ost-West-Ausdehnung ist es etwa 100 km. TNB markiert die Terra Nova Bucht mit unserer Referenzstation Gondwana (GOND).

on Earth. But the timing and magnitude of the plate motions leading to the development of this rift system remain poorly known, because of a lack of magnetic anomaly and fracture zone constraints on seafloor spreading. Magnetic data, gravity data and swath bathymetry were collected in several areas of the south Tasman Sea and northern Ross Sea. These results made it possible to calculate mid-Cenozoic rotation parameters for East and West Antarctica. These rotations show that there was roughly 180 km of separation in the western Ross Sea embayment in Eocene and Oligocene time. This episode of extension provides a tectonic setting for several significant Cenozoic tectonic events in the Ross Sea embayment including the uplift of the Transantarctic Mountains and the deposition of large thicknesses of Oligocene sediments. Inclusion of this East-West Antarctic motion in the plate circuit linking the Australian, Antarctic and Pacific plates removes a puzzling gap between the Lord Howe Rise and Campbell Plateau found in previous early Tertiary reconstructions of the New Zealand region. Determination of it also resolves a long-standing controversy regarding the contribution of deformation in this region to the global plate circuit linking the Pacific to the rest of the world (e.g. Behrendt et al. 1991, 1993, Cande et al. 2000, Decesari et al. 2007). The results obtained up to now indicate that considerable crustal deformation has taken place and is still ongoing.

GEODETICAL RESULTS

The Italian programme of repeated GPS-measurements carried out at well installed points in that area (Fig. 1; Mancini 2000, Mancini et al. 2004) revealed quite small, but significant deformations over a period of four years (seasons 1999-2000, 2000-2001, and 2002-2003, Capra et al. 2007). The analyses of the data obtained up to now provide absolute horizontal velocities ranging between 17 mm per year and 8 mm per year, with greater motions in the north. The relative motions obtained by subtraction of a rigid plate motion (using the results from the permanent GPS-station TNB1 installed at the Italian Mario Zucchelli Station) reveal neo-tectonics and may help to improve the understanding of the geologic development.

For the vertical, motions were detected with an average of +1.3 mm per year. Subtracting the velocities observed at the continuous station TNB1 the relative horizontal velocities are per year for the east direction, whereas for the vertical +0.4 mm per year were obtained (errors are in the order of ±0.1 mm). These are essential boundary conditions for the detection of the glacial isostatic adjustment (GIA) and other geophysical signals, and to redefine theory and other numerical models used without any direct measurement (Capra et al. 2007).

GRAVITY FIELD, ICE COVER AND ISOSTASY

Gravity research in the area has two different aims: First, of course, to derive the Bouguer anomaly for the investigation of the crustal structure. The second aim concerns the gravity changes induced by changes of the ice cover and/or tectonic deformation. In connection with air-borne measurements the Bouguer anomaly was already derived for the area of NVL (Reitmayr 2003). We hope to shed some more light on the gravity field and crustal dynamics in future by joint interpretation of the gravity and magnetic fields available in that area, also off-shore. This topic is under consideration in the frame of a research proposal by Jentzsch, Damaske and Läufer funded by DFG (doctoral thesis under preparation).

An explanation with a changing crustal thickness by isostatic models as well as models for glacial isostatic adjustment (GIA) is still lacking. The new measurements add new data, and they also add a dynamic component with increasing importance with time: Gravity variations measured on the surface to complement gravity variations derived from satellites.

With respect to the already observed vertical movements of about +0.4 mm per year and taking into account the available accuracy and resolution of repeated gravity measurements of about 10 μGal gravity variations should rise above the signal-to-noise ratio after some 20 years – additional signals, e.g. from mass-loss due to ice retreat could alter this estimation.

Ivins et al. (2003) derive vertical movements in the order of 1.5 mm per year in North Victoria Land with a gradient

of about 1 mm per year over our area. Further, SHEPHARD et al. (2012) report about new findings concerning ice retreat in West Antarctica and models of surface mass balance and glacial isostatic adjustment to estimate the mass balance. For the West Antarctic ice shield a dramatic mass-loss is documented for the past decade, which should be seen in gravity signal as well.

We used gravimeters in the same way the Nordic colleagues did concerning their work along the so-called Land-Uplift-Lines in Fennoscandia (MÄKINEN et al. 1985, EKMAN & MÄKINEN 1996): After several decades and many campaigns (repeated about every five years) they could distinguish between the free air effect and the Bouguer effect on gravity (visco-elastic response), and, thus, find a model for postglacial rebound for Fennoscandia.

Therefore, it is advisable to repeat the measurements every three to five years to create a reliable database, and to increase the points by the other available points of the Italian network.

MICRO-GRAVITY MEASUREMENTS AND PRELIMINARY RESULTS

The gravity measurements were carried out with the relative gravimeters G-085 and G-858 provided by the Technical University of Berlin (Geodesy and Geoinformatics), and the gravimeter G-662, owned by the Leibniz-Institute for Applied Geophysics, Hannover. All gravimeters are equipped with electrostatic feedback systems, which were carefully calibrated before the expedition. These three gravimeters were already in use by us and, thus, well known as some of the best gravimeters available in Germany (KRONER et al. 2006).

Every measurement consisted of at least three single readings, noted after at least two minutes after adjustment, repeated twice. We noted the value of the dial as well as the feedback voltage. In this way obvious miss-adjustments were revealed. Later, the mean of the remaining readings is used for the final adjustment of the network. It was intended to measure at all points at least three times to obtain nearly ten measurements each (with three gravimeters). The order of the measurements was always G-085 first, then G-858 and G-662. But due to the weather conditions it was not always possible to complete the tour as intended. Therefore, the distribution of the data is somewhat inhomogeneous. The order of the measurements as well as the connections realized are given in Table 1.

Depending on the local conditions like the horizontal and/or vertical distances between the helicopter landing spot and the point itself the time for completing the work at one point was about 40 minutes for the measurements (adjustment of the gravimeters and taking readings as described above) and up to 20 minutes for the transportation. Thus, it was possible to build up a routine to measure with several gravimeters one after another. The GPS-equipment was installed by the Italian colleagues at the beginning and removed just before the end of the season. Thus, we received averaged GPS-observations.

Table 2 contains all the points visited, their coordinates as well as the preliminary gravity differences obtained. We used Gondwana Station as reference station, and every day was started with taking measurements there; upon return, again a measurement was taken.

This led to the question concerning the number of stations possible during one flight. The best result was obtained when measuring six points plus the two reference measurements at Gondwana Station. This meant about eight hours measuring time plus more than two hours flight time. But we also had to experience the negative extreme. Only one station possible due to strong winds at the other places – and five hours work. To avoid breakdowns, it is recommended to use new batteries. We only suffered one battery breakdown from an old battery, which had to be replaced by a spare-one.

Difference measurements taken

GOND	-	TNB (B)	xxx xxx xxx
GOND	-	VL15	xxx xx xxx
GOND	-	VL07	xxx xxx xxx xxx
GOND	-	VL08	xxx
GOND	-	VL10	xxx xxx
GOND	-	VL11	xxx xxx
GOND	-	VL13	xx xxx
GOND	-	VL06	xxx xxx
GOND	-	VL18	xxx xxx
GOND	-	VL19	xxx
TNB (B)	-	TNB1 (ref)	xxx xxx
VL07	-	VL08	xxx xxx xxx
VL08	-	VL10	xxx xxx
VL11	-	VL13	xxx
VL13	-	VL17	xxx xx
VL15	-	TNB (B)	xxx
VL15	-	VL16	xx xxx
VL16	-	VL17	xx
VL16	-	VL18	xxx
VL17	-	VL19	xxx
VL18	-	VL19	xxx

Measurements at the individual points

GDW	xxx xxx xxx xxx xxx xxx xxx xxx xx xxx xxx xxx xxx xxx xxx xxx xxx xxx xxx xxx xxx xxx xxx xxx xxx xxx xxx xxx xxx
TNB (B)	xxx xxx xxx xxx
TNB1 (ref)	xxx
VL06	xxx
VL07	xxx xxx xxx
VL08	xxx xxx xxx
VL10	xxx xxx
VL11	xxx xxx
VL13	xx xxx xxx
VL15	xxx xx xxx
VL16	xx xxx xxx
VL17	xx xxx xxx
VL18	xxx xxx xxx
VL19	xxx xxx xxx

Tab. 1: GANOVEX X 2009–2010 measurement statistics; due to a breakdown of the battery of G-662 one loop could not be completed with this gravimeter. Therefore, in some cases only two crosses are given. Each x denotes one gravimeter.

Tab. 1: GANOVEX X 2009–2010: Zusammenstellung der Messungen. Jedes x steht für ein Gravimeter. Wegen Batterieausfalles am Gravimeter G-662 sind bei einigen Stationen nur zwei Geräte aufgeführt.

Name	GPS-No	North longitude	East longitude	Elevation above sea level [m]	Gravity differences to GOND [μm s^{-2}]
Gondwana	GOND	-74.633560	164.220855	10	0
Terra Nova building	TNB (B)	-74.698806	164.102943	15	61
Terra Nova Ref.	TNB1-GPS	-74.698806	164.102943	72	-172
Mt. Melbourne	VL06-GPS	-74.350001	164.690649	2732	-6,884
Mt. Monteagle	VL07-GPS	-73.759900	165.379302	2100	-6,147
Mt. Jiracek	VL08-GPS	-73.764285	163.739536	2655	-7,568
Archambault Ridge	VL10-GPS	-73.688456	162.768594	2619	-7,896
Mt. Baxter	VL11-GPS	-74.371428	162.541668	2362	-6,708
Mt. Larsen	VL13-GPS	-74.847797	162.204969	1510	-4,626
Inexpressible Island	VL15-GPS	-74.934264	163.715667	29	131
Cape Philippi	VL16-GPS	-75.232561	162.545487	311	-1,370
Evans Height	VL17-GPS	-75.095135	161.538744	683	-2,779
Starr Nunatak	VL18-GPS	-75.898533	162.593712	58	-571
Mc Daniel Nunatak	VL19-GPS	-75.804974	161.781615	809	-2,427

Tab. 2: Names and coordinates of GPS points and preliminary (rounded) gravity differences regarding GOND in μm s^{-2}; Terra Nova Ref. is the geodetic reference point on top of the hill above Mario Zucchelli Station; TNB (B) is the reference point inside a hangar where absolute gravity was measured. The higher resolution (nm s^{-2}) was provided by the precise data analyses (see Tab. 3). Our measurements at Mt. Melbourne were carried out by invitation of the Italian partner.

Tab. 2: Bezeichnungen und Koordinaten der GPS-Punkte und vorläufige Schweredifferenzen zu GOND in μm s^{-2}. Terra Nova Ref. Ist der geodätische Referenzpunkt auf der Spitze des Hügels direkt hinter der Mario Zucchelli Station. TNB (B) ist der Referenzpunkt innerhalb des Hangars, auf dem die Absolutschwere bestimmt worden ist. Die höhere Auflösung (nm s^{-2} wurde durch die Analysen möglich (Tab. 3). Unsere Messungen auf dem Mt. Melbourne fanden auf Einladung der italienischen Partner statt.

Name	GPS-No	Readings	Δg [nm s^{-2}]	rms [nm s^{-2}]
Gondwana	GOND	80	0	49
Terra Nova building	TNB	24	60 675	98
Terra Nova Ref.	TNB1-GPS	6	-174 128	191
Mt. Melbourne	VL06-GPS	6	-6 898 447	171
Mt. Monteagle	VL07-GPS	17	-5 700 586	110
Mt. Jiracek	VL08-GPS	16	-7 561 680	117
Archambault Ridge	VL10-GPS	12	-7 889 645	136
Mt. Baxter	VL11-GPS	12	-6 702 274	132
Mt. Larsen	VL13-GPS	14	-4 619 520	122
Inexpressible Island	VL15-GPS	16	132 199	109
Cape Philippi	VL16-GPS	16	-1 367 577	112
Evans Height	VL17-GPS	15	-2 771 065	115
Starr Nunatak	VL18-GPS	18	-570 838	107
Mc Daniel Nunatak	VL19-GPS	11	-2 426 388	135

Tab. 3. Names and GPS-nos. of the observed points, number of connections, derived gravity differences regarding GOND and errors in nm s^{-2}; TNB is the reference point inside a hangar where absolute gravity was measured.

Tab. 3: Namen und GPS-Nummern der Messpunkte, Anzahl der Verbindungen, abgeleitete Schweredifferenz zu GOND sowie Fehler in nm s^{-2}; TNB ist der Referenzpunkt innerhalb des Hangars an dem die Absolutschwere gemessen worden war.

In all, Gondwana Station was connected with ten stations out of the network of 13, and eleven stations were connected to each other at least three times. 30 measurements were carried out at the reference station Gondwana (GOND) alone, and 34 measurements were done at the other points of the network (always with all three gravimeters).

The data were evaluated using the software GRAV (Wenzel 1993 unpubl.), which was completed by us, especially concerning the introduction of the feedback values. The final adjustment of all data was already completed (Jentzsch et al. 2014). This required a careful screening of the data of the individual gravimeters in order to sort out bad data. The results are given in Table 3 (from Jentzsch et al. 2014).

As it looks like, local ice thicknesses are not disturbing the data at the points, because there, we could always measure on the rock. But the general ice and snow cover may become a problem. Here we would need spatial data of the whole area. Model computations will be used to check this effect. On the other hand, we have improved the tidal model used up to now by taking into account the ocean tides as well. There existed a tide gauge record over more than one year at Mario Zucchelli Station just 7 km opposite to Gondwana Station, which was made available by the Italian colleagues. The ocean tidal corrections improved the data considerably due to the small distances to the ocean.

Figure 2 shows an arrangement at point VL15 (Inexpressible Island). The reference point is on the upper end of the steel post just below the table screwed on it. This table proved to be unusable because of vibrations due to wind. Figures 3 & 4 give more details about the experiments, especially the steel post and the shielding against wind if necessary.

Depending on the weather the flights had to be planned and the schedules had to be adopted. In particular the strong catabatic winds proved to be very disturbing, measurements were simply impossible. On the other hand, we also experienced best conditions at critical points, unexpectedly. Thus, it was not possible to follow the previously worked out flight plan, and instead of 12 intended flights we had to use the helicopter 15 times (one flight invited by the Italian colleagues), and still we could not measure as much as we had planned. The flight distances are in the order of over 3,000 km.

FINAL RESULTS

Data analyses are already completed and Table 3 contains the results (from Jentzsch et al. 2014). Some figures can be stressed. The gravimeters are calibrated to 10^{-4}; although this

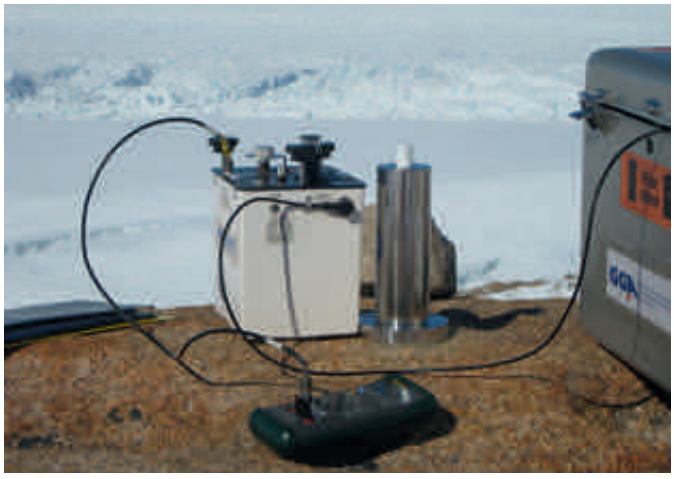

Fig. 3: Gravimeter G-662 at point Cape Philippi (VL16) beside the benchmark. In the background is the David Glacier continued by the Drygalski Ice Tongue to the left, (Photo: author).

Abb. 3: Messpunkt Cape Philippi (VL16) mit Gravimeter G-662 neben dem Edelstahl-Pfosten. Im Hintergrund ist der David Glacier mit der Drygalski Ice Tongue zur Linken, (Foto: Autor).

Fig. 2: Measurements at point VL15, Inexpressible Island. The table proved to be not usable due to unexpected vibrations. Here, G-662 is seen, the other two gravity meters are in the boxes behind. The arrow points to the top of the benchmark as the reference, (Photo: author).

Abb. 2: Messung an Punkt VL15, Inexpressible Island. Der aufgesetzte Tisch erwies sich als unbrauchbar wegen unerwarteter Vibrationen. Man sieht G-662, die anderen beiden Gravimeter im Hintergrund. Der Pfeil deutet auf den Bezugspunkt am Pfosten, (Foto: Autor).

Fig. 4: Measurements with G-858 at Mt. Jiracek (VL08). The boxes of the other gravimeters are used as windshields, the arrow points to the top of the benchmark. Circled below left is the helicopter pilot worrying for a developing whiteout, which appeared only some minutes later and forced us to abandon the measurement. The position of the pilot reveals that the climb up-hill was not that easy, (Photo: private).

Abb. 4: Messungen mit G-858 am Mt. Jiracek (VL08). Die beiden anderen Gravimeter dienen als Windschutz, der Pfeil deutet auf den Pfosten. Im Kreis sieht man den Piloten der zur Eile drängt, da sich ein „whiteout“ entwickelt; die Position des Pikoten zeigt, dass der Aufstieg zum Messpunkt nicht einfach war, (Foto: privat).

value was determined for the feedback only, we consider that the calibration of the dial is not better but similar. This means, that gravity differences between Gondwana and the high points like Mt. Jiracek or Archambault Ridge in the order of more than 6,500 μm s^{-2} (corresponding to 650 mGal, since 10 μm s^{-2} correspond to 1 mGal.) cannot be determined to better than 650 nm s^{-2} (or 65 μGal). This is not too bad, but by far not enough to separate the anticipated very small differences to be resolved later. But, the gravity differences between the points at about the same elevations seem reasonable for interpretations, because they are much smaller and, accordingly, the errors as well; and this is exactly what we need. Therefore, we tried to combine the points themselves rather than to link all the points to the reference GOND.

Although the set-ups of the gravimeters were more or less repeatable, there were some considerable differences due to wind and temperature conditions, which surely have consequences for the accuracy of the results. Thus, due to the environmental conditions we may not be able to achieve similar results concerning the errors as in our measurements at volcanoes of about ±100 nm s^{-2} to ±150 nm s^{-2} (±10 to ±15 μGal; JENTZSCH et al. 2004). But, as a positive result we can mention that under favourable conditions we received for a single loop between Gondwana Station and Mario Zucchelli Station an error of ±4 μGal (±40 nm s^{-2}), which can serve as a lower bound for the errors. Thus, we expect that the data will be useful for the purposes mentioned above.

DISCUSSION AND CONCLUSIONS

The work started with this project marks the starting point concerning the investigation of the relation of deformation and gravity field variations in the area of northern Victoria Land. The central question is if deformation is accompanied by gravity field variations or if there are additional effects causing changes in gravity, e.g. like changes in the ice cover. This can only be answered after about 20 years and several campaigns. The results could contribute as another boundary condition to the numerical modelling of other geophysical and geodetical data, as mentioned above. It is certainly not to be expected to find strong changes due to fast elevation changes, but such measurements should be started now to create data for later comparison. Because of climate changes a retreat of the glaciers will be a signal to be observed, and, thus, a contribution to glacial isostatic adjustment (GIA) can be expected, although no modeling was done yet. Thus, as the colleagues in Fennoscandia we expect to distinguish between the free air effect and the Bouguer effect on gravity to find a model for postglacial rebound.

The first experience worth mentioning concerns the transport of the gravimeters with the airplane as cabin luggage. Because of new flight restrictions they had to be transported without the batteries, and this transport had to be negotiated with the airline prior to purchasing the tickets. The connectors being prepared beforehand, the batteries were purchased in New Zealand during the two days between arrival of the plane and departure of the Italian research vessel to Terra Nova Bay. On the way back the batteries were put into the personal luggage and returned with the ship.

In the helicopters, the gravimeters were transported on the rear seats, on the seat cushions, to minimise vibrations. Since the elevation differences were up to 2,600 m, the dial was turned using a small electric motor.

Although we had quite fortunate conditions concerning the temperature and the wind it is recommended for further measurements to insulate the gravimeters, e.g. by a material wrapped around to protect the casing from cooling too fast. Since the gravimeters have to be used close to the benchmarks and due to the limited area of rock available for the installation it is not possible to use them inside a bigger case with bottom holes for the foot screws. Further, the gravimeter campaign had to fit into the overall schedule of the expedition leading to the effect that not all favourable times could be used for gravimetry.

Finally, one person operating three gravimeters meant quite a big job. But the capacity of the helicopter is limited, and the flights often had to be shared with other projects. Therefore, it was necessary to rely on the accompanying colleagues as well as the pilots to help carrying the gravimeters to the points. For the future the recommendation is to use four gravimeters and two observers, which would increase the number of observations in a shorter time.

From the technical point of view, the question if micro-gravity measurements are feasible at the GPS-points in NVL following the usual practice (several gravimeters together; precise repetition of set-ups) can be answered with YES (!). Thus, we want to recommend to continue these measurements including more points already available from the Italian partners in NVL.

ACKNOWLEDGMENTS

This work is a contribution to the expedition GANOVEX X planned and organised by the Federal Institute of Geosciences and Natural Resources (Bundesanstalt für Geowissen-schaften und Rohstoffe, BGR), Hannover. Part of the project (travel cost, spare parts) was funded within the *Schwerpunktprogramm Antarktisforschung* of the German Research Foundation (DFG), whereas the fieldwork was supported by BGR. The funding and logistic support are gratefully acknowledged. Thanks go also to the Italian side, Alessandro Capra and Marco Dubbini, for providing the permission to use the GPS stations as well as all necessary information. The measurements at the top of Mt. Melbourne were possible through the invitation of the Italian side. We are indebted to the Institute of Geodesy and Geoinformatics of the Technical University of Berlin for providing the gravimeters G-085 and G-858 as well as to the Leibniz Institute for Applied Geophysics, Hannover, for lending the gravimeter G-662.

The transport of the gravimeters in the plane as cabin luggage required two extra persons; Nadine John and Robert Schöner of our institute, also participating the expedition, thankfully volunteered to carry two gravimeters through check-in and customs.

The author needed help to carry the gravimeters to the measuring points; this help was provided by the colleagues who

shared the flights, as well as by the pilots – many thanks! Thanks also to my co-workers Stephanie Zeumann and Marco Naujoks as well as the students Franziska Bock and Tobias Nickschick for their contribution to carefully calibrate the gravimeters at the vertical base line in Hannover.

The suggestions of Lothar Viereck and one anonymous reviewer are gratefully acknowledged; the text was considerably improved. Last but not least I wish to thank Sieglinde Ott for many inspiring and fruitful discussions and for attracting my interest to new, non-geophysical aspects of polar research, the lichen.

References

Behrendt, J.C., LeMasurier, W.E., Cooper, A.K., Tessensohn, F., Trehu, A. & Damaske, D. (1991): Geophysical studies of the West Antarctic rift system.- Tectonics 10: 1257-1273.

Behrendt, J.C., Damaske, D. & Fritsch, J. (1993): Geophysical characteristics of the West Antarctic Rift system.- Geol. Jb. E47: 49-101.

Cande, S.C., Stock, J.M., Müller, D. & Ishihara, T. (2000): Cenozoic Motion between East and West Antarctica.- Nature 404: 145-150.

Capra, A., Mancini, F. & Negusini, M. (2007): GPS as a geodetic tool for geodynamics in northern Victoria Land, Antarctica.- Antarctic Science 19: 107-114.

Decesari, R,C, Wilson, D.S., Luyendyk, B.P. & Faulkner, M. (2007): Cretaceous and Tertiary extension throughout the Ross Sea, Antarctica.- US Geol. Surv. & National Acad. USGS OF-2007-1047, Short Research Paper 098; doi: 0.3 33/of2007-1047.srp098.

Dietrich, R., Dach, R., Engelhardt, G., Ihde, J., Korth, W., Kutterer, H.J., Lindner, K., Mayer, M., Miller, H., Menge, F., Muller, C., Niemeyer, W., Perlt, J., Pohl, M., Salbach, H., Schenke, H.W., Schone, T., Seeber, G., Veit, A. & Völksen, C. (2001): ITRF coordinates and plate velocities from repeated GPS campaigns in Antarctica – an analysis based on different individual solutions.- J. Geodesy 74: 756-766.

Dietrich, R., Rülke, A., Ihde, J., Lindner, K., Miller, H., Niemeyer, W., Schenke, H.W. & Seeber, G. (2004): Plate kinematics and deformation status of the Antarctic Peninsula based on GPS.- Global Planet. Change 42: 313-321.

Ekman, M. & Mäkinen, J. (1996): Recent postglacial rebound, gravity change and mantle flow in Fennoscandia.- Geophys. J. Internat. 126: 229-234.

Ivins, E.R., James, T.S. & Klemann, V. (2003): Glacial isostatic stress shadowing by the Antarctic ice sheet.- J. Geophys. Res. 108(B12), 2560, doi:10.1029/2002JB002182.

Jentzsch, G., Weise, A., Rey, C. & Gerstenecker, C. (2004): Gravity changes and internal processes – some results obtained from observations at three volcanoes.- PAGEOPH, Special Issue "Geodetic and geophysical effects associated to seismic and volcanic hazards", Pure Appl. Geophys. 161: 1415-1431.

Jentzsch, G., Ricker, R., Weise, A., Capra, A., Dubbini, M. & Zanutta, A. (2014): Micro-Gravity Measurements in Northern Victoria Land, Antarctica: A Feasibility Study.- In: C. RIZOS & P. WILLIS (eds), Earth on the Edge: Science for a Sustainable Planet; Proc. IAG Gen. Ass. Melbourne, Australia, June 28 – July 2, 2011. Series: Internat. Assoc Geodesy Sympos. 139: XIII, 617 p.

Kroner, C., Jahr, T., Naujoks, M. & Weise, A. (2006): Hydrological signals in gravity – foe or friend?.- Springer-Verlag, IAG-Cairns, Chapter 73: 504-510.

Mäkinen, J., Ekman, M., Midtsundstad, A. & Remmer, O. (1985): The Fennoscandian land uplift gravity lines 1966-1984.- Rep. Finnish Geodetic Inst. 85:4, 238 p.

Mancini, F. (2000): Geodetic activities: a new GPS network for crustal deformation control in Northern Victoria Land.- Terra Antartica Rep. 5: 23-28.

Mancini, F., Capra, A., Gandolfi, S., Sarti, P. & Vittuari, L. (2004): VLNDEF (Victoria Land Network for Deformation control) Monumentation during GANOVEX VIII.- ItaloAntartide XV: Survey and data processing; Terra Antartica 11: 35-38.

Reitmayr, G. (2003): Continuation of Gravity Measurements in Victoria Land and at the Oates Coast, Antarctica, during GANOVEX VII.- Geol. Jb. B 95:

Rymer, H. (1991): The Use of Microgravity for Monitoring and Predicting Volcanic Activity: Poa's volcano, Costa Rica.- Cahier Centre Europ. Geod. Seismol. 4: Proc. Geodyn. Instrument. Applied Volcanic Areas., 1990, Walferdange, Luxembourg, 325-331.

Shepherd, A., Ivins, E.R., Geruo, A, Barletta, V.R., Bentley, M.J., Bettadpur, S., Briggs, K.H., Bromwich, D.H., Forsberg, R., Galin, N., Horwath, M., Jacobs, S., Joughin, I., King, M.A., Lenaerts, J.T.M., Li, J., Ligtenberg, S.R.M., Luckman, A., Luthcke, S.B., McMillan, M., Meister, R., Milne, G., Mouginot, J., Muir, A., Nicolas, J.P., Paden, J., Payne, A.J., Pritchard, H., Rignot, E., Rott, H., Sørensen, L.S., Scambos, T.A., Scheuchl, B., Schrama, E.J.O., Smith, B., Sundal, A.V., van Angelen, J.H., van de Berg, W.J., van den Broeke, M.R., Vaughan, D.G., Velicogna, I., Wahr, J., Whitehouse, P.L., Wingham, D.J., Yi, D., Young, D. & Zwally, H.J. (2012): A Reconciled Estimate of Ice-Sheet Mass Balance.- Science 338: 1183-1189.

Wenzel, H.-G. (1993): Program package GRAVNA - Adjustment of gravity observations, Fortranprogram, Geodetic Inst. Univ. Karlsruhe, unpubl.

Polarforschung 84 (1), 23–38, 2014

The Ross-Orogenic Tiger Gabbro Complex (Northern Victoria Land, Antarctica): Insights into the Lower Crust of a Cambrian Island Arc

by Friedhelm Henjes-Kunst[1], Jürgen Koepke[2], Andreas Läufer[1], Solveig Estrada[1], Glen Phillips[3,4], Karsten Piepjohn[1], and Dominique Kosanke[2]

Abstract: Subduction related mafic/ultramafic complexes marking the suture between the Wilson Terrane and the Bowers Terrane in northern Victoria Land (Antarctica) are well-suited for evaluating the magmatic and structural evolution at the Palaeo-Pacific continental margin of Gondwana. One of these intrusions is the "Tiger Gabbro Complex" (TGC), which is located at the southern end of the island-arc type Bowers Terrane. The TGC is an early Palaeozoic island-arc related layered igneous complex characterized by extraordinarly fresh sequences of ultramafic, mafic and evolved lithologies and extensive development of high-temperature high-strain zones. The goal of the present study is to establish the kinematic, petrogenetic and temporal development of the TGC in order to evaluate the magmatic and structural evolution of the deep crustal roots of this Cambrian-aged island-arc. Fieldwork during GANOVEX X was carried out to provide insight into: (i) the spatial relations between the different igneous lithologies of the TGC, (ii) the nature of the contact between the TGC and Bowers Terrane, and (iii) the high-temperature shear zones exposed in parts of the TGC. Here, we report the results of detailed field and petrological observations combined with new geochronological data. Based on these new data, we tentatively propose a petrogenetic-kinematic model for the TGC, which involves a two-phase evolution during the Ross orogeny. These phases can be summarized as: (i) an early phase (maximum age c. 530 Ma) involving tectono-magmatic processes that were active at the deep crustal level represented by the TGC within the Bowers island arc and within a general NE–SW directed contractional regime and (ii) a late phase (maximum age c. 490 Ma) attributed to the late Ross orogenic intrusion of the TGC into the higher-crustal metasedimentary country rocks of the Bowers Terrane under NE–SW directed horizontal maximum stress and subsequent cooling.

Zusammenfassung: Subduktionsgebundene mafisch-ultramafische Komplexe markieren die Sutur zwischen dem Wilson Terrane und dem Bowers Terrane im nördlichen Victoria Land (Antarktis). Diese sind gut geeignet, um die magmatische und strukturelle Entwicklung am paläopazifischen Kontinentrand Gondwanas im Kambrium zu rekonstruieren. Eine dieser Intrusionen stellt der „Tiger Gabbro Complex" (TGC) am südlichen Ende des Inselbogenkomplexes des Bowers Terranes dar. Der TGC ist ein frühpaläozoischer geschichteter Magmatitkomplex mit Inselbogenaffinität, der durch außerordentlich frische Gesteinsabfolgen ultramafischer, mafischer und stärker differenzierter Lithologien und durch hoch-temperierte Scherzonen gekennzeichnet ist. Das Ziel dieser Arbeit ist die Klärung der kinematischen, petrogenetischen und zeitlichen Entwicklung des TGC, um so die magmatische und strukturelle Entwicklung der tief-krustalen Bereiche dieses kambrischen Inselbogenkomplexes zu rekonstruieren. Die Geländeaufnahmen während GANOVEX X wurden mit den Zielen durchgeführt, 1.) die räumlichen Zusammenhänge der verschiedenen Lithologien innerhalb des TGC, 2.) die Kontaktverhältnisse des TGC zu den umgebenden Metasedimentgesteinen und 3.) die Hochtemperaturscherzonen, die von einem Teilgebiet des TGC bekannt waren, zu untersuchen. Wir stellen hier die Ergebnisse der detaillierten Geländeuntersuchungen, von petrologischen Untersuchungen und von neuen geochronologischen Analysen vor. Basierend auf diesen Daten schlagen wir ein Modell vor, welches eine zweiphasige Entwicklung des TGC beinhaltet. Diese lässt sich zusammenfassen in: 1.) „Frühphase" (Maximalalter ca. 530 Ma) mit tektonomagmatischen Prozessen, die innerhalb der durch den TGC repräsentierten unteren Krustenbereiche des Bowers Terrane aktiv waren, und 2.) „Spätphase" (Maximalalter ca. 490 Ma), die der spät-Ross-orogenen Intrusion des TGC in die höherkrustalen metasedimentären Rahmengesteine des Bowers Terrane unter NE-SW gerichtetem horizontalem Hauptdruck sowie anschließender Abkühlung zugeordnet werden kann.

INTRODUCTION

Ultramafic to mafic complexes often mark sutures between collided continents or terranes. In northern Victoria Land (NVL) in Antarctica, the suture between the Wilson Terrane and the Bowers Terrane is marked by mafic to ultramafic intrusions, which bear valuable information on processes related to the magmatic evolution of island arc systems. These rocks are particularly wellsuited for evaluating the structural and geological evolution at the active continental margin of Palaeo-Victoria Land during the Cambrian (Rocchi et al. 1999, Capponi et al. 2003, Estrada & Jordan 2003, Rocchi et al. 2003, Tiepolo & Tribuzio 2008, Tribuzio et al. 2008).

There is currently a great interest in determining the origin of subduction-related mafic-ultramafic intrusive complexes. Unfortunately, these intrusions are rare and commonly volumetrically subordinate. It was suggested that they founder within the mantle because of their high density (for details see Behn & Kelemen 2006). Such intrusions are highly relevant to models for crustal development, because they potentially link upper mantle and lower crustal processes (Annen et al. 2006). Accordingly, understanding the emplacement and differentiation mechanisms of deep-seated magmatic bodies is crucial to understanding crustal growth mechanisms (DeBari 1994). Mafic and ultramafic intrusive rocks exposed along orogenic belts may thus be important sources of information on hidden crustal processes that occurred during subduction. Such rocks locally preserve relict mineral phases or complex zoning which is the record of variations in magma composition. Petrological results, when coupled with detailed geochronological data, can provide the timing of the different magmatic events and important constraints for the evolution of an orogen.

One of such suite of ultramafic-mafic, magmatic-arc related intrusives is the "Tiger Gabbro Complex" (TGC) at the southeastern termination and southwestern border of the Bowers Terrane in NVL (Ganovex Team 1987). The rocks of the TGC

[1] Bundesanstalt für Geowissenschaften und Rohstoffe (BGR), Stilleweg 2, D-30655 Hannover, Germany, <henjes-kunst@bgr.de>
[2] Institut für Mineralogie, Leibniz Universität Hannover, Callinstr. 3, D-30167 Hannover, Germany.
[3] Discipline of Earth Sciences, School of Environmental and Life Sciences, Science Building – SB110, The University of Newcastle, University Drive, Callaghan, NSW 2308, Australia.
[4] Geological Survey of New South Wales, 516 High Street, Maitland NSW 2320, Australia

Manuscript received 7 June 2014; accepted in revised form 21 October 2014.

are extraordinarily fresh and range from primitive olivine-pyroxene rich cumulates up to quartz-bearing diorites and anorthosites s.l.. In addition, in parts of the complex spectacular high-temperature shear zones are exposed. The present project was established to investigate the magmatic and structural evolution of the TGC by combining field work carried out during the GANOVEX X campaign in 2009/10 with geochronological and isotope geochemical analyses of samples taken during this expedition as well as from earlier GANOVEX campaigns. Our overarching aims for the project were: (i) to reconstruct the petrogenetic evolution of these cumulate rocks as a rare example of a deep-seated magmatic-arc related layered igneous complex, (ii) to investigate an affinity to either an oceanic or a continental magmatic-arc system and (iii) to provide insight into the final emplacement of the complex into its current structural position. The purpose of this paper, particularly, is to present field observations combined with first petrological and structural data as well as Ar-Ar age determinations. Results of ongoing isotope geochemical and geochronological studies and thermodynamic modeling will be published in later articles.

GEOLOGICAL BACKGROUND

The continental basement of NVL comprises three tectonic terranes (from SW to NE: the Wilson Terrane, the Bowers Terrane, and the Robertson Bay Terrane), which according to the model of KLEINSCHMIDT & TESSENSOHN (1987) were juxtaposed during the Cambro-Ordovician Ross Orogeny by accretionary processes above a westward dipping subduction zone (Fig. 1).

The Wilson Terrane represents the Palaeo-Pacific active continental margin of Gondwana. It mostly consists of low- to high-grade metasedimentary rocks (e.g., HENJES-KUNST & SCHÜSSLER 2003, HENJES-KUNST 2003) intruded by granitic to mafic plutons showing geochemical continental-arc affinity (Granite Harbour Intrusives; DI VINCENZO & ROCCHI 1999). The stratigraphically lower part of the Bowers Terrane is composed of intercalated low-grade metavolcanic and metasedimentary rocks that have traditionally been interpreted to represent a Middle to Late Cambrian intra-oceanic island arc (WEAVER et al. 1984). The metasedimentary rocks (Molar Formation) are turbiditic in nature and grade upwards into the shallow marine Mariner Formation. The upper part of the Bowers Terrane is built up by km-thick terrestrial deposits (Leap Year Group). The Robertson Bay Terrane is composed of turbiditic metasedimentary rocks of late Cambrian to Ordovician age (HENJES-KUNST & SCHÜSSLER 2003, HENJES-KUNST 2003). During the Ross Orogeny, accretion of the Bowers Terrane (together with the conjoined Robertson Bay Terrane to the east) to the eastern margin of the Wilson Terrane was accompanied by widespread folding and lower greenschist facies metamorphism. The suture zone between the Wilson and Bowers terranes, a key area for the construction of a geodynamic model for the Ross Orogeny in NVL (e.g., ROCCHI et al. 1999, ESTRADA & JORDAN 2003, ROCCHI et al. 2003, FEDERICO et al. 2006), is marked by the presence of mafic to ultramafic intrusions (Fig. 1). They have been interpreted to form the deeper crustal part of a juvenile magmatic-arc system of Cambrian age (TIEPOLO & TRIBUZIO 2008, TRIBUZIO et al. 2008).

One of these mafic bodies is the TGC, a layered intrusion located at the southeastern termination of the Bowers Terrane at the Ross Sea coast (Fig. 1). It crops out over an area of 35 km^2 at Dragontail Hills (southeastern Spatulate Ridge) and at Apostrophe Island (Fig. 2). Typical lithologies are pyroxenites, gabbros, gabbronorites, anorthosites s.l., and hornblende-plagioclase-rich pegmatoids (GANOVEX TEAM 1987, BRACCIALI et al. 2009). The complex exhibits well-exposed high-temperature shear zones. Geochronological data are scarce and generally not coherent. KREUZER et al. (1987) report a K-Ar age of 521 ±10 Ma on a hornblende from a pegmatoid. Subsequent Ar-Ar dating of this hornblende (RICCI & TESSENSOHN 2003) revealed two discrete plateau-like age intervals of 501 ±3 Ma, and 483 ±2 Ma, respectively. ROCCHI et al. (1999) and BRACCIALI et al. (2009) report a Sm-Nd isochron age of 535 ±21 Ma based on three whole-rock samples and an Ar-Ar step-heating age determination of a hornblende which again yields two discrete plateau-like age intervals of 510 ±10 Ma, and 499 ±6 Ma, respectively. Whole-rock trace-element geochemistry suggests a calc-alkaline character of the TGC (ROCCHI et al. 2003). More recent geochemical investigations and modeling (BRACCIALI et al. 2009) indicate a primitive low-K tholeiitic character and support the cumulate nature. Based on these data, BRACCIALI et al. (2009) interpret the TGC as a *"root of an island arc within the Palaeozoic margin of Gondwana"* and suggest a genetic link between the TGC and the metavolcanic rocks of the Cambrian Bowers Terrane.

From the study of the Bowers Terrane country rocks (Middle Cambrian Sledgers Group) to the north of the TGC, Engel (1987) reports a 4.5 km wide contact aureole with estimated temperatures of 800 °C at pressures of 0.2-0.4 GPa close to the contact. However, the contact between the TGC and metasedimentary and metavolcanic rocks of the Bowers Terrane remains a matter of discussion since it is only exposed in two steep cliffs at the northwestern and northeastern margins of the TGC (Fig. 2) which are not easily accessible. Based on helicopter-supported fieldwork, CAPPONI et al. (2003) and BRACCIALI et al. (2009) suggest that the contact between the TGC and the Bowers Terrane metasedimentary and metavolcanic rocks is of tectonic origin.

Geochemical and geochronological investigations also exist for two other mafic-ultramafic igneous complexes at the suture between the Wilson and Bowers terranes. The Niagara Icefall Intrusion (Fig. 1) is composed of pyroxenites, gabbronorites, ferrogabbronorites of cumulate origin with boninitic affinity (TRIBUZIO et al. 2008). From U-Pb zircon dating, a formation age of 514 ±2 Ma was concluded. According to TRIBUZIO et al. (2008), the Niagara Icefalls suite represents an igneous complex formed in an embryonic back-arc basin at the active continental margin of Gondwana in the Middle Cambrian. For the other mafic complex, the Husky Ridge Intrusion (Fig. 1), TIEPOLO & TRIBUZIO (2008) report the dominance of quartz diorites and amphibole-rich cumulates with sanukitic affinity (related to melts which originated by equiliration of subduction-derived sediment melts with a refractory mantle). From in-situ U-Pb geochronology on zircon grains, an age of 516 ±3 Ma was extracted, which is within its error limits identical to the age of the Niagara Icefall intrusion.

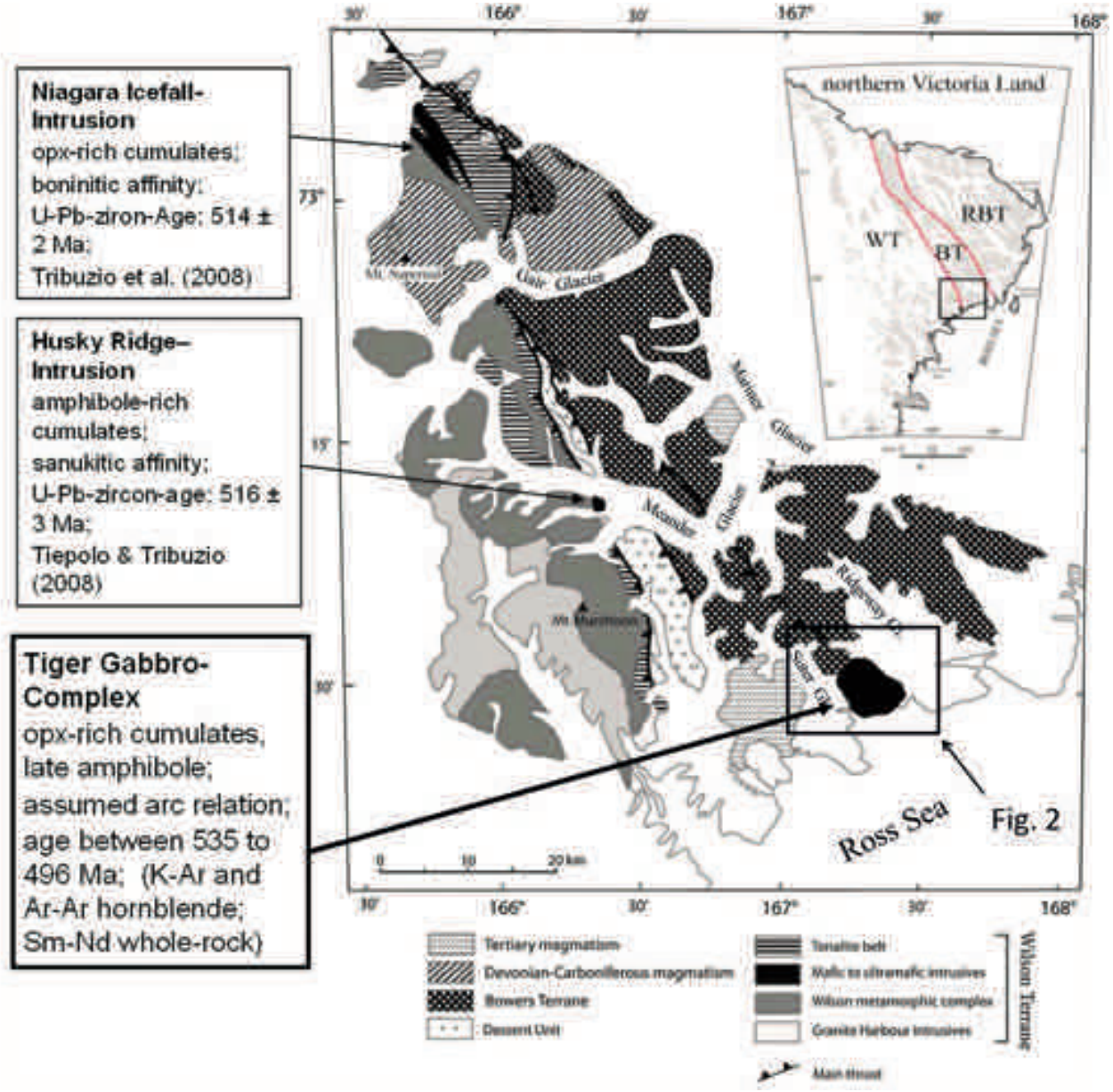

Fig. 1: Mafic to ultramafic igneous complexes with magmatic-arc relation at the suture between the Wilson and Bowers terranes. Map from TRIBUZIO et al. (2008). Inset northern Victoria Land: WT = Wilson Terrane; BT = Bowers Terrane; RBT = Robertson Bay Terrane. Tiger Gabbro Complex is located between the ice tongues of the Suter Glacier and the Ridgeway Glacier at the southeastern end of the Bowers Terrane.

Abb. 1: Mafische bis ultramafische Komplexe mit Inselbogenaffinität entlang der Sutur zwischen dem Wilson und Bowers Terrane. Karte von TRIBUZIO et al. (2008). Inset-Karte northern Victoria Land: WT = Wilson Terrane, BT = Bowers Terrane, RBT = Robertson Bay Terrane. Lage des Tiger Gabbro Complex zwischen den Eiszungen von Suter Glacier und Ridgeway Glacier am Südostende des Bowers Terrane.

OBJECTIVES OF A DETAILED INVESTIGATION OF THE TIGER GABBRO COMPLEX (TGC)

The TGC has the potential (i) to provide key information on hidden crustal processes that occurred during subduction along the eastern margin of Gondwana in the early Palaeozoic, and (ii) to provide general knowledge on details of the magmatic evolution and petrogenesis of island arcs. As mentioned above, published scientific results are rare, highly incomplete and leave open many questions, such as:

(i) What characterizes the lithological and geochemical diversity of the TGC? So far, only geochemical data for 10 whole-rock samples and trace-element data for 5 samples are published.

(ii) What characterizes the mineralogical diversity of the TGC? Earlier studies do not present a systematic description on the mineralogy of the compositional layering.

(iii) What is the formation age of the complex? The available geochronological data do not yield consistent age constraints because of methodical shortcomings. With respect to the Sm-Nd whole-rock age, there is no proof of initial Nd isotope equilibration in the complex based on the analysis of three samples only. Furthermore, the published Ar-Ar age determinations on hornblende yielded age spectra, which do not allow for a straightforward geological interpretation.

(iv) What is the composition of the parent melt(s)? The interpretation of BRACCIALI et al. (2009) is based on the modeling results performed on three samples only.

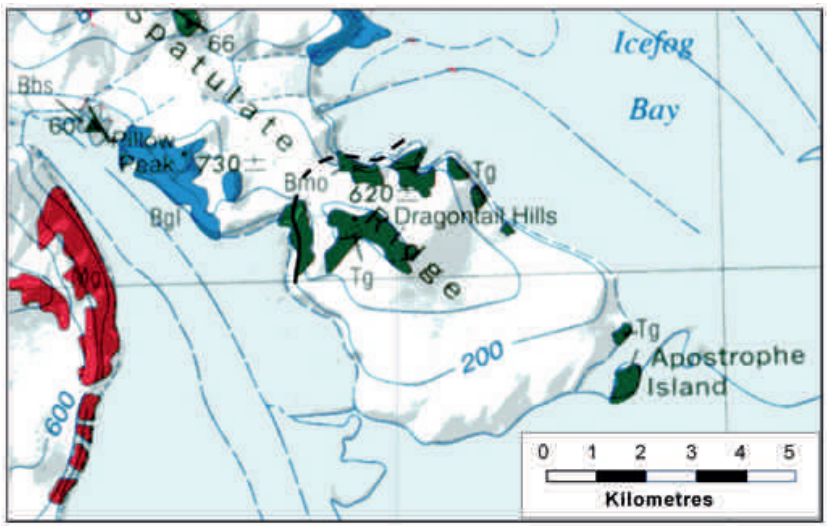

Fig. 2: Geological map of the area under investigation showing the outcrops of the Tiger Gabbro Complex ("Tg") in dark green (modified after CAPPONI et al. 1997). Outcrops of the TGC are known from the area of Dragontail Hills, southeastern end of Spatulate Ridge, and from Apostrophe Island to the southeast. The contact to metasedimentary rocks of the Bowers Terrane ("Bmo" in green) forming the country rocks to the NW is indicated by a black solid line. The contact to the north (dashed black line) is extrapolated from helicopter-based survey. Metavolcanic rocks of the Bowers Terrane ("Bgl") in blue; Cenozoic igneous rocks ("Mg") in red.

Abb. 2: Geologische Karte mit den Aufschlüssen des Tiger Gabbro Complex („Tg") in dunkelgrün (modifiziert nach CAPPONI et al. 1997). Aufschlüsse im TGC sind bekannt aus der Gegend Dragontail Hills, Südosten von Spatulate Ridge und von Apostrophe Island im Südosten des Gebietes. Der direkte Kontakt zu den metasedimentären Nebengesteinen des Bowers Terrane („Bmo" in hellgrün) im nördlichen Teil des TGC ist schwarz eingezeichnet (durchgezogene Linie = besucht; gestrichelt = extrapoliert nach Beobachtungen aus dem Hubschrauber). Metavulkanite des Bowers Terrane („Bgl") in blau; känozoische Magmatite („Mg") in rot.

Therefore, it is our attempt to establish a detailed petrogenesis of the TGC including its magmatic evolution, subsolidus cooling path, and high-temperature shearing history, with the aim to evaluate the geological evolution of deep crustal sequences supposed to have formed the root of an island-arc system. Here, we present the first results of petrographic investigations performed on samples collected during earlier GANOVEX campaigns, the results of the field work in the TGC in the frame of the GANOVEX X campaign and the results of preliminary geochronological investigations (Ar-Ar dating on amphibole). Building on the results of these first steps, we aim to conduct further investigations, which will include detailed (isotope) geochemical and geochronological studies and experimental modeling of the TGC.

RESULTS OF PRELIMINARY PETROGRAPHICAL INVESTIGATIONS

The work on the project was started in late 2009. From the rock repository of the Federal Institute for Geosciences and Natural Resources (BGR), a collection of about 20 samples of the Tiger Gabbro Complex (collected during GANOVEX III in 1982/83) was found suitable for petrographical, geochemical and in part microanalytical investigations.

Typical rocks of the TGC are gabbronorites, gabbros, anorthosites, pyroxenites, hornblende diorites, and hornblendites in order of decreasing abundance. They are characterized petrographically in the following.

• Gabbronorites to gabbros form by far the largest group among the plutonic rocks from the TGC (see below). They are mostly medium grained, granular rocks with subhedral crystal shapes (Figs. 3a, b). Those rocks sampled in the layered series of Dragontail Hills show a strong magmatic foliation, other rocks are isotropic. Beside plagioclase, clino- and orthopyroxene forming the principal phases, olivine, pargasite, and Fe-Ti oxides are present in minor amounts. Some rocks bear relatively high amounts of Fe-Ti oxides (max 5 vol.%) leading to the evolution of ferrogabbronorites. Pargasite always crystallized late, forming interstitial assemblages, often associated with Fe-Ti oxides. In one sample, small seams of orthopyroxene are visible surrounding olivine. Most rocks show signs of deformation, as cataclastic zones cutting the rocks, bands of fluid inclusions in the principal minerals, undulose extinction, and plastic deformation mostly recorded in bent plagioclases.

• Anorthosites are medium grained, isotropic rocks with granular texture and anhedral mineral shapes, bearing more than 95 vol.% plagioclase (Figs. 3c, d); the rest is composed of pargasite, oxide, and clinopyroxene. A record of deformation both in plastic and brittle regimes is present (bent plagioclase lamellae, cataclastic zones, undulose extinction).

• Pyroxenites are medium to coarse grained rocks consisting mainly of clinopyroxene and orthopyroxene (>90 vol.%) with additional pargasite, oxide, plagioclase in amounts <5 vol.% for each phase (Figs. 3e, f). The textures are granular, equigranular to seriate, mostly with subhedral mineral shapes. These rocks show in part a tectonic overprint both in the plastic and brittle regimes leading to mylonitic and cataclastic domains, respectively. Exsolution lamellae of orthopyroxene in clinopyroxene and vice versa are common. Some pyroxenes show shear-related bands of fluid inclusions implying that the shear process was associated with a fluid phase.

• Hornblende diorites are evolved rocks composed mainly of plagioclase and amphibole, associated with additional phases in minor amounts like clino- and orthopyroxene, oxide and quartz (Figs. 3g, h). Their textures are medium grained, granular, isotropic with subhedral crystal shapes. Signs of deformation both in the plastic and in the brittle regime are always visible (bent plagioclase lamellae, cataclastic bands, undulose extinction). While most gabbroic rocks of the TGC are very fresh, the hornblende diorites show a strong alteration (high amounts of chlorite, secondary albite).

• Gabbros s.l. sampled close to the high-temperature shear zones at Apostrophe Island typically show a porphyroclastic texture, expressed by mm- to cm-sized pyroxene and olivine porphyroclasts swimming in fine grained to cryptocrystalline mylonitic or cataclastic matrix (Figs. 3i, j). Neoblasts of the matrix and of domains surrounding the porphyroclasts show a granoblastic network, which includes also pargasite and Fe-Ti oxides (Fig. 3k). The porphyroclasts may bear bands of fluid

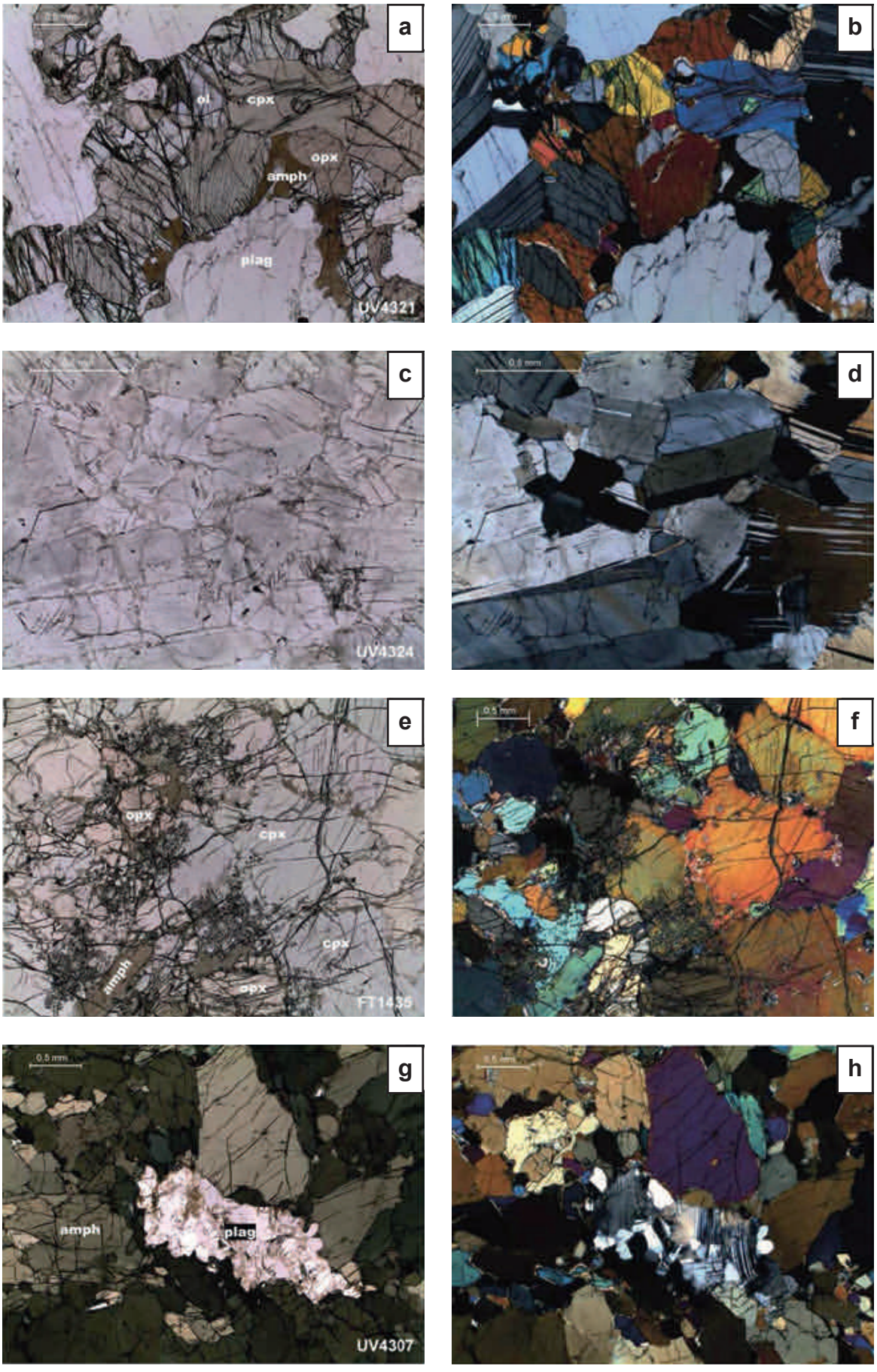

Fig. 3 / Abb. 3 continued ▶

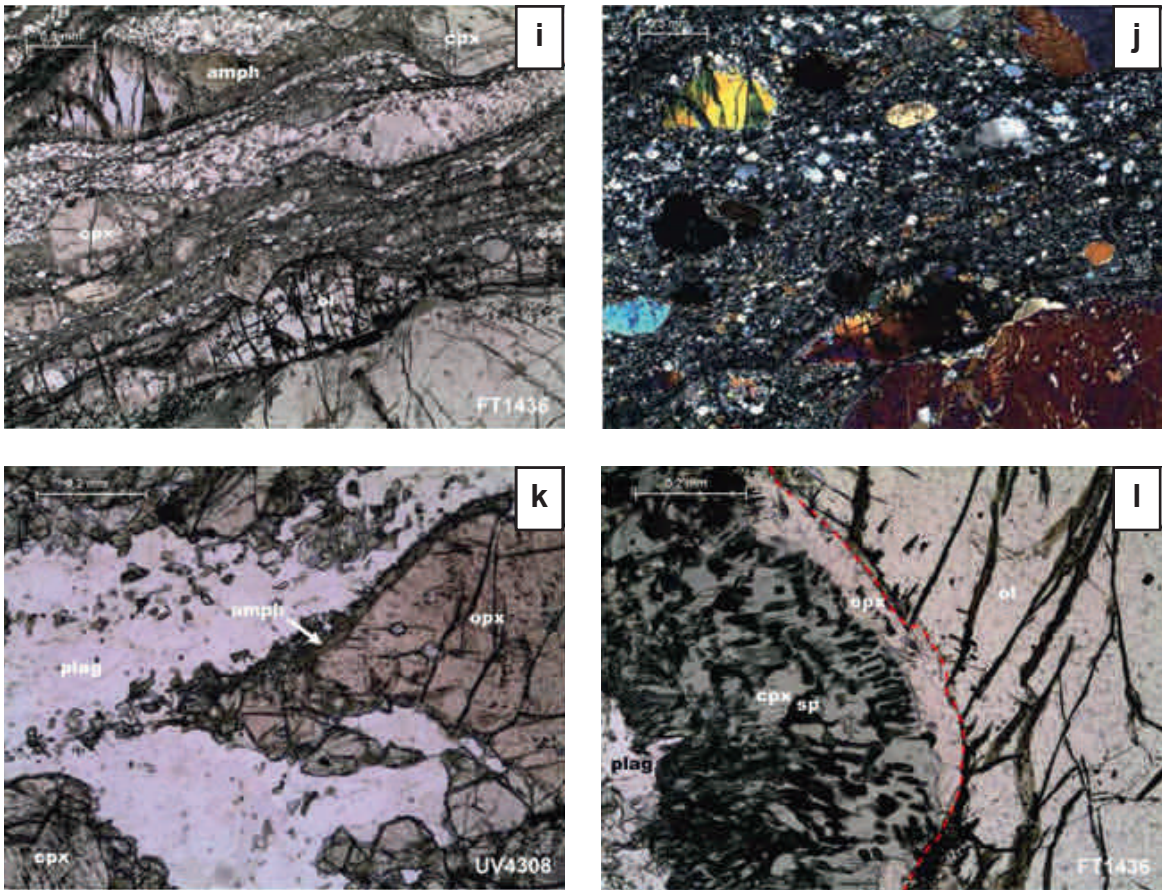

Fig. 3 a-l: Microphotographs of thin sections of samples of the Tiger Gabbro Complex from the BGR sample repository collected by F. Tessensohn and U. Vetter during GANOVEX III in 1982/83. Abbreviations: cpx = clinopyroxene, opx = orthopyroxene, ol = olivine, amph = amphibole, sp = spinel. (a, b) = sample UV4321 (Dragontail Hills): olivine-bearing primitive gabbronorite. Olivine, orthopyroxene, and clinopyroxene form mafic clusters; the textural relations imply the crystallization order ol > plag > opx = cpx > amph. a = plane-polarized light; b = cross-polarized light. (c, d) = sample UV4324 (Dragontail Hills): anorthositic gabbro. Plagioclase shows a pronounced foliation probably due to magmatic "sedimentation" or flow processes in the magma chamber and plastic deformation indicating high-temperature shearing under sub-solidus conditions; c = plane-polarized light; d = cross-polarized light. (e, f) = sample FT1435 (Apostrophe Island): pyroxenite showing characteristic cumulate structure of the more primitive rocks, suggesting co-crystallization of opx and cpx, and late crystallization of amph in the interstices; e = plane-polarized light; f = cross-polarized light. (g, h) = sample UV4307 (Apostrophe Island): the presence of nearly monomineralic hornblendite (>95 % amph) documents accumulation processes of hornblende in a hydrous magma chamber, implying that under certain circumstances (pressure, water activity, bulk composition) amph was on the liquidus; g = plane-polarized light; h = cross-polarized light. (i, j) = sample FT1436 (Apostrophe Island): gabbronorite from a mylonitic to ultramylonitic high-temperature shearzone. The rock shows marked porphyroclastic textures with porphyroclasts of ol, opx, cpx, and amph and a mylonitic to neoblastic matrix; i = plane-polarized light; j = cross-polarized light. (k) = Sample UV4308 (Apostrophe Island): detail of a mylonitic to ultramylonitic gabbronorite. The fine-grained, recrystallized granulitic matrix is composed of opx, cpx, plag, and amph. Amph forms fine granoblastic networks enclosing tiniest opx and cpx, indicating hydrous conditions during the high-T-shearing process; plane-polarized light. (l) = sample FT1436 (Apostrophe Island): symplectitic intergrowths of sp and cpx boarded by a thin seam of opx (boundary towards ol is marked by a dashed line in red) as reaction products between primary magmatic ol and plag, interpreted as the record of sub-solidus processes during cooling; plane-polarized light.

Abb. 3 a-l: Dünnschliff-Fotografien von Proben des Tiger Gabbro Complex aus dem BGR Probenarchiv. Die Probennahme erfolgte durch F. Tessensohn und U. Vetter während GANOVEX III (1982/83). Abkürzungen: cpx = Klinopyroxen, opx = Orthopyroxen, ol = Olivin, amph = Amphibol, sp = Spinell. (a, b) = Probe UV4321 (Dragontail Hills): Olivin-haltiger primitiver Gabbronorit. Olivin, Orthopyroxen und Klinopyroxen bilden mafische Anhäufungen, die von relativ spät auskristallisiertem, oft in Zwischenräumen vorliegendem Amphibol umgeben sind. Die Gefügebeziehungen implizieren eine Kristallisationsabfolge ol > plag > opx = cpx > amph; a = linear-polarisiertes Licht; b = gekreuzt-polarisiertes Licht. (c, d) = Probe UV4324 (Dragontail Hills): Anorthositischer Gabbro. Plagioklas mit deutlicher Foliation vermutlich aufgrund magmatischer "Sedimentation" oder Fließprozessen in der Magmenkammer und plastische, subsolidus Verformung infolge hochtemperierter Scherprozesse; c = linear-polarisiertes Licht; d = gekreuzt-polarisiertes Licht. (e, f) = Probe FT1435 (Apostrophe Island): Pyroxenit mit charakteristischen Kumulatstrukturen der primitiveren Gesteine, welcher gleichzeitige Kristallisation von Ortho- und Klinopyroxen und späte Kristallisation von Amphibol in den Zwischenräumen vermuten lässt; e = linear-polarisiertes Licht; f = gekreuzt-polarisiertes Licht. (g, h) = Probe UV4307 (Apostrophe Island): Das Auftreten von fast monomineralischen Hornblenditen (>95 % Amphibol) dokumentiert Akkumulationsprozesse von Hornblende in einer wasserreichen Magmenkammer und belegt, dass unter besonderen Umständen (Druck, Fluidaktivität, Gesamtzusammensetzung) Amphibol auf dem Liquidus liegt; g = linear-polarisiertes Licht; h = gekreuzt-polarisiertes Licht. (i, j) = Probe FT1436 (Apostrophe Island): Mylonitische bis ultramylonitische Hochtemperatur-Scherzone in einem Gabbronorit. Die Gesteine zeigen oft auffällige porphyroklastische Texturen mit Porphyroklasten aus Olivin, Orthopyroxen, Klinopyroxen und Amphibol und eine mylonitisch bis neoblastische Matrix; i = linear-polarisiertes Licht; j = gekreuzt-polarisiertes Licht. (k) = Probe UV4308 (Apostrophe Island): Detail eines mylonitisch bis ultramylonitischen Gabbronorits. Die feinkörnig rekristallisierte granulitische Matrix besteht aus Orthopyroxen, Klinopyroxen, Plagioklas und Amphibol. Der Amphibol bildet ein feinkörnig-granoblastisches Netzwerk, das sehr feinkörnige Pyroxene einschließt, und damit auf erhöhte Fluidaktivität während des hochtemperierten Scherprozesses hindeutet; linear-polarisiertes Licht. (l) = Probe FT1436 (Apostrophe Island): Symplektitische Verwachsungen von Spinell und Klinopyroxen mit dünnem Saum aus Orthopyroxen zu Olivin (die Grenze zum Olivin ist durch eine rot-gestrichelte Linie gekennzeichnet) als Reaktionsprodukte zwischen primärmagmatischem Olivin und Plagioklas, was als Hinweis auf Subsolidusprozesse während der Abkühlung gedeutet wird; linear-polarisiertes Licht.

inclusions, implying, together with the presence of amphibole in the neoblastic domains, that during the recrystallization processes under deformative conditions, a fluid-rich phase was present. Some porphyroclastic to mylonitic gabbros show characteristic reaction products between primary magmatic olivine and plagioclase consisting of thin orthopyroxene seams next to olivine and symplectitic intergrowths of spinel and clinopyroxene next to plagioclase, interpreted as the record of sub-solidus processes during cooling (Fig. 3l). Identical features were observed in gabbros from the Chilas Complex (Kohistan, NW Pakistan), which is regarded as world site for island-arc gabbros in the deep crust of a juvenile island arc (JAGOUTZ et al. 2007).

Microprobe analyses were performed on the rock-forming silicate minerals and in part oxide phases of selected samples using the Cameca SX 100 electron microprobe at the Institute for Mineralogy, Leibniz University Hannover. Details on the conditions of measurements can be found in Koepke et al. (2011). Data are archived in the database "PANGAEA" (http://doi.pangaea.de/10.1594/PANGAEA.810354) and presented in Table 1. The mineral analyses are presented complementary to the petrographical description of the major rock types but will not discussed in detail here.

Our petrographic characterization indicates that the TGC provides an ideal suite of rocks to achieve the goals of the project. First-order observations on different aspects of the petrogenesis of the TGC are:
(i) The presence of a whole suite of crystallization products from early cumulates (olivine-bearing pyroxenites) to chemically highly evolved rocks (anorthosites s.l.), enabling the possibility to establish the magmatic evolution.
(ii) The crystallization order: in pyroxenitic cumulates plagioclase crystallizes after pyroxene, while in gabbronorites plagioclase crystallizes before.
(iii) The dominance of gabbronoritic lithologies.
(iv) The role of amphibole which may form true cumulate rocks (hornblendites), poikilitic clusters, or interstitial crystals. Some amphiboles are definitely of magmatic origin, others can be interpreted as formed at subsolidus conditions.
(v) The record of significant high-temperature shear processes expressed by spectacular porphyroclastic to mylonitic textures in samples from Apostrophe Island. Samples with porphyroclastic to mylonitic textures are observed in different lithologies of the TGC at Apostrophe Island spatially not related to each other and thus indicate that the high-temperature shear processes are likely not related to a pervasive post-magmatic deformation event.
(vi) A well-developed cooling history. Some gabbros show characteristic symplectitic intergrowths, interpreted as the record of sub-solidus processes during cooling. Exsolution lamellas of orthopyroxene in clinopyroxene and vice versa are also common.

RESULTS OF FIELD WORK DURING GANOVEX X

Fieldwork conducted during GANOVEX X (2009/10) shows that gabbronorites s.l. and leucocratic plagioclase-rich cumulate rocks comprise the majority of the Dragontail Hills (southeastern Spatulate Ridge) whereas ultramafic cumulate rocks with very low plagioclase content are dominant at Apostrophe Island. At both localities, chemically evolved alkali feldspar-bearing igneous rocks, which are known as late differentiates from other well-studied layered intrusions like the Bushveld and Stillwater complexes, are absent. The gabbronorites s.l. at Dragontail Hills show well exposed rhythmic or intermittent layering that dips between 45° and 65° toward the southwest (Fig. 4a). Cross-bedding relationships were found (Fig. 4b). Thickness of the individual layers ranges from centimeter to meter. Compositionally, the layers vary between melanocratic gabbronoritic rocks that are low in plagioclase content and very leucocratic rocks composed almost exclusively of plagioclase (anorthosites s.l., Fig. 4c). Layers may either show graded variations in modal composition or uniform compositions. In addition, there are lenses of ultramafic rocks up to several hundred meters long orientated roughly parallel to the magmatic layering. Their thickness is generally less than hundred meters. Due to stronger weathering of the ultramafic rocks, no in-situ contact to the layered gabbronorites could be identified. However, based on the overall layered character of the whole sequence and the absence of intrusive relationships between the ultramafic rocks and the gabbronorites s.l. at Dragontail Hills, it is assumed that both form part of one major layered igneous sequence ("layered unit") which bears many similarities to banded series of large layered intrusions like the Bushveld, Stillwater or Skaergaard complexes. Especially the rhythmic and/or intermittent layering can only be explained by processes of crystallization, differentiation and layering typical for magma chambers of layered mafic intrusions (e.g. WINTER 2001).

The ultramafic rocks at Apostrophe Island do not show obvious layering. There is, however, clear evidence of interaction between these rocks and gabbronoritic rocks similar to those exposed at Dragontail Hills – but here without the characteristic igneous layering – from magma mixing/mingling relations between the two (Figs. 4d-f). The gabbronoritic rocks show intrusive contacts towards the ultramafic rocks and contain blocky to rounded enclaves and schlieren of ultramafic rocks. The enclaves either have sharp contacts or their margins are partially disintegrated and mixed up with gabbroic material (Fig. 4e). Very similar magma mixing/mingling relations between ultramafic cumulates and gabbroic to more evolved igneous rocks were described from other intrusive complexes in northern Victoria Land (e.g., at Teall Nunatak, southern Wilson Terrane; GIACOMINI et al. 2007). These structures indicate that emplacement of both rock types occurred nearly contemporaneously while they were still in a (partially) molten state. With respect to the dominance of ultramafic lithologies, the TGC at Apostrophe Island corresponds to the basal series of well characterized layered intrusions like the Bushveld or Stillwater complexes.

Localized high-temperature and high-strain shear zones were identified along the northern margin of Apostrophe Island at 73°31'05" S, 167°26'05" E. These shear zones range from narrow (<10 cm) planar low-angle mylonitic to wide (2-4 m) cataclastic shear zones. They are associated with synkinematic injections of plagioclase and phenocrystic hornblende-rich melts (Figs. 5a, b). Larger shear zones have formed by duplexing, with these melts injected along the dominant main deformation zones and from there into associated joint systems within the rock (Fig. 5b). Geometrically, the shear zones strike southeast–northwest (135-150°) and dip shallowly (25-40°)

Fig. 4 a-c: Field photographs of the Tiger Gabbro Complex (TGC). (a) = Tiger Gabbro from Dragontail Hills showing typical rhythmic to intermittent and in part graded layering on a cm scale; see hammer for scale. (b) = Magmatic crossbedding in TGC at Dragontail Hills; hammer for scale. (c) = Layering of very leucocratic rocks at Dragontail Hills. Modal composition varies between plagioclase-rich layers low in contents of mafic minerals (anorthositic gabbro) to nearly monomineralic anorthosite s.l.; hammer for scale. (d) = Ultramafic rocks (pale green) at Apostrophe Island intruded by and reacting with hornblende-plagioclase-rich melts (dark coloured) originating from the high-strain shear zone in the lower left of the photograph; see ice axe for scale. (e) = Relationships between dark coloured ultramafic rocks and lighter coloured gabbronoritic rocks resulting from magma mingling and mixing, see Figure 4 f for details; ice axe for scale. (f) = Schlieren of dark coloured ultramafic material in a lighter coloured gabbronoritic matrix bearing clear evidence of interaction of two magmas with different chemical and physical properties; ice axe for scale.

Abb. 4 a-c: Geländefotografien des Tiger Gabbro Complex (TGC). (a) = Tiger Gabbro von Dragontail Hills mit typischem rhythmischem bis wechsellagerndem und teilweise gradiertem Lagenbau im cm-Bereich; Hammerstiel als Maßstab. (b) = Magmatische Schrägschichtung im TGC bei Dragontail Hills; Hammer als Maßstab. (c) = Lagenbau in sehr leukokraten Gesteinen bei Dragontail Hills. Die modale Zusammensetzung variiert von Plagioklas reichen Lagen mit niedrigem Anteil an mafischen Mineralen (anorthositischer Gabbro) zu fast monomineralischen Anorthositen s.l.; (Hammer als Maßstab). (d) = Ultramafite (blass grün) auf Apostrophe Island, welche von Hornblende-Plagioklas reichen Schmelzen intrudiert und assimiliert werden. Die Hornblende-Plagioklas reichen Schmelzen entstammen der Hochtemperaturscherzone links unten im Bild; (Eispickel als Maßstab). (e) = Beziehungen zwischen dunklen ultramafischen Gesteinen und helleren gabbronoritischen Gesteinen, die aus Vermischungsprozessen des Magmas resultieren, weitere Details siehe Abbildung 4 f; Eispickel als Maßstab. (f) Schlieren aus dunklem ultramafischem Material in einer helleren gabbronoritischen Matrix geben Hinweis auf Interaktionen zweier Magmen mit unterschiedlichen chemischen und physikalischen Eigenschaften; Eispickel als Maßstab.

toward the northeast (Fig. 5c). A consistent lineation defined by elongate hornblende, epidote and chlorite crystals that shallowly plunge (20-40°) to the northeast (50-65°) indicates the direction of transport along the shear planes. Kinematic indicators include crystal-plastic structures with S-C relationships in the high-strain internal parts of the shear zones, dilational 'lock-up' structures and late-stage brittle structures such as Riedel shears. Crystal-plastic deformation of plagioclase and hornblende suggests minimum temperatures of 650-700 °C (e.g., PASSCHIER & TROUW 2005 and references therein). All these fabrics consistently indicate a reverse, top-to-SW directed sense of transport on the shear zones. Localized folding was also identified. Folds are open to closed and asymmetrically verge to the south. Fold hinges shallowly plunge to the northeast (~35° to 75°), with axial surfaces dipping moderately (~50°) to the southeast (~115°). Perpendicular to the shear zones are high-angle semi-brittle tension gashes, which are also filled by the plagioclase-hornblende-rich melts (Fig. 5a). The tension gashes strike southeast–northwest (~150°) and dip steeply (75°) to the southwest. As a result, it can be assumed that the high-temperature shear zones and the tension gashes formed nearly synchronously under localized very high strain. Equilibrium temperatures were calculated for the granulite-facies mylonitic matrix (Figs. 3i, j) of a porphyroclastic gabbro (FT1436) from a high-strain shear zone at Apostrophe Island to c. 800 °C based on the Ti-in-amphibole thermometer (ERNST & LIU 1998) and to c. 855 °C based on the hornblende-plagioclase thermometer (HOLLAND & BLUNDY 1994). A prerequisite for applying the Ti-in-amphibole thermometer is that the amphibole must coexist with a titanian phase. This is given in sample FT1436 where pargasite in the neoblastic matrix forms an equilibrium assemblage together with ilmenite. This geothermometer is regarded as semi-quantitative, but the application to gabbroic rocks was confirmed experimentally by KOEPKE et al. (2003).

Large elongated hornblende crystals within the shear zone shown in Figure 5b were dated by the Ar-Ar method (sample TG 101, Fig. 6). The sample yielded an age spectrum with a well defined high temperature four steps plateau characterized by 96.3 % of the released ^{39}Ar and an age value of 518.6 ±4.6 Ma. The geological significance of this Ar-Ar age is, however, unclear. It is well known that minerals formed in shear zones may contain radiogenic Ar not related to in-situ decay of K ("excess Ar", MCDOUGALL & HARRISON 2000). The excess Ar is related to radiogenic Ar released from sheared country rocks. Since the amount of likely excess Ar in a mineral with plateau-like age spectrum cannot be quantified, the c. 519 Ma age for amphibole TG 101 can only be regarded as a maximum formation age. Two further Ar-Ar analyses were

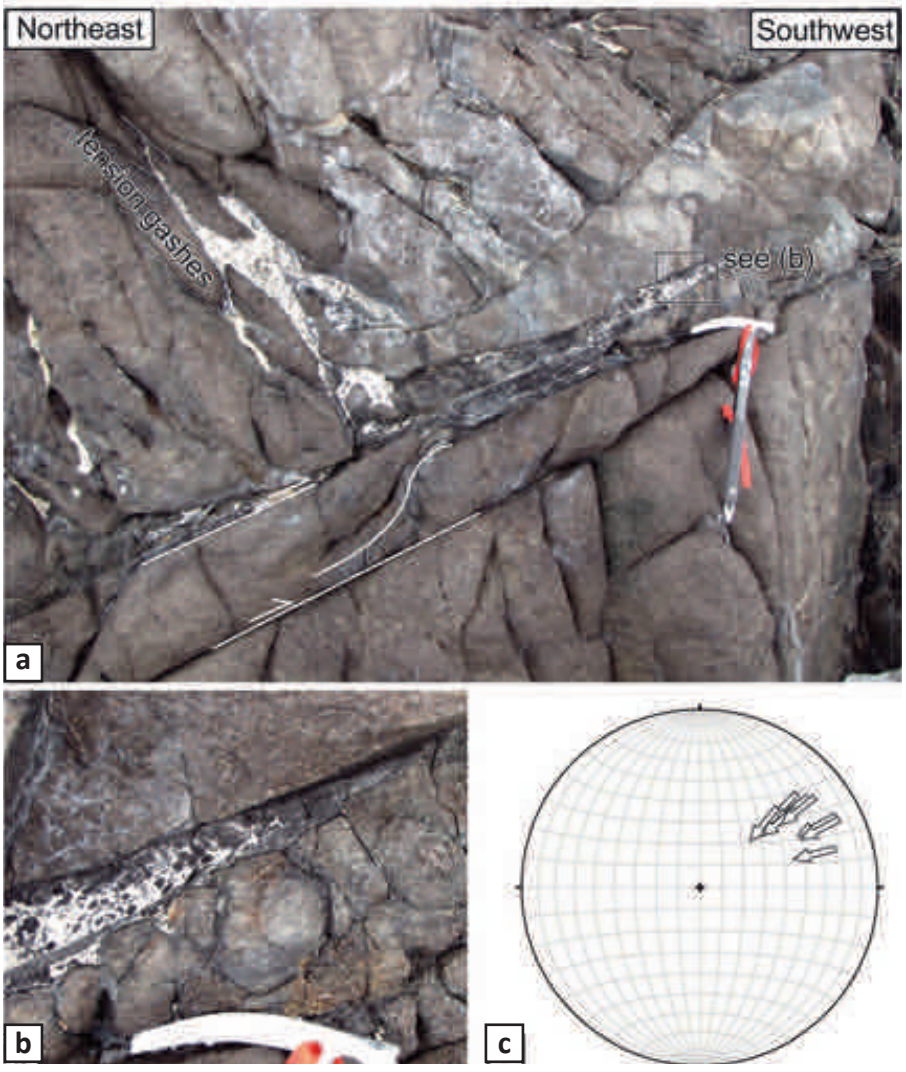

Figs. 5 a-c: Field photographs and structural data of a shear zone in the Tiger Gabbro Complex at Apostrophe Island. (a) = Low-angle reverse high-strain shear zone located at Apostrophe Island. S-C relations (with large hornblende crystals in S-position) confirm a reverse sense of transport. Tension gashes formed at high angles to the main shear zone are filled with plagioclase-hornblende melt injections. (b) = Close up of plagioclase-hornblende melt injected along the main shear plane. (c) = Equal area stereographic projection of hanging-wall transport vectors for high-strain zones identified at Apostrophe Island.

Abb. 5 a-c: Geländefotografien und Strukturdaten einer hochtemperierten Scherzone im Tiger Gabbro Complex bei Apostrophe Island. (a) = Flach einfallende, aufschiebende hochtemperierte Scherzone bei Apostrophe Island. S-C Gefüge (große Hornblende-Kristalle in S-Position) belegen den aufschiebenden Bewegungssinn. Dehnungsklüfte stehen in großem Winkel zur Hauptscherzone und sind gefüllt mit Plagioklas-Hornblende reichen Schmelzinjektionen. (b) = Nahaufnahme einer Plagioklas-Hornblende-reichen Schmelze, welche entlang der Scherzone injiziert ist. (c) = Stereographische Projektionen (untere Halbkugel) der Bewegungsvektoren des hangenden Blocks in den hochtemperierten Scherzonen von Apostrophe Island.

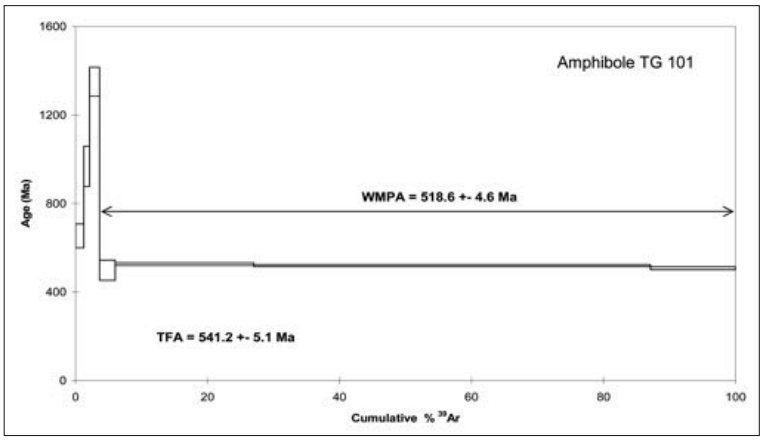

Fig. 6: Ar-Ar age spectrum of large hornblende crystals from the high-temperature shear zone at Apostrophe Island (see Fig. 5b); analyses performed by Actlabs (Canada).

Abb. 6: Ar-Ar Altersspektrum von großen Hornblenden aus der Hochtemperatur-Scherzone von Apostrophe Island (siehe Abb. 5b); Analysen durch Actlabs (Kanada).

performed on amphiboles separated from the TGC (Fig. 7). Sample UV4307 is a plagioclase hornblendite from Apostrophe Island. Hornblende crystals separated from this sample gave an age of 529.7 ±4.3 Ma. However, since the data points defining this age yield no isochron in the inverse isochron plot, this datum should also be interpreted with caution and can give only a rough age trend for the TGC. The second sample UV4335 represents a hornblende diorite from Dragontail Hills. Its amphibole yielded a spectrum with an age of 504.7 ±3.7 Ma.

The contact of the TGC to the country rocks of the Bowers Terrane was examined at a cliff on the northwestern side of Dragontail Hills. Here, gabbronoritic rocks of the layered unit of the TGC were found in contact to strongly contact-metamorphosed metasedimentary rocks of the Bowers Terrane approximately 75 m (GPS values) below the upper edge of the cliff (Fig. 8a). Close to the contact, the gabbronoritic rocks include small lenses of the metasedimentary country rock (Fig. 8b). There is no evidence for deformation neither in the gabbronorite nor in the country rock as would be expected for a tectonic emplacement of the TGC according to Capponi et al. (2003) and Bracciali et al. (2009). The metasedimentary rock exhibits abundant discontinuous and strongly welded quartz mobilisates in a zone, which extends several 10 metres away from the contact. Welding is highly chaotic (Fig. 8c) probably

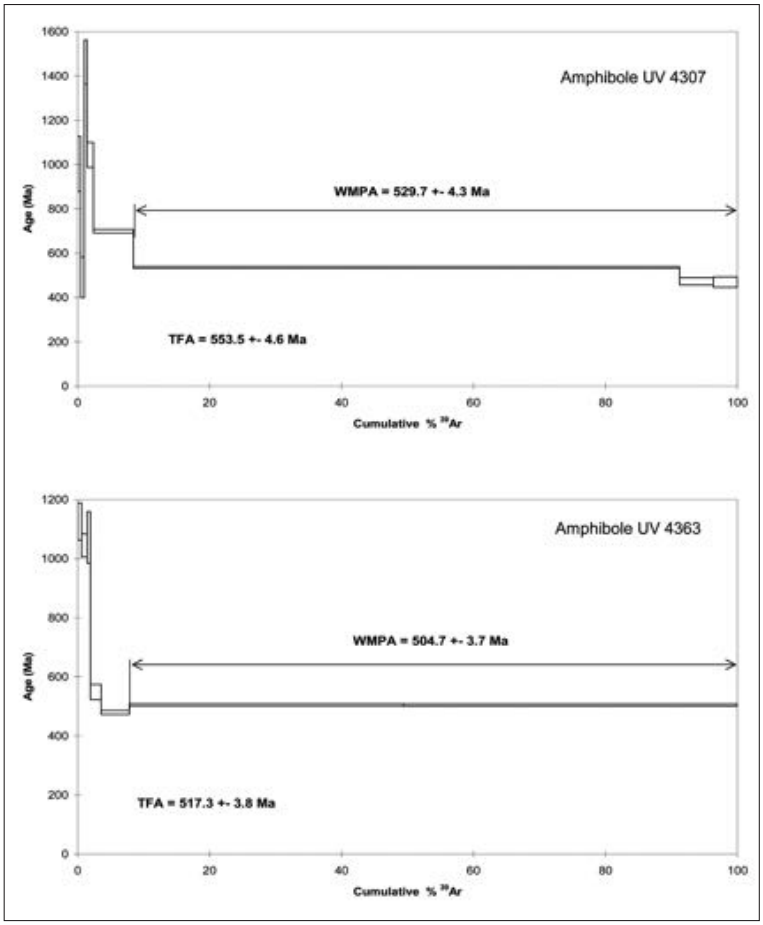

Fig. 7: Ar-Ar age spectra of amphiboles separated from a plagioclase hornblendite (UV 4307, top) from Apostrophe Island and from a hornblende diorite from Dragontail Hills (UV 4363, bottom); analyses by Actlabs (Canada).

Abb. 7: Ar-Ar Altersspektren von Amphibolen aus einem Plagioklas-Hornblendit (UV 4307, oben) von Apostrophe Island und einem Hornblende-Diorit von Dragontail Hills (UV 4363, unten); Analysen durch Actlabs (Kanada).

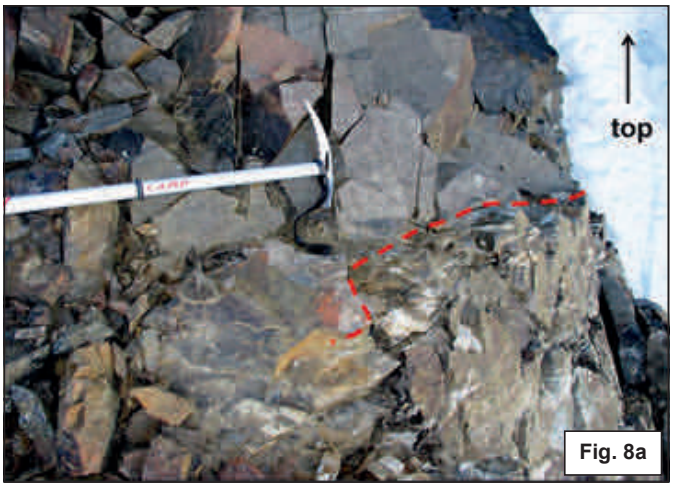

Figs. 8 a-c: Contact relationship between the Tiger Gabbro complex and metasedimentary rocks in a cliff at the northwest side of Dragontail Hills. (a) = Photograph of the contact (top: gabbroic rocks of the Tiger Gabbro Complex; bottom: metasedimentary rocks of the Bowers Terrane; ice axe for scale). The contact is marked by a red dashed line. At the left end of the dashed line, the contact is characterized by a mélange made up to about 90 % by lenses of metasedimentary rocks veined by gabbroic material (about 10 %). (b) = Lenses and schlieren of country rock in an undeformed gabbronorite from the contact of the TGC to metasediments of the Bowers Terrane (hammer for scale). (c) = Discontinuous and strongly welded quartz mobilisates in a metasedimentary rock directly at the contact to the TGC (marker for scale).

Abb. 8 a-c: Kontakt zwischen Tiger Gabbro Complex und Metasedimentgesteinen des Bower Terranes in einem Kliff an der Nordwestseite von Dragontail Hills (Axt als Maß). (a) = Übersichtsaufnahme des Kontakts (oben: gabbroide Gesteine des Tiger Gabbro Complex; unten: Metasedimentgesteinen des Bowers Terrane; Eisaxt als Maßstab). Die rot gestrichelte Linie markiert den Kontakt. Die gestrichelte Linie endet auf der linken Seite in einer Melange, die zu ca. 90 % aus Schlieren des Nebengesteins besteht, das von einem Netzwerk von gabbroidem Material (ca. 10 %) durchsetzt ist. (b) = Linsen und Schlieren von Nebengesteinen in einem undeformierten Gabbronorit am Kontakt des TGC zu Metasedimentgesteinen des Bowers Terrane (Hammer als Maßstab). (c) = Nicht durchgehende und stark verschweißte Quarzmobilisate in einem Metasedimentgestein direkt am Kontakt zum TGC (Marker als Maßstab).

due to plastic flow of the quartz mobilisates induced by very high contact metamorphic conditions. Engel (1987) suggested temperatures close to 800 °C at pressures of 0.2-0.4 GPa in the metasedimentary rocks at the contact. The contact relationships are best explained by a mechanism of forceful intrusion of the still very hot (>>800 °C) TGC into the country rocks at upper crustal levels.

INTERPRETATION AND CONCLUSIONS

Field evidence shows that the TGC is built up by two units: a layered sequence composed of subordinate ultramafic and mainly gabbronoritic to highly evolved anorthositic s.l. cumulate rocks ("layered unit") at Dragontail Hills on the one hand and a massif ultramafic unit showing clear evidence of magma mixing/mingling with gabbroic rocks (similar to the gabbronorite at Dragontail Hills) at Apostrophe Island on the other hand.

Based on our microprobe results, mylonitic gabbroic rocks in the prominent high-temperature shear zones of the TGC at Apostrophe Island record maximum temperature conditions close to the minimum temperature for water-triggered partial melting of gabbroic rocks (c. 870 °C, Beard & Lofgren 1991, Koepke et al. 2004). It is therefore likely that the plagioclase and phenocrystic hornblende-rich melts which synkinematically injected along dominant shear planes were generated by local anatexis during mylonitization. The consistent lineation trend in the shear zones as defined by the elongate hornblende, epidote and chlorite crystals documents that shearing occurred under decreasing temperature conditions. Since later recrystallization processes are not evident and the shear zones show consistent deformational (from mylonitic to

cataclastic) and mineralogical (from high to low-temperature phases) records, we infer that they were formed during the late stage emplacement of the TGC from deeper crustal levels into the Bowers Terrane country rocks at higher-crustal levels and subsequent cooling.

Contact relation between gabbronoritic rocks of the layered unit and country rocks of the TGC at the NW cliff of Dragontail Hills unequivocally demonstrates the intrusive nature of the TGC. Evidence for a tectonic emplacement is missing. Instead, emplacement of the TGC by a mechanism of forceful intrusion at upper crustal levels (ENGEL 1987) seems likely. Bearing in mind that the protoliths of the country rocks, metasedimentary and metavolcanics rocks of the Sledgers Group (Bowers Terrane), have a Middle to Late Cambrian age (summarized in TESSENSOHN & HENJES-KUNST 2005), the age of emplacement of the TGC into the surrounding higher-crustal country rocks must be approximately 490 Ma or younger. This, however, does not exclude that formation of the TGC occurred already earlier in the Cambrian since its cumulate structures are typical for crystallization and accumulation processes occurring in a deeper crustal magma chamber.

We tentatively propose that the TGC records a two-stage evolution during the Ross Orogeny, i.e. an early phase with a maximum age of c. 530 Ma and a late phase with a maximum age of 490 Ma. The first one is related to magmatic processes that were active at deep crustal levels. At that time, the TGC likely crystallized as the lower crustal root zone of the Bowers island arc (BRACCIALI et al. 2009). The latter phase, on the other hand, may be attributed to the late Ross orogenic emplacement of the TGC as a still very hot magmatic complex into the higher-crustal metasedimentary country rocks of the Bowers Terrane under NE–SW directed horizontal maximum stress followed by cooling of the whole complex.

Based on the kinematic data collected from high-temperature shear zones at Apostrophe Island, we suggest that the TGC was deformed by northeast over southwest thrusting. This transport direction is in line with the general NE-SW directed contractional regime reconstructed for the Palaeo-Pacific active continental margin of East Gondwana at that time (e.g., KLEINSCHMIDT & TESSENSOHN 1987). For instance, major thrust zones and cogenetic minor backthrusts in the Wilson Terrane (e.g., Exiles and Wilson thrust system, FLÖTTMANN & KLEINSCHMIDT 1991, LÄUFER et al. 2006, 2011) or at the Bowers Terrane to Robertson Bay Terrane boundary (Millen Thrust Zone, e.g., CRISPINI et al. 2014, PHILLIPS et al. 2014) reveal both southwest and northeast directed reverse tectonic transport and are generally attributed to the late Ross Orogeny.

Further detailed petrological, (isotope) geochemical and geochronological investigations are needed to unravel processes of the magmatic evolution of the TGC. Especially, reliable age data are needed to verify the existing Ar-Ar and Sm-Nd age data and to test the proposed two-stage model. The results so far, however, indicate that the TGC is well suited for evaluating the magmatic and structural evolution of the island-arc type Bowers Terrane at the active continental margin of Palaeo-Victoria Land during the Ross Orogeny and for an in-depth comparison with other examples of exhumed deeper sections of magmatic arc or spreading systems.

ACKNOWLEDGMENT

Franz Tessensohn is sincerely thanked for introducing us into the TGC field relations. Glen Phillips would like to thank the Bundesanstalt für Geowissenschaften und Rohstoffe (BGR) for invitation to GANOVEX X. The fieldwork during the GANOVEX X expedition would not have been possible without the logistic support by the crew of the M/V "Italica" and pilots and mechanics of HELICOPTERS NEW ZEALAND (HNZ). Special thanks are due to the NZ field guide Brian Straite who assisted in the field. This study was supported by the Deutsche Forschungsgemeinschaft (Grant KO 1723/11-1 to J. Koepke) in the framework of the priority program "Antarctic Research with comparative investigations in Arctic ice areas", which is gratefully acknowledged. F. Tessensohn and U. Schüssler are thanked for their careful reviews, which helped to clarify important aspects of the study.

References

Annen, C., Blundy, J.D. & Sparks, R.S.J. (2006): The genesis of intermediate and silicic magmas in deep crustal hot zones.- J. Petrol. 47: 505-539.

Behn, M.D. & Kelemen, P.B. (2006): Stability of arc lower crust: insights from the Talkeetna arc section, south central Alaska, and the seismic structure of modern arcs.- J. Geophys. Res. Solid Earth 111: B11207.

Beard, J.S. & Lofgren, G.E. (1991): Dehydration melting and water-saturated melting of basaltic and andesitic greenstones and amphibolites at 1, 3, and 6.9 kb.- J. Petrol. 32: 365-401.

Bracciali, L., Di Vincenzo, G., Rocchi, S. & Ghezzo, C. (2009): The Tiger Gabbro from northern Victoria Land, Antarctica: the roots of an island arc within the early Palaeozoic margin of Gondwana.- J. Geol. Soc. London 166: 711-724.

Capponi G., Meccheri M. & Oggiano G. (1997): Antarctic Geological 1:250,000 Map series. Coulman Island Quadrangle, (Victoria Land).- Museo Nazionale dell'Antartide, Sezione di Scienze della Terra, Siena, Italy.

Capponi, G., Crispini, L., Di Vincenzo, G., Ghezzo, C., Meccheri, M., Palmeri, R. & Rocchi, S. (2003): Mafic rocks of the Bowers Terrane and along the Wilson-Bowers Terrane boundary: Implications for a geodynamic model of the Ross Orgeny in Northern Victoria Land, Antarctica.- Geophys. Res. Abstr. 5: 05843.

Crispini, L, Federico, L. & Capponi, G. (2014): Structure of the Millen Schist Belt (Antarctica): clues for the tectonics of northern Victoria Land along the paleo-Pacific margin of Gondwana.- Tectonics 33: 420-440, doi:10.1002/2013TC003414.

DeBari, S.M. (1994): Petrogenesis of the Fiabala gabbroic intrusion, northwestern Argentina, a deep-crustal syntectonic pluton in a continental magmatic arc.- J. Petrol. 35: 679-713.

Di Vincenzo, G. & Rocchi, S. (1999): Origin and interaction of mafic and felsic magmas in an evolving late orogenic setting: the Early Paleozoic Terra Nova Intrusive Complex, Antarctica.- Contrib. Mineral. Petrol. 137: 15-35.

Engel, S. (1987): Contact metamorphism by the layered gabbro at Spatulate Ridge and Apostrophe Island (North Victoria Land, Antarctica).- Geol. Jb. B 66: 275-301.

Ernst, W.G. & Liu, J. (1998): Experimental phase-equilibrium study of Al- and Ti-contents of calcic amphibole in MORB – a semiquantitative thermobarometer.- Amer. Mineral. 83: 952-969.

Estrada, S. & Jordan, H. (2003): Early Paleozoic island arc volcanism in the Bowers terrane of northern Victoria Land, Antarctica.- Geol. Jb. B95: 183-207.

Federico, L., Capponi, G. & Crispini, L. (2006): The Ross Orogeny of the transantarctic mountains: a northern Victoria Land perspective.- Int. J. Earth Sci. 95: 759-770.

Flöttmann, T. & Kleinschmidt, G. (1991): Opposite thrust systems in northern Victoria Land, Antarctica: Imprints of Gondwana's Paleozoic accretion.- Geology 19: 45-47.

Ganovex Team (1987): Geological map of North Victoria Land, Antarctica, 1 : 500 000, explanatory notes.- Geol. Jb. B66: 7-79.

Giacomini, F., Tiepolo, M., Dallai, L. & Ghezzo, C. (2007): On the onset and evolution of the Ross Orogeny magmatism in North Victoria Land, Antarctica.- Chem. Geol. 240: 103-128.

Henjes-Kunst, F. & Schüssler, U. (2003): Metasedimentary units of the Cambro-Ordovician Ross Orogen in northern Victoria Land and Oates Land: Implications for their provenance and geotectonic setting from

loc[a]	phase[b]	no.[c]	SiO_2	TiO_2	Al_2O_3	Cr_2O_3	FeO	MnO	MgO	CaO	Na_2O	K_2O	F	Cl	Total	Mg#[d]	An[e]
UV4307 (plagioklase hornblendite)																	
Al	amph	5	44.44	1.09	12.18	n.a.	12.00	0.20	13.80	11.33	1.99	0.18	3.47	0.02	100.69	67.22	
			0.63	*0.10*	*0.60*		*0.37*	*0.02*	*0.59*	*0.22*	*0.16*	*0.03*	*1.62*	*0.01*			
	plag	10	46.43	-	33.88	-	0.14	-	-	17.56	1.62	-	n.a.	n.a.	99.64		85.67
			0.58		*0.55*		*0.06*			*0.60*	*0.29*						
UV4308 (layered gabbro)																	
Al	amph	6	42.72	3.65	12.69	n.a.	11.28	0.12	12.66	11.62	2.64	0.25	-	-	97.64	66.67	
			0.46	*0.18*	*0.19*		*0.24*	*0.02*	*0.23*	*0.15*	*0.10*	*0.02*					
	plag	9	53.07	-	29.56	-	-	-	-	12.34	4.63	0.05	n.a.	n.a.	99.65		59.53
			0.77		*0.34*					*0.59*	*0.26*	*0.03*					
	opx	10	52.76	0.34	2.51	-	18.85	0.39	24.90	0.94	-	-	n.a.	n.a.	100.71	70.19	
			0.49	*0.31*	*0.38*		*0.72*	*0.06*	*0.64*	*0.85*							
	cpx	10	50.72	1.02	4.66	-	7.85	0.18	13.26	21.92	0.69	-	n.a.	n.a.	100.31	75.07	
			0.42	*0.07*	*0.25*		*0.53*	*0.03*	*0.37*	*0.84*	*0.05*						
UV4309 (microgabbronorite)																	
Al	amph	20	41.19	3.50	14.32	n.a.	10.15	0.10	13.35	11.49	2.96	0.78	0.47	-	98.30	70.11	
			0.36	*0.26*	*0.35*		*0.43*	*0.02*	*0.53*	*0.19*	*0.14*	*0.10*	*0.79*				
	plag	21	52.66	-	29.98	-	-	-	-	12.67	4.42	0.13	n.a.	n.a.	99.87		60.80
			0.64		*0.48*					*0.52*	*0.30*	*0.02*					
	opx	14	53.16	0.30	3.16	-	15.94	0.32	26.82	1.09	-	-	n.a.	n.a.	100.78	75.00	
			0.21	*0.06*	*0.32*		*0.36*	*0.04*	*0.32*	*0.50*							
	cpx	13	50.29	1.10	5.06	-	6.91	0.18	14.34	21.50	0.75	-	n.a.	n.a.	100.12	78.73	
			0.34	*0.12*	*0.20*		*0.35*	*0.05*	*0.38*	*0.53*	*0.09*						
	ol	15	38.02	-	-	-	26.05	0.34	36.59	-	-	-	n.a.	n.a.	101.00	71.47	
			0.21				*0.36*	*0.05*	*0.46*								
UV4314 (layered gabbro)																	
Al	amph	15	43.47	2.34	12.38	n.a.	10.30	0.10	14.43	11.86	2.28	0.24	-	0.03	97.43	71.41	
			0.30	*0.04*	*0.25*		*0.47*	*0.02*	*0.25*	*0.17*	*0.06*	*0.02*		*0.00*			
	plag	8	47.91	-	33.19	-	-	-	-	16.52	2.31	-	n.a.	n.a.	99.93		79.84
			0.07		*0.05*					*0.08*	*0.05*						
	opx	15	53.24	0.17	2.70	-	16.97	0.33	26.52	0.67	-	-	n.a.	n.a.	100.60	73.59	
			0.25	*0.04*	*0.62*		*0.75*	*0.04*	*0.73*	*0.19*							
	cpx	8	51.81	0.47	3.30	-	7.08	0.18	14.66	22.43	0.47	-	n.a.	n.a.	100.38	78.68	
			0.07	*0.04*	*0.05*		*0.15*	*0.08*	*0.06*	*0.08*	*0.05*						
UV4316 (hornblende pyroxenite)																	
Al	amph	10	43.40	2.18	12.20	n.a.	9.72	0.08	14.54	12.14	2.59	0.08	-	-	96.93	72.74	
			0.67	*0.21*	*0.43*		*0.41*	*0.02*	*0.49*	*0.18*	*0.10*	*0.03*					
	opx	17	53.74	0.17	2.80	-	14.86	0.27	27.47	0.92	-	-	n.a.	n.a.	100.23	76.73	
			0.45	*0.03*	*0.37*		*0.61*	*0.04*	*0.68*	*0.80*							
	cpx	13	50.33	0.72	4.95	0.18	6.48	-	13.82	22.65	0.54	-	n.a.	n.a.	99.66	79.16	
			0.31	*0.07*	*0.36*	*0.05*	*0.21*		*0.18*	*0.30*	*0.09*						
UV4393 (ferrogabbronorite)																	
Al	amph	8	42.81	3.11	12.37	n.a.	10.48	0.11	13.51	11.64	2.47	0.33	-	0.04	96.86	69.68	
			0.57	*0.27*	*0.51*		*0.28*	*0.03*	*0.36*	*0.20*	*0.10*	*0.06*		*0.01*			
	plag	9	49.01	-	31.89	-	0.18	-	-	15.35	2.90	0.03	n.a.	n.a.	99.36		74.43
			0.77		*0.48*		*0.05*			*0.63*	*0.34*	*0.00*					
	opx	27	53.03	0.21	3.24	-	16.26	0.30	25.32	0.78	-	-	n.a.	n.a.	99.15	73.52	
			0.33	*0.05*	*0.35*		*0.55*	*0.04*	*0.55*	*0.46*							
	cpx	12	50.07	0.78	4.70	0.16	6.66	0.17	13.44	22.57	0.58	-	n.a.	n.a.	99.13	78.24	
			0.89	*0.26*	*0.69*	*0.05*	*0.35*	*0.05*	*0.36*	*0.40*	*0.06*						
FT1435 (amphibole-bearing pyroxenite)																	
Al	amph	9	43.89	2.03	13.31	n.a.	7.32	-	15.78	11.91	2.48	0.23	-	0.03	96.98	79.36	
			0.73	*0.19*	*0.45*		*0.25*		*0.33*	*0.15*	*0.13*	*0.11*		*0.00*			
	opx	10	54.26	0.14	2.78	-	12.22	0.24	29.79	0.62	-	-	n.a.	n.a.	100.05	81.29	
			0.62	*0.03*	*0.25*		*0.29*	*0.06*	*0.24*	*0.20*							
	cpx	8	51.39	0.50	4.14	0.18	5.03	-	14.97	22.44	0.58	-	n.a.	n.a.	99.23	84.13	
			0.22	*0.06*	*0.32*	*0.03*	*0.20*		*0.31*	*0.46*	*0.06*						
FT1436 (porphyroclastic layered gabbro)																	
Al	amph	5	42.99	1.71	13.58	n.a.	8.37	0.09	14.83	12.22	3.04	0.12	-	0.02	96.96	75.96	
			0.45	*0.16*	*0.20*		*0.36*	*0.02*	*0.42*	*0.24*	*0.05*	*0.01*		*0.00*			
	plag	13	47.88	-	32.81	-	0.16	-	-	16.59	2.35	-	n.a.	n.a.	99.79		79.58
			1.05		*0.59*		*0.19*			*0.75*	*0.49*						
	cpx	6	51.19	0.57	4.47	0.24	5.78	0.14	13.44	22.97	0.59	-	n.a.	n.a.	99.39	80.57	
			0.67	*0.13*	*0.96*	*0.07*	*0.25*	*0.04*	*0.29*	*0.94*	*0.24*						
	ol	20	38.80	-	-	-	21.52	0.27	37.93	-	-	-	n.a.	n.a.	98.52	75.86	
			0.26				*0.34*	*0.04*	*0.72*								
	ilm	1	-	52.86	-	-	43.57	1.15	2.13	-	-	-	n.a.	n.a.	99.72	8.03	

Table 1 continued ▶

loc[a]	phase[b]	no.[c]	SiO_2	TiO_2	Al_2O_3	Cr_2O_3	FeO	MnO	MgO	CaO	Na_2O	K_2O	F	Cl	Total	Mg#[d]	An[e]
UV4341 (ferrogabbronorite)																	
DH	amph	10	41.87	2.21	10.60	n.a.	18.08	0.17	9.89	11.03	1.70	1.60	-	0.57	97.73	49.38	
			0.46	*0.14*	*0.31*		*0.35*	*0.02*	*0.38*	*0.17*	*0.07*	*0.09*		*0.05*			
	plag	10	56.23	-	27.40	-	0.16	-	-	9.76	6.72	0.59	n.a.	n.a.	100.84		43.15
			0.62		*0.39*		*0.03*			*0.36*	*0.30*	*0.03*					
	opx	20	50.71	0.16	1.25	-	28.12	0.55	18.67	0.77	-	-	n.a.	n.a.	100.23	54.21	
			0.41	*0.04*	*0.12*		*0.36*	*0.06*	*0.34*	*0.11*							
	cpx	6	51.55	0.40	2.42	-	12.44	0.28	11.77	21.08	0.50	-	n.a.	n.a.	100.44	62.79	
			0.58	*0.10*	*0.33*		*0.70*	*0.05*	*0.32*	*0.52*	*0.05*						
	ilm	9	-	49.88	-	-	49.13	0.60	0.23	-	-	-	n.a.	n.a.	99.84	0.84	
				0.80			*0.64*	*0.05*	*0.04*								
UV4321 (olivine gabbronorite)																	
DH	amph	9	40.76	3.50	14.27	n.a.	10.55	0.11	13.18	11.39	3.24	0.82	-	0.02	97.87	69.01	
			0.36	*0.08*	*0.32*		*0.18*	*0.03*	*0.29*	*0.15*	*0.08*	*0.05*		*0.00*			
	plag	9	50.22	-	31.49	-	0.18	-	-	14.43	3.94	0.12	n.a.	n.a.	100.38		66.50
			0.28		*0.16*		*0.06*			*0.16*	*0.12*	*0.01*					
	opx	10	53.10	0.46	2.74	0.12	15.98	0.32	26.05	1.37	-	-	n.a.	n.a.	100.15	74.40	
			0.31	*0.23*	*0.14*	*0.04*	*0.30*	*0.04*	*0.32*	*0.41*							
	cpx	8	49.79	1.08	4.78	0.19	7.89	0.20	14.04	20.59	0.74	-	n.a.	n.a.	99.30	76.04	
			0.26	*0.05*	*0.24*	*0.03*	*0.78*	*0.04*	*0.65*	*1.21*	*0.04*						
	ol	7	37.66	-	-	-	26.33	0.36	35.76	-	-	-	n.a.	n.a.	100.11	70.77	
			0.13				*0.39*	*0.03*	*0.28*								
UV4324 (anorthosite)																	
DH	amph	10	42.59	1.68	13.10	n.a.	11.38	0.25	13.79	11.44	1.51	0.80	0.26	0.16	96.98	68.35	
			0.42	*0.20*	*0.32*		*0.86*	*0.02*	*0.38*	*0.20*	*0.12*	*0.04*	*0.02*	*0.00*			
	plag	11	51.13	-	30.22	-	0.29	-	-	13.66	3.80	0.15	n.a.	n.a.	99.25		65.97
			0.74		*0.51*		*0.04*			*0.66*	*0.37*	*0.03*					
	mt	6	-	-	-	0.20	92.83	-	-	-	-	-	n.a.	n.a.	93.04		
						0.03	*0.29*										
UV4327 (gabbronorite)																	
DH	amph	10	42.50	2.87	12.63	n.a.	11.39	0.13	13.31	11.61	1.85	0.45	-	0.04	96.79	67.58	
			0.50	*0.18*	*0.26*		*0.13*	*0.03*	*0.36*	*0.18*	*0.17*	*0.02*		*0.00*			
	plag	10	48.20	-	32.66	-	0.23	-	-	15.79	3.00	0.06	n.a.	n.a.	99.93		74.19
			0.22		*0.08*		*0.08*			*0.13*	*0.08*	*0.01*					
	opx	20	52.97	0.22	2.65	-	17.27	0.36	25.99	0.99	-	-	n.a.	n.a.	100.44	72.85	
			0.20	*0.03*	*0.12*		*0.44*	*0.06*	*0.38*	*0.63*							
	cpx	10	51.17	0.72	3.62	-	7.33	0.18	13.90	22.58	0.43	-	n.a.	n.a.	99.93	77.17	
			0.40	*0.09*	*0.51*		*0.12*	*0.06*	*0.27*	*0.48*	*0.06*						
UV4333 (layered gabbronorite)																	
DH	amph	10	43.27	2.87	12.03	n.a.	10.37	0.08	14.66	11.48	2.34	0.46	-	0.01	97.58	71.61	
			0.38	*0.13*	*0.30*		*0.53*	*0.02*	*0.23*	*0.14*	*0.10*	*0.02*		*0.00*			
	plag	10	48.56	-	32.04	-	0.26	-	-	15.60	3.22	0.06	n.a.	n.a.	99.74		72.57
			0.24		*0.19*		*0.04*			*0.16*	*0.08*	*0.01*					
	opx	10	53.65	0.25	2.69	-	15.48	0.29	26.15	0.87	-	-	n.a.	n.a.	99.37	75.07	
			0.13	*0.02*	*0.13*		*0.15*	*0.05*	*0.28*	*0.32*							
	cpx	16	50.32	0.89	4.47	-	6.95	0.17	14.25	21.95	0.61	-	n.a.	n.a.	99.60	78.52	
			0.29	*0.06*	*0.19*		*0.60*	*0.05*	*0.57*	*0.97*	*0.08*						
UV4335 (gabbronorite)																	
DH	amph	16	40.85	3.50	13.55	n.a.	11.65	0.13	13.06	11.32	3.27	0.38	-	0.02	97.73	66.66	
			0.27	*0.51*	*0.20*		*0.27*	*0.02*	*0.40*	*0.26*	*0.11*	*0.02*		*0.00*			
	plag	21	48.66	-	32.46	-	0.22	-	-	15.72	3.15	0.05	n.a.	n.a.	100.26		73.18
			0.66		*0.46*		*0.05*			*0.59*	*0.36*	*0.01*					
	opx	21	52.30	0.40	3.29	-	17.01	0.34	25.42	1.43	-	-	n.a.	n.a.	100.19	72.70	
			0.33	*0.24*	*0.29*		*0.38*	*0.05*	*0.42*	*0.57*							
	cpx	16	49.70	0.95	4.67	-	8.12	0.22	13.99	21.20	0.69	-	n.a.	n.a.	99.54	75.45	
			0.85	*0.10*	*0.38*		*0.53*	*0.04*	*0.65*	*0.81*	*0.04*						
	ilm	8	0.35	49.00	-	0.19	46.09	3.81	0.07	0.31	-	-	n.a.	n.a.	99.84	0.28	
			1.00	*0.54*		*0.05*	*0.95*	*0.26*	*0.03*	*0.78*							
UV4342 (ferrogabbronorite)																	
DH	amph	8	42.58	1.72	12.12	n.a.	13.95	0.11	12.16	11.76	1.17	1.59	0.01	0.29	97.48	60.85	
			0.31	*0.03*	*0.15*		*0.18*	*0.02*	*0.25*	*0.13*	*0.10*	*0.04*	*0.00*	*0.01*			
	plag	10	56.67	-	26.79	-	0.26	-	-	9.39	6.86	0.58	n.a.	n.a.	100.55		41.71
			0.46		*0.36*		*0.07*			*0.42*	*0.23*	*0.02*					
	opx	9	51.39	0.18	1.52	-	25.95	0.52	19.41	1.01	-	-	n.a.	n.a.	99.99	57.15	
			0.31	*0.03*	*0.15*		*0.72*	*0.08*	*0.31*	*0.82*							
	cpx	9	51.02	0.34	2.37	-	11.30	0.25	12.47	21.39	0.52	-	n.a.	n.a.	99.67	66.31	
			0.21	*0.04*	*0.11*		*0.44*	*0.04*	*0.19*	*0.28*	*0.02*						
	ilm	8	-	49.88	-	-	49.81	0.79	0.08	-	-	-	n.a.	n.a.	100.56	0.28	
				0.52			*0.43*	*0.08*	*0.03*								

Table 1 continued ▶

loc[a]	phase[b]	no.[c]	SiO_2	TiO_2	Al_2O_3	Cr_2O_3	FeO	MnO	MgO	CaO	Na_2O	K_2O	F	Cl	Total	Mg#[d]	An[e]
UV4343 (gabbronorite)																	
DH	amph	10	43.78	1.20	9.76	n.a.	15.94	0.16	11.91	11.46	1.62	1.26	0.54	0.36	98.00	57.13	
			0.50	*0.28*	*0.66*		*0.65*	*0.02*	*0.59*	*0.14*	*0.59*	*0.11*	*0.77*	*0.06*			
	plag	10	57.36	-	26.91	-	0.20	-	-	9.19	6.27	0.49	n.a.	n.a.	100.42		43.52
			0.29		*0.13*		*0.05*			*0.15*	*0.17*	*0.09*					
	opx	10	51.64	0.55	1.64	-	25.12	0.51	19.65	1.33	-	-	n.a.	n.a.	100.43	58.24	
			0.74	*0.86*	*0.12*		*0.79*	*0.07*	*0.34*	*0.51*							
	cpx	10	51.26	0.40	2.32	-	11.63	0.31	12.55	20.88	0.52	-	n.a.	n.a.	99.86	65.80	
			0.39	*0.08*	*0.29*		*0.62*	*0.06*	*0.36*	*0.70*	*0.07*						
	ilm	4	-	45.63	-	-	52.65	0.67	-	-	-	-	n.a.	n.a.	98.96		
				0.50			*0.31*	*0.04*									
UV4355 (gabbronorite)																	
DH	amph	10	42.15	3.50	12.56	n.a.	13.85	0.17	11.86	11.15	1.89	0.47	-	0.04	97.65	60.43	
			0.37	*0.66*	*0.37*		*0.16*	*0.03*	*0.11*	*0.15*	*0.08*	*0.04*		*0.01*			
	plag	10	53.04	-	29.69	-	-	-	-	12.71	4.50	0.10	n.a.	n.a.	100.04		60.60
			0.39		*0.18*					*0.27*	*0.14*	*0.01*					
	opx	9	52.11	0.18	2.24	-	21.32	0.42	22.21	1.30	-	-	n.a.	n.a.	99.79	65.00	
			0.50	*0.03*	*0.15*		*0.57*	*0.03*	*0.76*	*0.79*							
	ilm	5	0.08	49.98	0.06	-	47.43	2.57	0.08	-	-	-	n.a.	n.a.	100.19	0.30	
			0.13	*0.53*	*0.07*		*0.64*	*0.07*	*0.11*								
UV4362 (hornblende diorite)																	
DH	plag	4	66.64	-	21.26	-	-	-	-	2.07	11.00	-	n.a.	n.a.	100.98		9.43
			0.37		*0.69*					*0.35*	*0.12*						
UV4363 (hornblende diorite)																	
DH	amph	8	41.12	3.83	12.35	n.a.	15.11	0.24	11.37	10.62	2.55	0.41	0.25	0.04	97.87	57.29	
			0.32	*0.21*	*0.14*		*0.32*	*0.03*	*0.22*	*0.05*	*0.05*	*0.01*	*0.01*	*0.01*			
	plag	6	52.01	-	30.13	-	0.16	-	-	13.19	4.18	0.07	n.a.	n.a.	99.73		63.57
			0.61		*0.49*		*0.05*			*0.53*	*0.29*	*0.03*					
	opx	6	52.23	0.29	2.53	-	20.21	0.47	23.03	1.12	-	-	n.a.	n.a.	99.88	67.01	
			0.26	*0.08*	*0.23*		*0.68*	*0.07*	*0.50*	*0.62*							
	cpx	5	50.35	0.91	3.86	-	9.07	0.24	13.62	21.86	0.50	-	n.a.	n.a.	100.42	72.80	
			0.53	*0.07*	*0.28*		*0.92*	*0.06*	*0.71*	*0.08*	*0.04*						
	ilm	7	-	49.93	-	-	50.16	1.52	-	-	-	-	n.a.	n.a.	101.61		
				0.52			*0.40*	*0.08*									
	mt	6	-	0.09	0.19	-	93.12	-	-	-	-	-	n.a.	n.a.	93.41		
				0.09	*0.14*		*0.75*										
FT1476 (ferrogabbronorite)																	
DH	amph	16	43.12	1.74	10.57	n.a.	16.97	0.15	10.27	11.34	1.17	1.54	-	0.29	97.16	51.89	
			0.70	*0.37*	*0.45*		*0.26*	*0.03*	*0.18*	*0.19*	*0.27*	*0.10*		*0.11*			
	bio	21	37.76	4.13	14.87	n.a.	12.16	-	15.44	-	0.08	9.60	-	0.12	94.16	69.36	
			0.44	*0.25*	*0.34*		*1.18*		*0.64*		*0.04*	*0.26*		*0.01*			
	plag	17	57.66	-	26.26	-	0.19	-	-	8.84	6.20	0.69	n.a.	n.a.	99.83		42.35
			0.44		*0.22*		*0.04*			*0.24*	*0.19*	*0.08*					
	opx	20	51.19	0.13	1.17	-	28.02	0.55	17.08	1.12	-	-	n.a.	n.a.	99.28	52.07	
			0.21	*0.04*	*0.12*		*0.89*	*0.06*	*0.32*	*0.88*							
	cpx	14	51.21	0.38	2.37	-	12.13	0.29	11.23	21.21	0.50	-	n.a.	n.a.	99.32	62.26	
			0.38	*0.06*	*0.36*		*0.77*	*0.04*	*0.28*	*0.86*	*0.06*						
	ilm	12	-	48.25	-	-	50.41	0.48	0.23	-	-	-	n.a.	n.a.	99.36	0.80	
				0.85			*0.87*	*0.07*	*0.19*								

Tab. 1: Compositions of minerals from gabbroic rocks of the Tiger Gabbro Complex.
loc[a] = locality: AI = Apostrophe Island; DH = Dragontail Hills; **phase**[b]: amph = amphibole; cpx = clinopyroxene; ilm = ilmenite; mt = magnetite; ol = olivine; opx = orthopyroxene; pl = plagioclase; bi = biotite; **no.**[c] = number of analyses; **Mg#**[d] = MgO/(MgO + FeO^{tot})•100, molar; **An**[e] = An content of the plagioclase (mol %); **-** = below limit of detection; **n.a.** = not analyzed; **FeO** = FeO^{tot}; **italics** = one standard deviation

Tab. 1: Mineralzusammensetzung von gabbroiden Gesteinen des Tiger Gabbro Complex.
loc[a] = Probenlokalität: AI = Apostrophe Island, DH = Dragontail Hills (Spetulate Ridge); **phase**[b]: amph = Amphibol, cpx = Klinopyroxen, ilm = Ilmenit, mt = Magnetit, ol = Olivin, opx = Orthopyroxen, pl = Plagioklas, bi = Biotit; **no.**[c] = Anzahl der Analysen; **Mg#**[d] = molares MgO/(MgO + FeO^{tot})•100; **An**[e] = An-Gehalt von Plagioklas (in mol %); **-** = unterhalb der Nachweisgrenze; **n.a.** = nicht analysiert; **FeO** = FeO^{tot}; **kursiv** = einfache Standardabweichung.

geochemical and Nd-Sr isotope data.- Terra Antartica 10(3): 105-128.

Henjes-Kunst, F. (2003): Single-crystal Ar-Ar laser dating of detrital micas from metasedimentary rocks of the Ross orogenic belt at the Pacific margin of the Transantarctic Mountains, Antarctica.- In: D.K. FÜTTERER (ed), Antarctic Contributions to Global Earth Sciences. - 9th Int. Symp. Ant. Earth Sci., Terra Nostra 2003/4: 150-151.

Holland, T.J.B. & Blundy, J. (1994): Non-ideal Interactions in calcic amphiboles and their bearing on amphibole plagioclase thermometry.- Contrib. Mineral. Petrol. 116: 433-447.

Jagoutz, O., Muntener, O., Ulmer, P., Pettke, T., Burg, J.P., Dawood, H. & Hussain, S. (2007): Petrology and mineral chemistry of lower crustal intrusions: the Chilas Complex, Kohistan (NW Pakistan).- J. Petrol. 48: 1895-1953.

Kleinschmidt, G. & Tessensohn, F. (1987): Early Paleozoic westward directed subduction at the Pacific margin of Antarctica.- In: G. MCKENZIE (ed): Gondwana Six: Structure, Tectonics and Geophysics, Amer. Geophys. Union AGU, Washington D.C., Geophys. Monogr. 40: 89-105.

Kreuzer, H., Höhndorf, A., Lenz, H., Müller, P. & Vetter, U. (1987): Radiometric ages of pre-Mesozoic rocks from northern Victoria Land, Antarctica. In: G. MCKENZIE (ed): Gondwana Six: Structure, Tectonics, and Geophysics, Amer. Geophys. Union AGU, Washington D.C., Geophys. Monogr. 40: 31-47.

Koepke, J., Berndt, J. & Bussy, F. (2003): An experimental study on the shallow-level migmatization of ferrogabbros from the Fuerteventura Basal Complex, Canary Islands.- Lithos 69: 105-125.

Koepke, J., Feig, S.T., Snow, J. & Freise, M. (2004): Petrogenesis of oceanic plagiogranites by partial melting of gabbros: An experimental study.- Contrib. Mineral. Petrol. 146: 414-432.

Koepke, J., France, L., Müller, T., Faure, F., Goetze, N., Dziony, W. & Ildefonse, B. (2011): Gabbros from IODP Site 1256 (Equatorial Pacific): Insight into axial magma chamber processes at fast-spreading ocean ridges.- Geochem. Geophys. Geosyst. 12: doi:10.1029/2011GC003655.

Läufer, A.L., Kleinschmidt, G. & Rossetti, F. (2006): Late-Ross structures in the Wilson Terrane in the Rennick Glacier area (northern Victoria Land, Antarctica).- In: D.K. FÜTTERER, D. DAMASKE, G. KLEINSCHMIDT, H. MILLER & F. TESSENSOHN (eds), Antarctica: Contributions to Global Earth Sciences, Springer-Verlag, Berlin Heidelberg New York: 195-204.

Läufer, A.L., Lisker, F. & Phillips, G. (2011): Late Ross-orogenic deformation of basement rocks in the northern Deep Freeze Range, Victoria Land, Antarctica: the Lichen Hills Shear Zone.- Polarforschung 80(2): 60-70.

McDougall, I. & Harrison, T.M. (2000): Geochronology and thermochronology by the $^{40}Ar/^{39}Ar$ method.- Oxford Univ. Press, New York, 2nd Edition, 1-269.

Passchier, C.W. & Trouw, R.A.J. (2005): Microtectonics.- Springer-Verlag, Berlin Heidelberg New York, 2nd Edition: 1-366.

Phillips, G., Läufer, A. & Piepjohn, K. (2014): Geology of the Millen Thrust System, northern Victoria Land, Antarctica.- Polarforschung 84: 39–47 (this volume)

Ricci, C.A. & Tessensohn, F. (2003): The Lanterman–Mariner suture: Antarctic evidence for active margin tectonics in Paleozoic Gondwana.- Geol. Jb. B85: 303-332.

Rocchi, S., Di Vincenzo, G., Tonarini, S. & Ghezzo, C. (1999): The Tiger Gabbro of northern Victoria Land: Age, affinity and tectonic implications.- 8th Internat. Sympos. Antarctic Earth Sci. ISAES, Progr. & Abstracts, Wellington, NZ Abstract Volume: 270.

Rocchi, S., Capponi, G., Crispini, L., Di Vincenzo, G., Ghezzo, C., Meccheri, M. & Palmeri, R. (2003): Mafic rocks at the Wilson-Bowers Terrane transition and within the Bowers Terrane: Implications for a geodynamic model of the Ross Orogeny.- Terra Antartica Rep. 9: 145-148.

Tessensohn, F. & Henjes-Kunst, F. (2005): Northern Victoria Land Terranes, Antarctica: far travelled or local products?- In: A.P.M. VAUGHAN, P.T. LEAT & R.J. PANKHURST (eds), Terrane Processes at the Margins of Gondwana, Geol. Soc. London, Spec. Publ. 246: 275-291.

Tiepolo, M. & Tribuzio, R. (2008): Petrology and U-Pb zircon geochronology of amphibole-rich cumulates with sanukitic affinity from Husky Ridge (northern Victoria Land, Antarctica): Insights into the role of amphibole in the petrogenesis of subduction-related magmas.- J. Petrol. 49: 937-970.

Tribuzio, R., Tiepolo, M. & Fiameni, S. (2008): A mafic-ultramafic cumulate sequence derived from boninite-type melts (Niagara Icefalls, northern Victoria Land, Antarctica).- Contrib. Mineral. Petrol. 155: 619-633.

Weaver, S.D., Bradshaw, J.D. & Laird, M.G. (1984): Geochemistry of Cambrian volcanics of the Bowers Supergroup and implications for the Early Palaeozoic tectonic evolution of northern Victoria Land, Antarctica.- Earth Planet. Sci. Lett. 68: 128-140.

Winter, J.D. (2001): An introduction to igneous and metamorphic petrology.- Prentice Hall, 1-697.

Polarforschung 84 (1), 39–47, 2014

Geology of the Millen Thrust System, Northern Victoria Land, Antarctica

by Glen Phillips[1,2], Andreas Läufer[3] and Karsten Piepjohn[3]

Abstract: Rocks of the Millen Schists were analysed during GANOVEX X (2009/10) to evaluate the nature of the contact between the Ross-age Bowers and Robertson Bay Terranes in northern Victoria Land. The majority of this work was carried out in proximity to the Millen Thrust System, a major structure that separates the whole Millen Shear Belt into two overlying tectonic units. The Millen Shear Belt has been widely acknowledged to represent the tectonic contact between the two terranes. Lithological similarities between the rocks in the hanging wall and footwall of the Millen Thrust System and those located in the Bowers and Robertson Bay Terranes support this suggestion. The structural history of the Millen Schists can be divided into three stages: (i) formation of isoclinal folds and pervasive S1 foliation that largely parallels bedding S0; (ii) upright D2 folding along northwest-southeast axes and (iii) localised D3 high-strain that was dominantly related to reverse transport along the Millen Thrust System. Interpretations based on field observations and the available geochronological data supports a model where: (i) sub-horizontal northeast-southwest directed pure shear shortened the juxtaposed (by the late Cambrian) Bowers and Robertson Bay terranes; (ii) strain localisation along the Millen Thrust System resulted in the development of a complex finite strain pattern in the Millen Schists, which records evidence of dominant northeast directed reverse transport with minor lateral displacement.

Zusammenfassung: Während der BGR-Expedition GANOVEX X (2009/10) wurden Gesteine der Millen Schists untersucht, um die Kontaktzone zwischen den ross-orogenetischen Bowers und Robertson Bay Terranes Nord-Victoria-Lands besser charakterisieren zu können. Die Untersuchungen wurden hauptsächlich in unmittelbarer Nähe des Millen-Überschiebungssystems durchgeführt, ein bedeutendes Strukturelement, das den gesamten Millen Shear Belt in zwei übereinanderliegende tektonische Einheiten teilt. Der Millen Shear Belt wird als der tektonische Kontakt zwischen beiden Terranes angesehen. Ähnliche Lithologien im hangenden und im liegenden Block des Millen-Überschiebungssystems, nämlich im Bowers- und Robertson Bay Terran, stützen diese These. Die strukturelle Entwicklung der Millen Schists kann in drei Stadien unterteilt werden: (1) Bildung isoklinaler Falten D1 und eine überwiegend schichtungsparallele penetrative S1-Foliation. (2) aufrechte Faltung D2 parallel NW-SE streichender B2-Faltenachsen. (3) lokale intensive Verformung D3 hauptsächlich im Zusammenhang mit aufschiebenden Bewegungen entlang des Millen-Überschiebungssystems. Die Interpretation der Geländebeobachtungen und existierender geochronologischer Daten stützen ein Modell, in dem (1) eine subhorizontale NE-SW gerichtete reine Scherung eine tektonische Verkürzung der (ab dem späten Kambrium) direkt aneinander grenzenden Bowers und Robertson Bay Terranes bewirkte und (2) die Konzentration intensiver Verformung entlang des Millen-Überschiebungssystems zur Bildung eines komplexen finiten Verformungsmusters in den Millen Schists führte, das einen nach NE überschiebenden tektonischen Transport mit untergeordneten Lateralbewegungen belegt.

INTRODUCTION

One of the main aims of GANOVEX X (German Antarctic North Victoria Land Expedition 2009/10) was to examine the kinematic history of the major tectonic contacts that define the architecture of northern Victoria Land. Representing part of the 18000 km long Terra-Australis Orogen (CAWOOD 2005), northern Victoria Land was largely assembled during the Ross Orogeny, which developed out of response to subduction along the margin of Gondwana. The geological record of northern Victoria Land therefore holds vital clues into the evolution of the Ross Orogeny and the nature of subduction and accretion along the Antarctic segment of the Terra-Australis Orogen.

Two conflicting geodynamic models are presented in the literature to explain the geological architecture of northern Victoria Land. The first model interprets the three main tectonic units, namely the Wilson, Bowers and Robertson Bay Terranes (Fig. 1; 'Terrane' is used to be consistent with the literature; see ROLAND et al. 2004 for discussion) as 'far travelled', with collision resulting in their accretion from the down-going plate onto the overriding Gondwana margin (BRADSHAW et al. 1985). The second model requires a supra-subduction setting for the Gondwana margin, where the development and assembly of the terranes took place on the overriding plate and in close proximity to the continental plate (ROLAND et al. 2004,

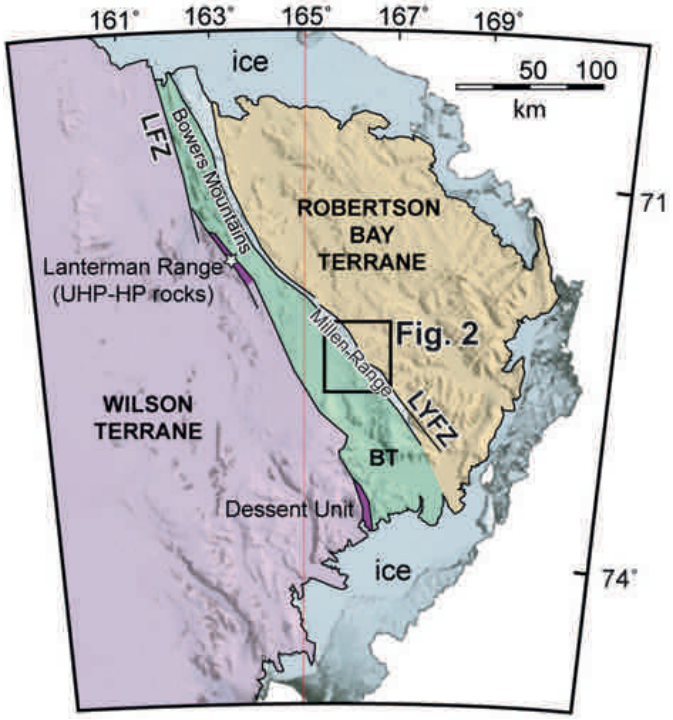

Fig. 1: Geological map of northern Victoria Land showing the distribution of the main terranes and tectonic boundaries. Abbreviations: BT = Bowers Terrane; LFZ = Lanterman Fault Zone; LYFZ = Leap Year Fault Zone.

Abb. 1: Geologische Karte von Nord-Victoria-Land mit der Lage der drei Terranes und ihrer tektonischen Grenzen.

[1] Discipline of Earth Sciences, The University of Newcastle, Callaghan, Australia.
[2] Geological Survey of New South Wales, Maitland, Australia.
[3] Bundesanstalt für Geowissenschaften und Rohstoffe, Hannover, Germany.

Manuscript received 29 May 2014; accepted in revised form 13 August 2014.

ROCCHI et al. 2011). These models demand contrasting settings for major tectonic contacts that separate the Wilson, Bowers and Robertson Bay terranes. For the 'far travelled' model, the terrane boundaries would be sutures, marking the site(s) of collision and accretion. For the supra-subduction model, the terrane boundaries represent internal fault zones that facilitated the translation of terranes along the continental foreland. To test these two models, the tectonic contact between the Robertson Bay and Bowers Terranes (defined by the Millen Schists) was analysed during GANOVEX X. Here we present the preliminary results of fieldwork, kinematic analysis and subsequent interpretations of these new data. These results are incorporated with existing studies of the Millen Schists and its western boundary, the Leap Year Fault Zone, to present a comprehensive kinematic history of the tectonic contact between the Bowers and Robertson Bay Terranes.

GEOLOGICAL SETTING

The general architecture of the Ross Orogen in northern Victoria Land comprises the inboard Wilson Terrane, the Bowers Terrane and the outboard Robertson Bay Terrane (Fig. 1). As detailed descriptions of these terranes have been published (GANOVEX TEAM 1987, ROLAND et al. 2004, TESSENSOHN & HENJES-KUNST 2005, ROCCHI et al. 2011), only brief descriptions of each terrane will be presented here. Separating these terranes are (i) the Lanterman Fault Zone between the Wilson and Bowers Terranes and (ii) the Millen Shear Belt, a high-strain structural unit between the Bowers and Robertson Bay Terranes). The Leap Year Fault Zone and the Handler (previously Lillie) Fault are generally regarded to represent the two boundary faults of the Millen Shear Belt in the west and in the east, respectively (e.g., CRISPINI et al. 2014). The Millen Thrust System represents the main structural element of the Millen Shear Belt, separating the Millen Schists into an upper and lower tectonic unit (e.g., CAPPONI et al. 2003). As the Millen Thrust System provides the central theme of this paper, a detailed description of this structure, along with the associated rocks of the Millen Schist is presented.

The Wilson Terrane is made up of variably metamorphosed (greenschist to granulite facies) rocks that are intruded by plutonic and volcanic rocks of the Granite Harbour suite (GREW et al. 1984). Isotopic data points to a Cambrian to Early Ordovician age (520-480 Ma) for the timing of magmatism, high-grade metamorphism and deformation (BORG et al. 1987, HENJES-KUNST et al. 2004, SCHÜSSLER et al. 2004). The Lanterman Fault Zone defines the eastern margin of the Wilson Terrane and its contact with the Bowers Terrane (Fig. 1). Significantly, it contains blocks of ultrahigh to high-pressure metamorphic rocks (located in the Lanterman Range and Dessent Unit; Fig. 1) and evidence of a complex, high strain structural evolution (ROLAND et al. 1984, GIBSON 1984). In contrast to the largely siliciclastic nature of the Wilson Terrane, the Bowers Terrane ranges from basal units of mafic volcanics, carbonates, greywakes and mudstones, followed by shallow marine limestone, mudstones and sandstone, which are capped by coarse grained conglomerate, quartzite and mudstones of continental character (LAIRD et al. 1982). In comparison to the relatively higher levels of strain identified along the western boundary of the Bowers Terrane (Black Spider Greenschist), a single generation of upright variably plunging, northwest-southeast trending folds characterises the interior of the terrane (Fig. 2b; GIBSON et al. 1984). To the east of the Bowers Terrane, the Robertson Bay Terrane comprises a monotonous package of turbidites and subordinate fossiliferous limestones (Fig. 2a-b; WRIGHT et al. 1984). Similar to the Bowers Terrane, the deformation style of the Robertson Bay Terrane is relatively homogeneous and comprises a single generation of upright folds (KLEINSCHMIDT & SKINNER 1981).

Originally acknowledged to represent the main tectonic contact between the Bowers and Robertson Bay Terranes, the northwest-southeast trending Leap Year Fault Zone records a complex tectonic history (BRADSHAW et al. 1985). Evidence of contractional, extensional and strike-slip transport along the fault zone supports this complex dynamic evolution (WRIGHT 1982, JORDAN et al. 1984). The Millen Schists are exposed east of this fault zone and provide evidence of a more complex kinematic deformation history compared to the interiors of the Bowers and Robertson Bay Terranes (TESSENSOHN 1984, CAPPONI et al. 2003). FINDLAY (1986) regarded the Millen Schists as the basal mylonitic reverse shear zone marking the contact between the overlying Robertson Bay

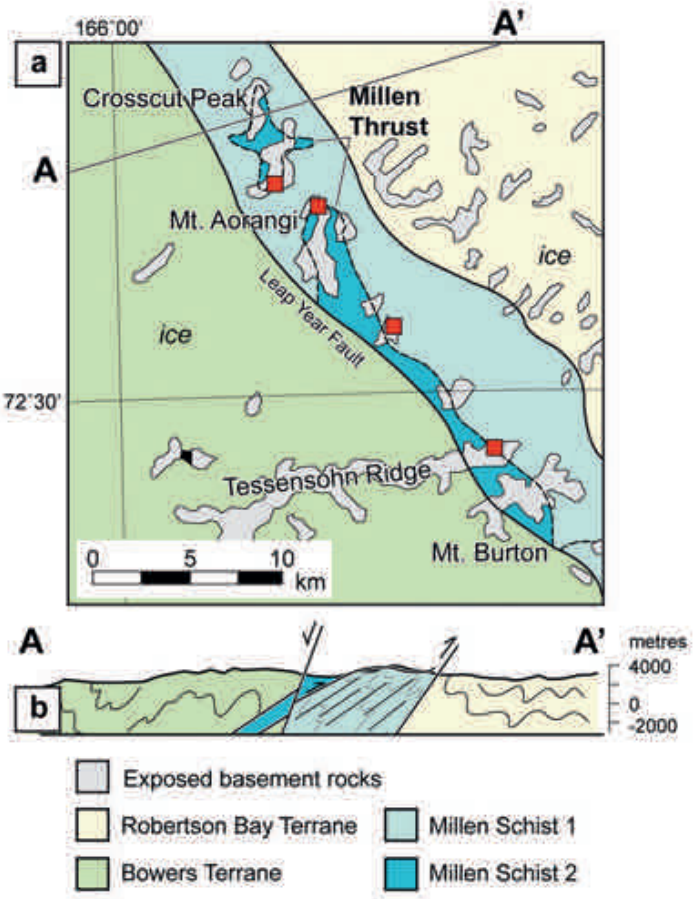

Fig. 2: (a) = Geological map of the Millen Range. Visited localities (red filled squares) and locations of the Millen Thrust (dashed line) are shown. (b) = Schematic cross section through the Bowers and Robertson Bay Terranes (Revised from MECCHERI et al. 2004). Note the location of cross section A-A' is shown on the geological map.

Abb. 2: (a) = Geologische Karte der Millen Range mit den besuchten Lokationen (rote Quadrate) und der Lage der Millen-Überschiebung (gestrichelte Linie). (b) = Schematisches Profil durch das Bowers- und Robertson-Bay-Terrane (verändert nach MECCHERI et al. 2004). Die Lage des Profils A-A' ist in der geologischen Karte (a) markiert.

Terrane metasedimentary sequences and the underlying metasedimentary and metavolcanic rocks of the Bowers Terrane. This led Bradshaw (1987) to use the term Millen Shear Zone to describe the Bowers-Robertson Bay terrane boundary because rocks of both terranes are tectonically mixed within a broad zone rather than a single linear fault and that the actual terrane boundary is therefore located within the whole shear belt (cf. Roland et al. 2004).

Based on previous work carried out in the Millen Range, two main rock units have been suggested to make up the Millen Schists (Capponi et al. 2003). Of these two units, there is a lower package that comprises metaphyllites, metagreywakes and metalimestones (shown as Millen Schist 1 in Figure 2a-b) and an upper package of volcanoclastic sandstones (shown as Millen Schist 2 in Figure 2a-b). Whereas the contact between these two units, termed the Millen Thrust (Capponi et al. 2003; Fig. 2a) or Crosscut-Aorangi Thrust (Crispini et al. 2014), consistently records a reverse sense of transport, the direction of transport remains disputed (either NE over SW (Findlay 1986) or NW over SE (Bradshaw 1985, Wright, 1985).

The Millen Schists record two well-developed foliations (S1 and S2; Capponi et al. 2003). S1 is parallel to bedding and forms in an axial planar orientation to rare isoclinal folds (Capponi et al. 2003). S2 is a steeply dipping, northwest-southeast striking crenulation cleavage that is oriented parallel to the axial plane of asymmetric northwest-southeast trending F2 open folds (Capponi et al., 2003). The timing relations proposed by these authors are that transport along the Millen Thrust was coeval with the formation of the S1 fabric. Sparse K-Ar and Ar/Ar data from these rocks constrain the timing of deformation along the Millen Thrust to the late Cambrian (c. 505–500 Ma; Wright & Dallmeyer 1991).

FIELD OBSERVATIONS FROM THE MILLEN RANGE

Four locations in the Millen Range were visited during GANOVEX X. These locations were selected to assess the nature of deformation along the Millen Thrust System and to identify rock types in the direct hanging wall and footwall of the contact. From SE to NW, the visited localities were (Fig. 2): (i) the eastern most point of Tessensohn Ridge (73°32'16.6'' S / 166°39'42.3'' E); (ii) an unnamed ridge (72°23'22.5''S / 166° 22'16.9'' E); (iii) the northern ridge of Mount Aorangi (72°23' 24.1'' S / 166°22'29.1'' E) and (iv) the southern ridge of Crosscut Peak (72°21'51.7''S / 166°18'54.1'' S). Owing to clear similarities in the structural histories identified at locations (i), (ii) and (iv), these kinematic data are compiled in Figure 4. The exposure of the Millen Thrust System at location (iii) results in a more complex structural history and, as a result, data are presented separately (Fig. 5).

At the easternmost point of Tessensohn Ridge, a fine transposed fabric comprising bedding (S0) and an S1 foliation is crenulated around a northwest-southeast striking, sub-vertically dipping crenulation cleavage (S2; Fig. 3a, 4b). The transposed nature of the S0 and S1 fabrics is supported by petrography, where an alignment of fine-grain white mica is observed parallel to bedding. Quartz fibres on S0/S1 surfaces have an average plunge of 40-60° towards ~240° and record evidence of flexural slip along bedding surfaces. The dominant S2 cleavage is also warped around rare F3 axes that strike northwest-southeast and dip sub-vertically, which could be interpreted to be related to strike-slip displacements in the Millen Schists.

At the unnamed ridge, deformed siltstones record evidence of open to closed metre- to cm-scale folds (Fig. 3b). Bedding is again paralleled by a fine-grained slatey S1 cleavage, which together are folded into a number of upright, asymmetric F2 folds that plunge 5-20° toward the southeast and verge to the northeast (Figs. 3b, 4a, 4c). The S0/S1 fabric dominantly strikes northwest-southeast and dips variably (10-70°) to the northeast and southwest (Fig. 4a). At this locality, we also observed minor evidence that the Millen Schists were affected by two phases of late- and/or post-Ross lateral shearing indicated by two sets of quartz veins: (i) an older phase with NW-SE trending dextral off-sets of thin NNE-SSW striking veins, and (ii) a younger NW-SE trending sinistral reactivation with thick veins oriented in an en-echelon-type geometry that suggests left-lateral shear along a NNW-SSE striking principle deformation zone.

At the northern ridge of Mount Aorangi, the Millen Thrust is clearly exposed (Fig. 5a; Wright & Findlay 1984). A detailed inspection of the rocks distal and proximal to the contact was undertaken to assess the nature of deformation along the fault zone. Distal to the contact, rocks are partly recrystallised

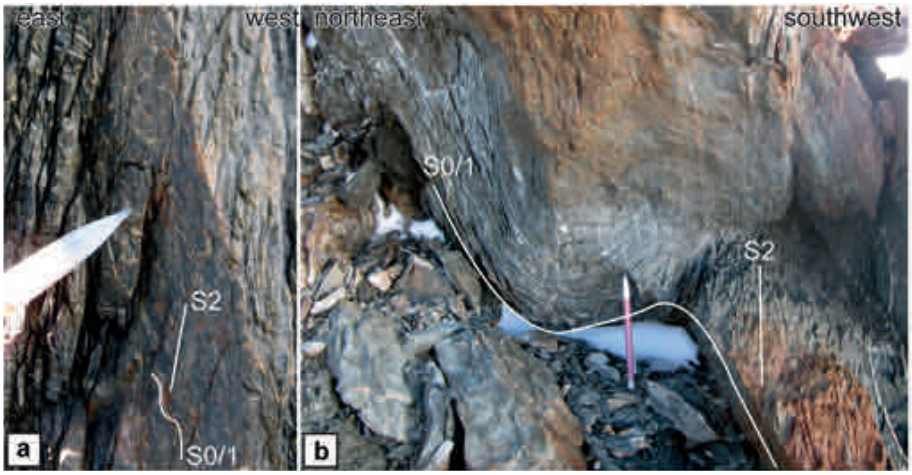

Fig. 3: Field photographs of the Millen Schists distal to the Millen Thrust. (a) = S2 crenulation cleavage identified at the eastern part of Tessensohn Ridge. (b) = Open folded S0/S1 and associated upright S2 identified at an unnamed ridge in the Millen Range.

Abb. 3: Geländefotos der Millen Schists in einiger Entfernung zur Millen-Überschiebung. (a) = S2 Krenulationsschieferung im Ostteil von Tessensohn Ridge. (b) = Offen verfaltetes S0/S1 und damit assoziierte aufrechte S2-Schieferung auf einem namenlosen Rücken in der Millen Range.

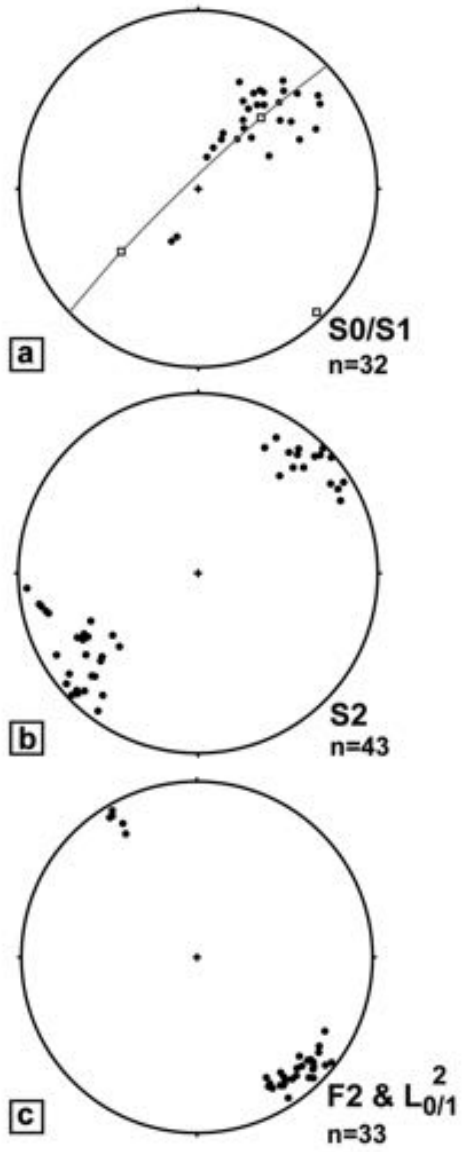

Fig. 4: Kinematic data collected from field locations away from the Millen Thrust zone (i.e., eastern Tessensohn Ridge, unnamed ridge and Crosscut Peak. (a) = S0/S1 data (as poles) and calculated best-fit girdle showing the profile plane of F2 folds. (b) = Orientations of S2 (as poles). (c) = Orientations of F2 folds and L0/12 intersection lineations.

Abb. 4: Kinematische Geländedaten von Lokationen in einiger Entfernung von der Millen-Überschiebung (östlicher Tessensohn Ridge, einem namenlosen Rücken und Crosscut Peak). (a) = S0/S1 Daten (als Polpunkte) und daraus gerechneter Großkreis der F2-Faltenprofilebene. (b) = Orientierungen der S2-Flächen (als Polpunkte). (c) = Orientierungen von F2-Falten und L0/12-Schnittlinearen.

poorly sorted matrix supported sandstones that are dominated by angular clasts of quartz and minor plagioclase. Regions of higher D2 strain contain dynamically recrystallised metasiltstones comprising a strong S2 foliation. This foliation is axial planar to cm-scale F2 folds that are defined by a composite S0/S1 fabric (Fig. 6a). F2 folds plunge 5-20° to the northwest (Fig. 5c; 6a). Evenly spaced (~30 cm) bedding parallel shear zones are also ubiquitous and show a reverse sense of transport on southeast-northwest striking, steeply dipping (60-75 °C to southwest and northeast) planes (Figs. 5b-c, 6b). These zones could represent syn-D2 flexural slip along bedding surfaces, or, a later D3 structural event. Closer to the Millen Thrust contact, the S2 fabric is shortened into cm- to m-scale open F3 folds that wrap around axial planes striking 140-160 °C and dipping 60-80° to the east (Fig. 5d). Due to the identification of these F3 folds, we suggest that the bedding parallel shearing described above was the response of a D3 event (as shown in Fig. 5b).

The Millen Thrust is folded and dominantly parallels the S0/S1 fabric (Fig. 6c). In the hanging wall of the contact, green schists are exposed atop of poorly sorted siliciclastic rocks in the footwall. Local offsets of the Millen Thrust along the sub-vertical S2 fabric are also common. In the direct fault zone, S-C fabrics show a reverse sense of movement (Fig. 6d). Below the fault zone, F3 folds are tight to isoclinal, plunge moderately (~30°) to the southeast (~160°) are folded around axial planes that parallel the thrust. Even though the Millen Thrust is folded by F2 structures, S-C fabrics consistently record a reverse sense of transport (Fig. 5e). As a result, reverse transport along the contact must have taken place after F2 folding; otherwise opposite shear sense indicators would be recorded on the opposing limbs of the folded thrust. Rocks in the hanging wall show a simple kinematic history with upright F2 folds defined by S0/1 and the development of an upright S2 foliation (Fig. 6e). S2 in these rocks strikes to the southeast-northwest and dips steeply (~80°) to the northeast, whereas the F2 folds shallowly plunge (~20°) toward the southeast (140-150°).

At Crosscut Peak, a dominant slatey cleavage strikes northwest-southeast and dips steeply (> 65°) to sub-vertically. Rare examples of folded bedding, sub-parallel quartz veins and a parallel micaceous cleavage (S1; identified microscopically) indicates that this main foliation is S2. Bedding and S1 strike to the northwest-southeast and have a moderate to shallow dip (25-55°) toward the southwest (Fig. 4a). F2 folds and intersection lineations plunge between 3 to 20° to the southeast (Fig. 4c). A second orientation of slatey cleavage showing a varying intensity across the outcrop forms at an acute angle to the S2 fabric (~330/55 W). Microscopic analysis does not reveal clear overprinting relationships between the two fabrics, which instead, show an anastomosing relationship. As a result, the two fabrics probably formed during the same event, and reflect subtle change in stress field orientation. At higher structural levels, the Millen Thrust is again exposed along the northern face of Crosscut Peak (Fig. 7). Viewed during helicopter reconnaissance, a contact between a lower package of open folded rocks and an upper package of apparently massive rocks was identified (Fig. 7). Interestingly, the fault at this location cuts across bedding on the western limb, yet is parallel to bedding on the eastern limb of the fold.

DISCUSSION

The provenance and kinematic evolution of the Millen Schists has direct implications for geodynamic models of the Ross Orogeny. With respect to the competing geodynamic models of the Ross Orogeny, the Millen Schists should represent one of either: (i) an exotic terrane that was accreted to the Bowers Terrane (Tessensohn & Henjes-Kunst 2005) or (ii) an internal transport surface between the Bowers and Robertson Bay Terranes (Capponi et al. 2003). The provenance of the Millen Schists provides a test for these models, as the exotic model requires a contrasting provenance to the neighbouring

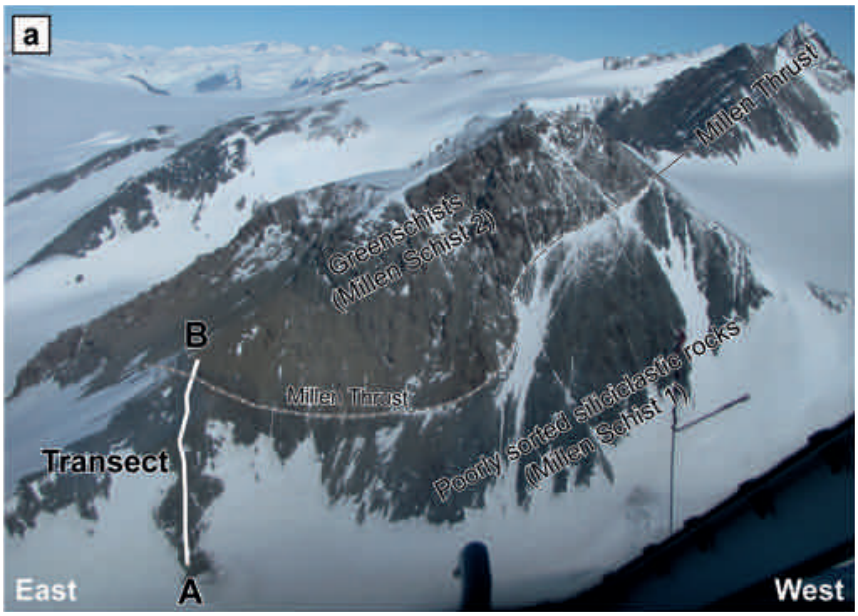

Fig. 5: Summary of key observations and data collected in close proximity to the Millen Thrust at Mt Aorangi. (a) = Photograph is taken looking south from a helicopter and shows the architecture of the geological units, the location of the Millen Thrust and the location of the field traverse A-B. A cross-sectional view of this transect (looking east) is below (A-B) with key overprinting observations and structural data shown. (b) = Schematic diagram of S0 to S3 overprinting relationships. (c) = Kinematic data from S0/S1, S2, L0/12 and S3 shear planes. (d) = Complex overprinting relationships in closer proximity to the fault surface. (e) = Orientations of S2 and S3 S-C fabrics in the direct hanging wall of the fault zone.

Abb. 5: Zusammenfassung der Schlüsselbeobachtungen und Daten in unmittelbarer Nähe zur Millen-Überschiebung am Mt. Aorangi. (a) = Foto aus dem Hubschrauber mit dem Aufbau der geologischen Einheiten, der Lage der Millen-Überschiebung und der Lage der Geländetraverse A-B. (b) = Schematisches Diagramm mit Überschneidungskriterien von S0 bis S3. (c) = Kinematische Daten von S0/S1, S2, L0/12 und S3-Scherflächen. (d) = Komplexe Überschneidungskriterien in größerer Nähe zur Störungsfläche. (e) Orientierungen von S2 (links) und S3-formende SC-Gefüge (rechts) im Hangendblock unmittelbar über der Störungsfläche.

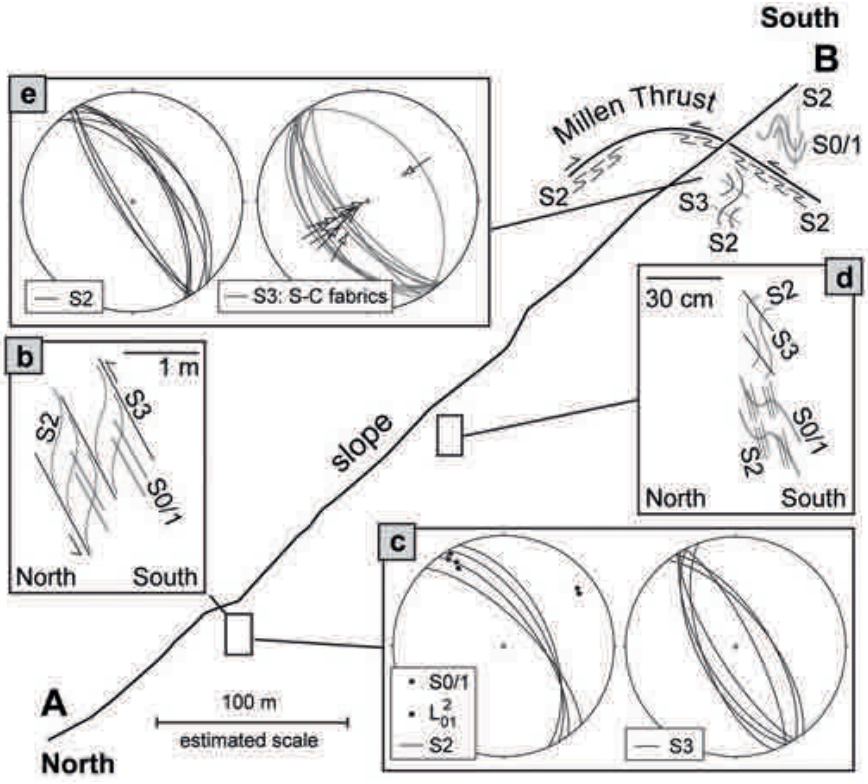

terranes, whereas the internal model requires lithological similarities. Based on field observation and microscopy, the rock units located in the hanging wall and footwall of the Millen Thrust comprise volcanoclastic sandstones and poorly sorted siliciclastic sandstones, respectively. Similarities with rock units of the largely volcanoclastic Sledgers Group of the Bowers Terrane and the siliciclasitc rocks of the Robertson Bay Group supports a local provenance for the rocks of the Millen Schists (JORDAN et al. 1984, CAPPONI et al. 2003). The Millen Thrust therefore represents a transport surface between the rocks of the Bowers and Robertson Bay Terranes. As a result, clues into the juxtaposition of these terranes can be inferred from the kinematic record of the Millen Schists.

The kinematic evolution of the Millen Schists involved three main stages of deformation. The first was largely identified petrographically, and involved the formation of a bedding parallel foliation that developed in an axial planar orientation to small isoclinal folds of bedding. Away from the Millen Thrust, the S0/S1 foliation is folded into upright asymmetric folds (F2) that plunge at low angles (5-20°) to the southeast and northwest (Fig. 5a-c). A sub-vertical S2 cleavage, which is the dominant foliation identified at most outcrops, is aligned along the axial plane of these folds. Whereas fold structures of similar orientation are also reported from the Bowers and Robertson Bay Terranes, these structures are associated with a single deformation event (D1; MECCHERI et al. 2004). Asym-

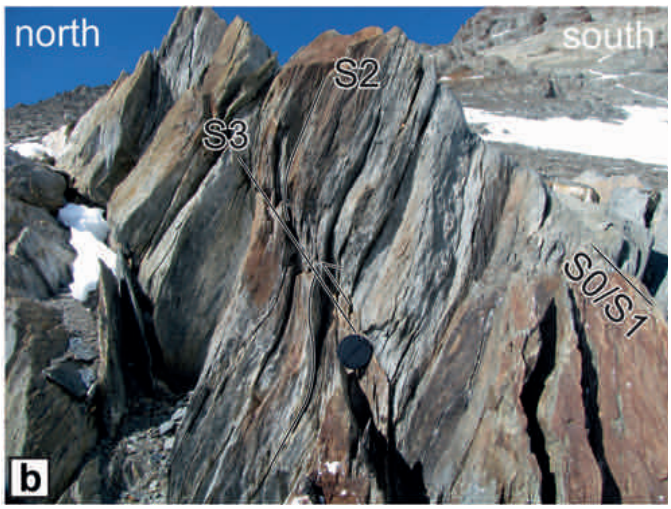

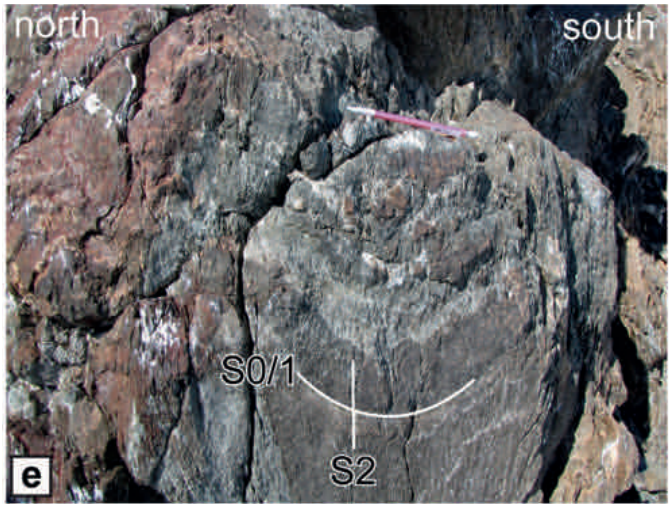

Fig. 6: Field photographs of the Millen Schists in close proximity to the Millen Thrust. (a) = Folded S0/S1 and the dominant S2 foliation. (b) = Reverse offset of S2 along high-angle, bedding parallel S3 shear planes. (c) = The folded thrust zone parallel to bedding. (d) = S-C fabrics (D3) showing a reverse sense of transport on the fault zone. (e) = Upright folds in the hanging wall of the thrust zone.

Abb. 6: Geländefotos der Millen Schists in unmittelbarer Nähe zur Millen-Überschiebung. (a) = Verfaltetes S0/S1 und dominierende S2 Foliation. (b) = Aufschiebende Versätze von S2 entlang steiler, schichtungsparalleler S3-Scherflächen. (c) = Verfaltete Störungszone, parallel zur Schichtung. (d) = SC-Gefüge (D3) mit aufschiebender Bewegung der Überschiebungszone. (e) = Aufrechte Falten im Hangendblock der Überschiebungszone.

Fig. 7: Photograph of the Millen Thrust exposed at Crosscut Peak. Photograph was taken from helicopter.

Abb. 7: Blick nach Süden aus dem Hubschrauber auf die Millen-Überschiebung am Crosscut Peak.

metric F2 folds in the lower units of the Millen Schists (i.e., Millen Schist 1) consistently verge to the northwest and indicate that the primary direction of tectonic transport along the Millen Thrust was probably also in this direction (Capponi et al. 2003). This is in contrast to the neighbouring Bowers and Robertson Bay Terranes, which record neutral vergence. It can therefore be reasonably suggested that the Millen Schists record the transportation of the Bowers Terrane over the Robertson Bay Terrane. However, owing to the dominant upright orientation of the S2 cleavage, the majority of this transport was probably facilitated by a low angle detachment located below the Millen Schists (i.e., as in Kleinschmidt 1992 for the Robertson Bay Terrane).

Toward the Millen Thrust, the intensity of D3 strain increases. Distal to the contact, D3 strain is recorded by the localised formation of open F3 warps and evenly spaced reverse shear planes. At the contact, a <1 m wide zone contains cm-scale S-C fabrics that consistently record a reverse shear sense indicators. The contact consistently strikes northwest-southeast, yet owing to the presence of metre-scale F2 folds, dips to the northeast and southwest. The change in dip, yet consistent reverse sense of transport along the contact may be responsible for previous conjecture surrounding the direction of transport along the fault zone (Bradshaw 1985, Wright 1985, Findlay 1986). As S-C fabrics on both northeast and southwest dipping limbs of the contact record a reverse sense of transport, folding of the contact must have taken place prior to the D3 thrusting; otherwise, reverse and normal transport direction would be recorded by fold limbs dipping in opposing directions. Based on this relationship, F2 folding of the contact between the Bowers and Robertson Bay Terrane must have taken place prior to the localisation of higher strain (D3) along the Millen Thrust. Whereas absolute constraints are not available to confirm the timing of D2 and D3 deformations, a clear similarity in the stress field responsible for their development (cf. Figs 4a-b, 5e) supports their synchronicity. We therefore view the deformation process in the high strain components of the Millen Schists as a localisation of high strain (responsible for D3 structures) along pre-existing weaknesses in a progressively folded tectonic pile.

Jordan et al. (1984) published an account of the structural geology of the Millen Schists exposed in the Bowers Mountains (see Fig. 1). These authors recognised the following structures: (i) a dominant S1 cleavage that strikes northwest to north and dips steeply to the east; (ii) associated F1 isoclinal folds that plunge steeply to near horizontally in the plane of S1; (iii) an S2 crenulation cleavage that strikes northwest to north and dips steeply to the east and west; (iv) F2 crenulations plunge shallowly to the southeast, and to a lesser extent, northwest and (v) an east- and west-dipping spaced S3 cleavage that forms axial planar to dextral kink folds. Similarities and disparities exist between the kinematic frameworks of the Bowers Mountains and Millen Range. Firstly, S1 forms axial planar to F1 isoclinal folds and forms the dominant foliation in the Bowers Mountains; S1 in the Millen Range is in contrast sub-parallel to bedding and crenulated/folded around the dominant S2 fabric. Secondly, the orientations of the S1 and S2 (Bowers Mountains) and S2 (Millen Range) foliations consistently strike northwest-southeast and dip steeply to the east or west. Thirdly, the localised formation of F3 warps and kinks that may indicate normal movement along the main fault zones is reported from both of the locations. Therefore, apart from variable levels of D1 and D2 strain, which can explain the different intensities of the D1 and D2 structures at either location, the kinematic framework of both regions is remarkably consistent. Of further significance, potential evidence of normal movement along the Leap Year Fault (Capponi et al. 2003, Crispini et al. 2014) and likely also according to the interpretation of our own data set of the Millen Thrust System signifies a more complex structural history than a simple thrust surface. We therefore prefer the term Millen Shear Belt for the whole zone taking into account a polydeformational history not only linked to reverse movements along the Millen Thrust System alone.

Available stratigraphic and isotopic data from northern Victoria Land (summarised in Tessensohn & Henjes-Kunst 2005) provides constraints on the timing of deformation of the Millen Schists. If the units of the Millen Schists represent components of the Bowers and Robertson Bay Terranes, a constraint on the timing of deformation is the age of sediment deposition in these terranes. Isotopic data collected from detrital zircon (only Robertson Bay Terrane; Fioretti et al. 2003) and mica (both Bowers (Molar Formation) and Robertson Bay Terranes; Henjes-Kunst 2003) limits the timing of sediment deposition in these terranes to after c. 490 Ma (excluding single analysis populations). Based on these constraints, the timing of deformation must be after 490 Ma. Interestingly, this time period marks the cessation of convergent deformation in the neighbouring Delamerian Orogeny of southeastern Australia (Foden et al. 2006), and is younger than the main phase of deformation in the Pensacola Mountains (Rowell et al. 2001). Whereas the reasons for these along strike variations (with respect to the greater Terra Australis Orogen) in deformation age remain beyond the scope of the present paper, our work supports an Early Ordovician (or even younger) deformation age for the rocks of the Millen Schists. The c. 505-500 Ma age obtained from Ar-Ar analyses by Wright & Dallmeyer (1991) are too old in this regard. On the other hand, Crispini et al. (2014) and Di Vicenzo et al. (2014) report a much younger age of c. 460 Ma for the oldest deformation along the Millen Thrust System based on recent Ar-Ar analyses of metamorphic white mica.

A second implication of our work is that the Bowers and Robertson Bay Terranes may have formed as a single tectonic entity throughout the Middle to Late Cambrian, rather than far removed arc and continental terranes (Kleinschmidt et al. 1987). Whereas this interpretation is favoured by several workers (Roland et al. 2004, Crispini et al. 2014), the provenance of the two terranes does raise significant questions. The Bowers Terrane comprises a volcanic basement associated with volcanoclastic rocks that are overlaid by terrestrial quartzites. The volcanic components of this pile are suggested to represent a rifted intra-oceanic arc (Weaver et al. 1984). The rocks of the Robertson Bay Terrane are derived from a proximal mature continental source (Henjes-Kunst et al. 2004) with limited evidence of volcanic detritus. The character of the Robertson Bay Terrane is therefore surprising given its outboard position and its inferred isolation from the only known continental source (i.e., the Wilson Terrane) by the Bowers Terrane. Whereas the far-travelled migration of sediments parallel to the trench could explain the enigmatic character of the Robertson Bay Group, the highly angular nature

and poorly sorted character of the rocks does not support a distal sedimentary source. Alternatively strike-slip displacement provides a mechanism to explain the current positioning of the two terranes (WEAVER et al. 1984); as a matter of fact, evidence for strike-slip to oblique-slip transport was reported for both boundary faults of the Millen Shear Belt (WRIGHT 1982, JORDAN et al. 1984, CRISPINI et al. 2014) and minor evidence of lateral displacements in the Millen Schists was also found in our target area. This led CRISPINI et al (2014) to interpret the structural setting of the Millen Range as the result of left-lateral pop-up tectonics.

The current work supports the significance of the Millen Schists as a key unit recording evidence of assembly processes in a convergent margin orogen. In addition to the Leap Year Fault, the Lanterman Fault Zone that is located in a more inboard position (Fig. 1), accommodates northeast-directed thrusting along a southwest-dipping fault zone. Given the comparatively low levels of finite strain recorded by the internal parts of the Bowers and Robertson Bay Terranes, it is reasonable to suggest that the Leap Year and Lanterman Fault Zones accommodated the majority of strain in the outboard part of the Ross Orogen in the northern Victoria Land sector (GIBSON & WRIGHT 1985). A contrasting geometry is observed in the inboard parts of the orogen, where opposite directed thrust systems are located in the Wilson Terrane (i.e., the Exiles and Wilson Thrusts; FLÖTTMANN & KLEINSCHMIDT 1991). Interestingly, classical fold and thrust belt models do predict this contrasting detachment architecture in outboard and inboard parts of orogenic belts. Analogue modelling (DAVIS et al. 1983) shows this, where basal shear results in the development of opposite directed thrust systems in the rear of the deforming wedge and consistently dipping detachment zones in the front of the wedge. The geometry of the major detachments in northern Victoria Land is therefore consistent with this architecture, which, in this case, would require southwest-directed dextral shear below northern Victoria Land. This deformation regime is consistent with southwest-directed subduction below northern Victoria Land throughout the late Cambrian to at least early Ordovician.

CONCLUSION

The Millen Schists record evidence of a polyphase deformation history that is more complex than the internal deformation patterns of the Bowers and Robertson Bay Terranes. The development of F1 isoclinal folds and S1 foliation resulted in the transposition of bedding and cleavage to form a composition S0/S1 fabric. Shortening of this fabric into upright, asymmetric folds was responsible for the development of the dominant northwest-southeast striking sub-vertical slatey S2 cleavage. F2 folds verge to the northeast, supporting the widely acknowledged conclusion that tectonic transport during the Ross Orogeny in northern Victoria Land was toward the northeast. The contact between the two main units of the Millen Schists record evidence of a more complex kinematic history, where folds attributed to normal movement along the contact are proximally located to S-C fabrics recording a reverse sense of movement. Owing to the consistent reverse sense recorded by S-C fabrics on both northeast and southwest dipping segment of the Millen Thrust, reverse transport must have taken place after folding of the contact. Based on the observations made at the contact, the Millen Thrust is suggested to represent a significant flexural slip surface, rather than a major tectonic boundary that facilitated the juxtaposition of two exotic terranes. This interpretation is further supported by lithological similarities between the rocks exposed in the hanging wall and footwall of the Millen Thrust System and the neighbouring Bowers and Robertson Bay Terranes. Available timing constraints limit the maximum timing of deformation in the Millen Schists to the early to middle Ordovician.

ACKNOWLEDGMENTS

Glen Phillips would like to thank the German Bundesanstalt für Geowissenschaften und Rohstoffe (BGR) for invitation to GANOVEX X. The field-work during GANOVEX X would not have been possible without the logistic support by the crew of the RV "Italica" and pilots and mechanics of Helicopters New Zealand (HNZ). Special thanks are due to the NZ field guide Brian Straite who assisted during the field work. Last-not-least, many thanks to the whole expedition team for stimulating discussions during and after the expedition.

References

Borg, S.G., Stump, E., Chappell, B.W., McCulloch, M.T., Wyborn, D., Armstrong, R.L. & Holloway, J.R. (1987): Granitoids of Northern Victoria Land, Antarctica: Implications of chemical and isotopic variation to regional crustal structure and tectonics.- Amer. J. Sci. 287: 127-169.

Bradshaw, J.D., Weaver, S.D. & Laird, M.G. (1985): Suspect Terranes and Cambrian Tectonics in Northern Victoria Land, Antarctica.- In: D.G. HOWELL (ed), Tectonostratigraphic Terranes of the Circum-Pacific Region, Circum Pacific Council for Energy and Mineral Resources, Earth Science Series 1: 467-479.

Bradshaw, J.D. (1985): Terrane boundaries and terrane displacements in northern Victoria Land, Antarctica.- Geol. Soc. Austral. Abstr. 14: 30-33.

Bradshaw, J.D. (1987): Terrane boundaries and terrane displacement in northern Victoria Land, Antarctica.- In: E.C. LEITCH & E. 12 42: 199-205.

Capponi G., Carosi, R., Meccheri, M. & Oggiano, G. (2003): Strain analysis in the Millen Range of Northern Victoria Land, Antarctica.- In: F. TESSENSOHN & C.A. RICCI (eds), Aspects of a Suture Zone, Geol. Jb. Reihe B: 223-251.

Cawood, P.A. (2005): Terra Australis Orogen: Rodinia breakup and development of the Pacific and Iapetus margins of Gondwana during the Neoproterozoic and Paleozoic.- Earth Sci. Rev. 69: 249-279.

Crispini, L., Federico, L. & Capponi, G. (2014): Structure of the Millen Schist Belt (Antarctica): clues for the tectonics of northern Victoria Land along the paleo-Pacific margin of Gondwana.- Tectonics 33: 420-440, doi:10.1002/2013TC003414.

Davis, D., Suppe, J. & Dahlen, F.A. (1983): Mechanics of fold-and-thrust belts and accretionary wedges.- J. Geophys. Res. Solid Earth 88: 1153-1172.

Di Vicenzo, G., Grande, A. & Rossetti, F. (2014): Paleozoic siliciclastic rocks fromnorthern Victoria Land (Antarctica): Provenance, timing of deformation, and implication for the Antarctica-Australia connection.- Geol. Soc. Amer. Bull., doi: 10.1130/B31034.1.

Findlay, R.H. (1986): Structural geology of the Robertson Bay and Millen terranes, northern Victoria Land, Antarctica.- In: E. STUMP (ed), Geological Investigations in Northern Victoria Land, Antarctica, Res. Series 46: 91-114, AGU, Washington, D.C., doi:10.1029/AR046p0091.

Fioretti A.M., Black P., Henjes-Kunst F. & Visonà D. (2003): Detrital zircon age patterns from a large gneissic xenolith from Cape Phillips granite and from Robertson Bay Group metasediments, northern Victoria Land, Antarctica.- In: D.K. FÜTTERER (ed), 9th Internat. Sympos. Antarctic Earth Sciences (ISAES IX) Antarctic Contributions to Global Earth Sciences, Programme & Abstracts. Terra Nostra 2003/4: 94-95.

Flöttmann, T. & Kleinschmidt, G. (1991): Opposite thrust systems in northern Victoria Land, Antarctica: Imprints of Gondwana Paleozoic accretion.- Geology 19: 45-47.

Foden, J., Elburg, M.A., Dougherty-Page, J. & Burtt, A. (2006): The Timing and duration of the Delamerian Orogeny: Correlation with the Ross Orogen and Implication for Gondwana Assembly.- J. Geology 114: 189-210.

GANOVEX Team (1987): Geological map of North Victoria Land, Antarctica, 1:500 000, explanatory notes, Geol. Jb. B 66, 7-79.

Gibson, G.M. (1984): Deformed conglomerates in the Eastern Lanterman Range, North Victoria Land, Antarctica.- In: N.W. ROLAND (ed), GANOVEX III, Geol. Jb. Reihe B, 1: 117-141.

Gibson, G.M., Tessensohn, F. & Crawford, A. (1984): Bowers supergroup rocks west of the Mariner Glacier and possible greenschist facies equivalents.- In: N.W. ROLAND (ed), GANOVEX III, Geol. Jb. Reihe B, 1: 289-318.

Gibson, G.M. & Wright, T.O. (1985): Importance of thrust faulting in the tectonic development of northern Victoria Land, Antarctica.- Nature 315: 480-483.

Grew, E.S., Kleinschmidt, G. & Schubert, W. (1984): Contrasting metamorphic belts in North Victoria Land, Antarctica.- In: N.W. ROLAND (Ed) GANOVEX III, Geol. Jb. Reihe B, 1: 253-263.

Henjes-Kunst, F. (2003): Single-crystal Ar-Ar laser dating of detrital micas from metasedimentary rocks of the Ross-orogenic belt at the Pacific margin of the Transantarctic Mountains, Antarctica.- In: D.K. FÜTTERER (Ed) 9th Internat. Sympos. Antarctic Earth Sciences (ISAES IX), Antarctic Contributions to Global Earth Sciences, Potsdam, Programme & Abstracts, Terra Nostra 2003/4: 150-151

Henjes-Kunst, F., Roland, N.W., Dunphy, J.M. & Fletcher, I.R. (2004): SHRIMP U-Pb dating of high-grade migmatites and relates magmatites from northwestern Oates Land (East Antarctica): Evidence for a single high-grade event of Ross-Orogenic age.- Terra Antartica 11: 67-84.

Jordan, H., Findlay, R., Mortimer, M., Schmidt-Thomé, Crawford, A. & Müller, P. (1984): Geology of the Northern Bowers Mountains, north Victoria Land, Antarctica.- In: N.W. ROLAND (ed) GANOVEX III, Geol. Jb. Reihe B, 1: 57-81.

Kleinschmidt, G. & Skinner, D.N.B. (1981): Deformation styles in the basement rocks of northern Victoria Land, Antarctica.- Geol. Jb. B 41, 155-199.

Kleinschmidt, G., Tessensohn, F. & Vetter, U. (1987): Paleozoic accretion at the Paleopacific margin of Antarctica.- Polarforschung 57: 1-8.

Kleinschmidt, G. (1992): Structural observations in the Robertson Bay Terrane and their implications.- Polarforschung 60: 128-132.

Laird, M.G., Bradshaw, J.D. & Wodzicki, A. (1982): Stratigraphy of the late Precambrian and early Paleozoic Bowers Supergroup, northern Victoria Land, Antarctica.- In: C. CRADDOCK (ed), Antarctic Geoscience, 535-542, Madison (University Wisconsin Press).

Meccheri, M., Pertusati, P.C. & Tessensohn, F. (2004): Explanatory notes to the geological and structural map of the area between the Aviator Glacier and Victory Mountains, Northern Victoria Land, Antarctica.- In: F. TESSENSOHN & C.A. RICCI (eds), Aspects of a Suture Zone, Geol. Jb Reihe B: 223-251

Rocchi, S., Bracciali, L., Di Vincenzon, G., Gemelli, M. & Ghezzo, C. (2011): Arc accretion to the early Paleozoic Antarctic margin of Gondwana in Victoria Land.- Gondwana Res. 19: 594-607.

Roland, N.W., Gibson, G.M., Kleinschmidt, G. & Schubert, W. (1984): Metamorphism and structural relations of the Lanterman Metamorphics, North Victoria Land, Antarctica.- In: N.W. ROLAND (ed). GANOVEX III, Geol. Jb. Reihe B, 1: 319-361.

Roland, N.W., Läufer, A.L. & Rossetti, F. (2004): Revision of the Terrane Model of Northern Victoria Land (Antartica).- Terra Antartica 11: 55-65.

Rowell, A.J., Van Schmus, Storey, A.H., Fetter, A.H. & Evans, K.R. (2001): Latest Neoproterozic to Mid-Cambrian age for the main deformation phases of the Transantarctic Mountains: new stratigraphic and isotopic constraints from the Pensacola Mountains, Antarctica.- J. Geol. Soc. 158: 295-308.

Schüssler, U., Henjes-Kunst, F., Talarico, F. & Flöttmann, T. (2004): High-grade crystalline basement of the northwestern Wilson Terrane and Oates Coast: New petrological and geochronological data and implications for its tectonometamorphic evolution.- Terra Antartica 11, 15-34.

Tessensohn, F. & Henjes-Kunst, F. (2005): Northern Victoria Land Terranes, Antarctica: far-travelled of local products.- In: A.P.M. VAUGHAN et al. (eds), Terrane Processes at the Margins of Gondwana, Geol. Soc. London Spec. Publ. 246: 275-291.

Tessensohn, F. (1984): Geological and tectonic history of the Bowers Structural Zone, North Victoria Land, Antarctica.- In: N.W. ROLAND (ed) GANOVEX III, Geol. Jb. Reihe B, 1: 371-396.

Weaver, S.D., Bradshaw, J.D. & Laird, M.G. (1984): Geochemistry of Cambrian volcanic of the Bowers Supergroup and implications for the early Palaeozoic tectonic evolution of northern Victoria Land, Antarctica.- Earth Planet. Sci. Lett. 68: 128-140.

Wright, T.O. (1982): Structural study of the Leap Year Fault.- Antarctic J. United States XVII-5: 11-13.

Wright, T.O. & Findlay, R.H. (1984): Relationships between the Robertson Bay Group and the Bowers Supergroup – New progress and complications from the Victory Mountains, North Victoria Land.- Geol. Jb. B60: 105-116.

Wright, T.O. & Dallmeyer, R.D. (1991): The age of cleavage development in the Ross Orogen, northern Victoria Land, Antarctica: evidence from $^{40}Ar/^{39}Ar$ whole rock slate ages.- J. Struct. Geol. 13: 677-690.

Wright, T.O., Ross, R.J. & Repetski, J.E. (1984): Newly discovered youngest Cambrian or oldest Ordovician fossils from the Robertson Bay terrane (formerly Precambrian), northern Victoria Land, Antarctica.- Geology 12: 301-305.

Wright, T.O. (1985): Late Precambrian and early Paleozoic tectonism and associated sedimentation in northern Victoria Land, Antarctica.- Geol. Soc. Amer. Bull. 96: 1332-1339.

Polarforschung 84 (1), 49–58, 2014

Sedimentological Field Investigations on the Takrouna Formation (Permian, Beacon Supergroup) in Northern Victoria Land, Antarctica

by Robert Schöner[1] and Nadine John[1]

Abstract: The deposits of the Takrouna Formation (Permian) were target of sedimentological field work during the 10th "German North Victoria Land Expedition" (GANOVEX X, 2009/2010). Four complete and several small sections were logged within six different mountain ranges in the northern part of Victoria Land. Lithofacies types of the studied sedimentary succession mainly comprise fluvial conglomerates and coarse- to fine-grained sandstones, and enable a subdivision in preliminary units. The lithofacies characteristics also allow tracing the transition of more proximal and distal parts of the fluvial system of the Takrouna Formation. Coarse-grained successions in the eastern part of the study area were probably deposited close to the basin margin. Further west sedimentary successions are overall finer and show a great variety of facies and fluvial architecture. They most likely represent locations close to the basin axis. At the basin margin the river system remained highly energetic in contrast to a more variable depositional environment towards the basin axis.

Zusammenfassung: Die Ablagerungen der Takrouna Formation (Perm) waren Ziel sedimentologischer Untersuchungen während der 10. „Deutschen Nord-Viktorialand-Expedition" (GANOVEX X 2009/2010). In insgesamt sechs Gebirgszügen wurden vier vollständige und mehrere kurze Profile sedimentologisch aufgenommen. Die Lithofaziestypen umfassen größtenteils fluviatile Konglomerate und Grob- bis Feinsandsteine. Die Geländebefunde erlauben eine vorläufige Unterteilung der sedimentären Abfolge in mehrere Einheiten und eine Unterscheidung zwischen proximalen und mehr distalen Bereichen des ehemaligen Flusssystems. Durchgehend grobkörnige Abfolgen im östlichen Teil des Untersuchungsgebietes wurden vermutlich nahe des Beckenrandes abgelagert. Die weiter westlich gelegenen Profile sind insgesamt feinkörniger und hinsichtlich Fazies und fluviatiler Architektur variabler. Sie wurden distaler abgelagert, wahrscheinlich im Bereich der Beckenachse.

INTRODUCTION

During the 10th German North Victoria Land Expedition (GANOVEX X) in the Austral summer 2009/2010, the Permian Takrouna Formation and locally the underlying deposits of supposed glacial origin were target of sedimentological fieldwork. Sedimentary rocks of the Takrouna Formation are exposed in several mountain ranges in the northern part of Victoria Land (Figs. 1 & 2). The current knowledge on the Takrouna Formation is based on field campaigns that were carried out in the 1970s and 1980s by Dow & Neall (1974), Walker (1983), Collinson & Kemp (1983), and Collinson et al. (1986). Although previous investigations indicate the Fluvial nature of the Takrouna Formation, the available data does not allow drawing a consistent picture of the depositional evolution of the roughly north-south oriented sedimentary basin. Sections from different parts of the basin could not be correlated so far. The major target of this field campaign was investigating the sedimentary inventory of the Takrouna Formation in detail throughout the exposed stratigraphic range. The localities selected are lined along two east-west and north-south trending axes in order to work out lateral changes across and along the basin. Detailed logging of vertical sections in combination with the study of large two-dimensional exposures (cliff faces) will help to better understand the sedimentological and stratigraphic evolution of the Permian succession in northern Victoria Land. The results will also allow comparing this basin with other contemporaneous basins in the Transantarctic Mountains.

This report provides a brief overview over the fieldwork on the Takrouna Formation carried out during GANOVEX X. Coordinates and elevations given in this report were recorded by GPS (WGS 84). Samples taken systematically will serve for further petrographical and provenance analytical studies as well as for biostratigraphic investigations.

GEOLOGICAL SETTING AND STRATIGRAPHY

Sedimentary rocks of the Beacon Supergroup of the Transantarctic Mountains rest unconformably on pre-Devonian basement composed of metamorphic and igneous rocks. The Beacon Supergroup was deposited in Devonian to Early Jurassic times in a sedimentary basin at the Panthalassan margin of Gondwana (Barrett 1991). It can be subdivided into the Devonian Taylor Group, and the Upper Carboniferous to Lower Jurassic Victoria Group. In northern Victoria Land, the Victoria Group consists of an unnamed basal diamictite unit and the overlying Takrouna Formation (Upper Carboniferous (?) to Permian; Dow & Neall 1974), the Triassic to Lower Jurassic Section Peak Formation (Collinson et al. 1986, Schöner et al. 2011), and the Lower Jurassic Shafer Peak Formation (Schöner et al. 2007). Volcaniclastic deposits of local phreatomagmatic eruptions are crosscutting the Section Peak and the Shafer Peak formations, and are also intercalated within the Lower Jurassic part of the sedimentary succession (Viereck-Götte et al. 2007, Schöner et al. 2007).

During the Late Carboniferous and earliest Permian northern Victoria Land was located close to the South Pole and affected by continental glaciation. After the retreat of the glaciers and the beginning of glacially controlled sedimentation (Laird & Bradshaw 1981, Skinner 1981), a fluvial system was established probably during Early Permian times. Permian sedimentary rocks of the Central Transantarctic Mountains and of Victoria Land were deposited in two different basins,

[1] Friedrich-Schiller-Universität Jena, Institut für Geowissenschaften, Burgweg 11, D-07749 Jena, Germany, <robert.schoener@gmx.de>, <nadine.jo@gmx.de>

Manuscript received 03 June 2014; accepted in revised form 06 November 2014.

which were separated by the Ross High (COLLINSON et al. 1994). Paleocurrent data indicate overall sediment transport-directions towards the south in the Central Transantarctic Mountains, and towards the north in Victoria Land. The Ross High apparently became inactive during the Triassic, when a north-oriented drainage system established throughout the Transantarctic Basin (BARRETT 1991, COLLINSON et al. 1994). However, there is no continuous record of Permian to Triassic sedimentation in northern Victoria Land. Outcrops of Permian deposits occur only in the northern part, whereas Triassic deposits have only been described from the southern part of northern Victoria Land. The emplacement of large volumes of mafic magma during the late Early Jurassic (Ferrar Group) led to the intrusion of mafic dolerite sills into the Beacon Supergroup, and to the deposition of a thick sequence of lava flows.

LOGISTICAL CONSTRAINTS AND SCHEDULE

To carry out sedimentological investigations on the approximately 300 m thick Takrouna Formation, five small satellite camps were planned at key localities. Four of these camps could be realized in Boggs Valley (Helliwell Hills), at De-Goes Cliff (Morozumi Range), in the northern Alamein Range, and close to Neall Massif (Figs. 1 & 2). These areas were investigated within five to eight days depending on weather conditions and helicopter availability. The field party consisted of Nadine John, Robert Schöner and Mike Aitkinson (field guide) and was equipped with one Polar tent (kitchen tent) and three lightweight geodetic tents (Fig. 5). People and equipment were transferred from camp to camp by two helicopter loads. The camp at Boggs Valley had to be carried to a more sheltered location after the first night due to strong catabatic winds. Walking distances from the camps to the outcrops varied between 1 km and 5 km. In total, 27 days were spent in the camps between January 03 and 29 2010. Helicopter supported reconnaissance surveys to key outcrops that could not be reached from the camps were originally planned at the beginning and end of the field campaign, and in combination with each camp move. However, apart from one short stop on a plateau above Boggs Valley (section 1BT, Tab. 1), all reconnaissance flights were cancelled owing to poor weather conditions or limited helicopter availability. After the last camp was closed down these reconnaissance flights could be partly completed. In total, helicopter reconnaissance was limited to one full day and two half days, which were used for brief visits of outcrops in the Lanterman Range, the Morozumi Range, the southern Freyberg Mountains, the Retreat Hills, and additionally for two outcrops of the Triassic Section Peak Formation at Vulcan Hills and Timber Peak (Figs. 1 & 2, Tab. 1). Sedimentological fieldwork was carried out for 18.5 days in total, which is equivalent to 64 % of the time spent in the working area, and about 30 % of the time spent on the expedition.

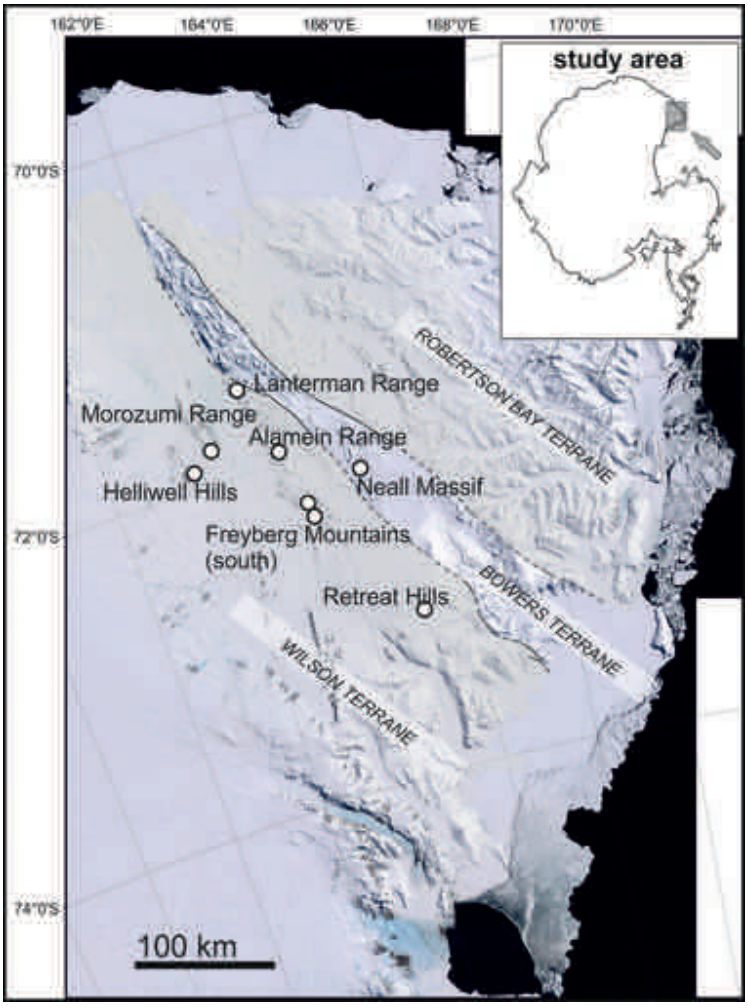

Fig. 1: Map of northern Victoria Land indicating the studied Permian sections in the Rennick Glacier region (compiled using satellite images from USGS-LIMA, 2009).

Abb. 1: Karte des nördlichen Victoria Land mit den untersuchten permischen Aufschlüssen im Bereich des Rennick Glacier (zusammengestellt auf Basis von USGS-LIMA, 2009).

RESULTS OF FIELD INVESTIGATIONS

Helliwell Hills

Exposures of the Takrouna Formation in the Helliwell Hills occur in Boggs Valley, southeast of Mt. Remington and south of Mt. Bresnahan. Since reconnaissance flights previous to the field period could not be carried out, the locality Boggs Valley, exposing the largest known outcrops with a thickness of 225 m (COLLINSON et al. 1994), was chosen for the first camp.

The outcrops at the nearly NE-SW trending valley were examined between January 03 and 08 2010 (Fig. 8). A continuous 3 km section was studied at the northern side of the valley and a cumulative thickness of about 180-190 m was measured. The sedimentary rocks are separated into several units by mafic dolerite sills of the Ferrar Group, which are thicker than the exposed sedimentary units. These sills also form the top of the peaks surrounding Boggs Valley. A 120 m section of the lower part of the sedimentary succession was studied in detail at the SE-facing cliff near the eastern end of the valley (section BV, Fig. 2, Tab. 1). Parts of the upper succession were investigated between two thick sills about 3 km further WSW, above a small plateau directly north of the valley (section BT). Additionally, sedimentological features and sedimentary architecture were studied on a cliff in the central part of the valley.

Boggs Valley (section BV)

The basement is exposed along the valley floor and consists predominantly of meta-sedimentary rocks belonging to the Rennick Schists, which comprise a variety of quartzites and finer-grained meta-sediments. Acidic igneous intrusive bodies contain partly high amounts of tourmaline and increase in abundance towards the western end of the valley (Fig. 3). The basal 15 m to 20 m of the sedimentary succession above the basement are covered by scree. The exposed succession starts with beige to medium-grey fine-grained clastic deposits

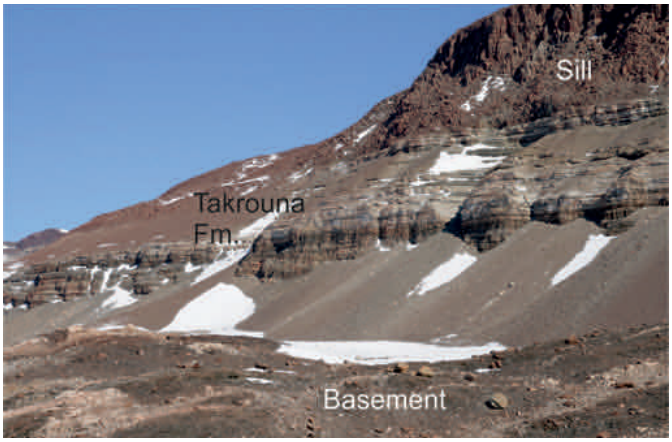

Fig. 3: Outcrop of the Takrouna Formation at the NW side of Boggs Valley in between basement and dolerite sill (Ferrar Group). The basement consists of Rennick Schists (dark) and acidic intrusives (bright). The sedimentary section was measured about 1 km further to the NE (section BV).

Abb. 3: Aufschluss der Takrouna Formation an der NW-Flanke von Boggs Valley zwischen Grundgebirge und einem Lagergang der Ferrar Group. Das Basement besteht hier aus Rennick Schists (dunkel) and felsischen Intrusiva (hell). Das Profil wurde ca. 1 km weiter im NE aufgenommen (Profil BV).

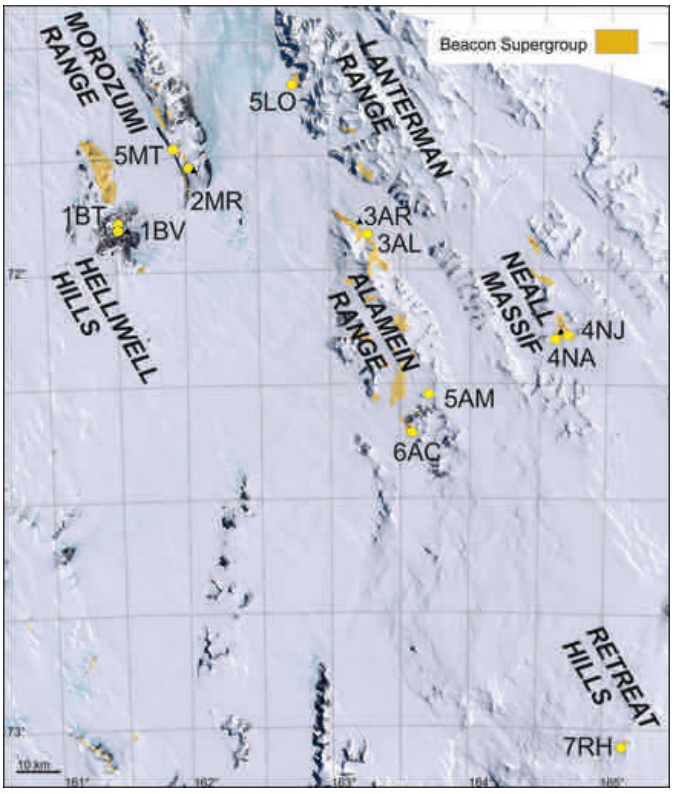

Fig. 2: Map of the working area showing outcrops of the Takrouna Formation in northern Victoria Land, including field camps and the studied localities: AC = Monte Cassino, AL = unnamed peak 10 km northwest of Takrouna Bluff, AM = Moawhango Névé, AR = Northern Alamein Range cliff, BT = Plateau directly north of Boggs Valley, BV = Boggs Valley, LO = Spur north of the Orr glacier, MR = DeGoes Cliff, MT = Plateau northwest of DeGoes Cliff, NA = West end of Neall Massif ridge, NJ = Central part of Neall Massif ridge, NM = East end of Neall Massif ridge, RH = southern peak of Retreat Hills. Map compiled using satellite images from USGS-LIMA (2009) and the geological map of GANOVEX-Team (1987).

Abb. 2: Karte des Arbeitsgebietes mit Aufschlüssen der Takrouna Formation im nördlichen Victoria Land einschließlich der Feldlager und der untersuchten Lokalitäten: AC = Monte Cassino, AL = unbenannter Berg 10 km nordwestlich des Takrouna Bluff, AM = Moawhango Névé, AR = Nördliches Kliff der Alamein Range, BT = Plateau unmittelbar nördlich von Boggs Valley, BV = Boggs Valley, LO = Felsrücken nördlich des Orr Glacier, MR = DeGoes Cliff, MT = Plateau nordwestlich von DeGoes Cliff, NA = westliches Ende des Felsrückens im Neall Massif, NJ = zentraler Teil des Felsrückens im Neall Massif, NM = östliches Ende des Felsrückens im Neall Massif, RH = südlicher Felsgipfel der Retreat Hills. Kartengrundlage zusammengestellt auf Basis von USGS-LIMA (2009) und GANOVEX-Team (1987).

followed by several sandy fining-up units. A mafic dolerite sill intrusion is exposed about 60 m above the base of the valley floor. The top of the sill and the overlying deposits are covered beneath scree. Further up, the exposed sequence continues with predominantly medium-grained sandstone showing ripple cross-lamination and less abundant trough crossbedding. At the top of this unit, paleo-soil relics such as root traces and iron-bearing concretions were observed. The overlying part of the section (71°54.137' S, 161°32.350' E, 840 m) is characterized by a laterally continuous light-beige coloured, pebble- and cobble-dominated conglomeratic layer that introduces a succession of fining-up units typically comprising coal-bearing fine-grained deposits at the top. Paleocurrent directions were measured throughout the sections using mainly trough cross-strata, or trough axis where exposed, as well as some planar cross-stratified beds. Measurements at section BV yield mean paleocurrent directions towards the NW.

Area	Locality	Section	Longitude S	Latitude E	Elevation (m) a.s.l.	Base	Top	working from	Formation
Helliwell Hills	Boggs Valley	1BV	71°54.0'	161°32.7'	760	Rennick Schists	Ferrar sill	camp	Takrouna Fm.
	Boggs Valley top	1BT	71°74.8'	161°26.0'	1360	Rennick Schists	Ferrar sill	helicopter	Takrouna Fm.
Moruzumi Range	De Goes Cliff	2MR	71°47.2'	161°59,0'	810	Morozumi Phyllites	Ferrar sill	camp	glacial deposits, Takrouna Fm.
	Morozumi Range top	5MT	71°41.6'	161°49.9'	1360	Ferrar sill	not exposed	helicopter	Takrouna Fm.
Freyberg Mountains	Alamein Range	3AL	71°55.0'	163°11.9'	1320	Granite Harbour Intrusives	Ferrar sill	camp	glacial deposits Takrouna Fm.
	Alamein Range cliff	3AR	71°53.6'	163°07.6'	1000	not exposed	Ferrar sill	camp	Takrouna Fm.
	Moawhango Névé	5AM	72°15.7'	163°30.1'	1810	not exposed	not exposed	helicopter	Takrouna Fm.
	Monte Cassino	6AC	72°21.4'	163°34.0'	1570	not exposed	Ferrar sill	helicopter	Takrouna Fm.
Neall Massif	Neall Massif east	4NM	72°08.8'	164°43.6'	2070	Molar Formation metasediments	not exposed	camp	glacial deposits
	Neal Massif camp	4NJ	72°08.6'	164°39.6'	1990	Ferrar sill	Ferrar sill	camp	Takrouna Fm.
	Neal Massif west	4NA	72°08.5'	164°31.2'	1790	Ferrar sill	not exposed	camp	glacial deposits Takrouna Fm.
Lanterman Range	S' spur N' Orr Glacier	5LO	71°35.2'	162°45.7'	530	Lanterman Metamorphics	not exposed	helicopter	glacial deposits Takrouna Fm.
Retreat Hills	Retreat Hills	7RH	73°02.9'	165°11.0'	3020	not exposed	not exposed	helicopter	Takrouna Fm.
Vulcan Hills	Vilcan Hills	7VH	73°40.1'	163°40.0'	2760	Granite Harbour	Ferrar sill	helicopter	Section Peak Fm.
Timber Peak	Timber Peak	8TI	74°11'	162°31'	2840	Ferrar sill	Ferrar sill	helicopter	Section Peak Fm.

Tab. 1: Outcrops of Permian / Permo-Carboniferous deposits investigated during GANOVEX X (2009/2010). Coordinates and elevations were taken by GPS (WGS 84).

Tab. 1: Aufschlüsse permischer / permokarboner Ablagerungen, die während GANOVEX X (2009/2010) untersucht wurden. Koordinaten und Höhen wurden mittels GPS (WGS 84) aufgezeichnet.

Plateau directly north of the valley (section BT)

A short helicopter stop was used to note the most important features and to sample the upper sedimentary rocks above a major dolerite sill (section BT). During this brief stop an approximately 20-25 m thick, cross-bedded sandstone unit was noticed, containing horizons with intense bioturbation of predominantly *Skolithos*-like burrows.

Morozumi Range

The Takrouna Formation is exposed in the western part of the Morozumi Range in the area between Jupiter Amphitheatre and Paine Ridge. The most complete section with a thickness of 280 m has been briefly described from DeGoes Cliff in the southern Morozumi Range by WALKER (1983).

We re-investigated this section from a field camp located west of the cliff during January 08 and 16, 2010 (section MR; Figs. 2 & 8, Tab. 1). The best exposures, found at the steep, east-facing, about 6 km long DeGoes Cliff, are located north of a prominent ice cliff (Fig. 4). A second outcrop on a plateau on top of a thick mafic dolerite sill was visited during a reconnaissance survey about 10 km further NNW (section MT).

DeGoes Cliff (section MR)

At the base of the sedimentary section, a heterogeneous, poorly sorted conglomerate forms a thin, discontinuous unit above the basement. It contains basement clasts up to 30 cm in size and fill up to 6 m of local paleo-relief. Fluvial conglomerate and sandstone of the Takrouna Formation were deposited either above this unit or, locally, directly on top of basement rocks. The erosive base of the conglomerate can be traced over a minimum distance of 1 km along the cliff and shows local scours of up to 1 m depth. The lowermost deposits of the Takrouna Formation at DeGoes Cliff are approximately 45 m of cross-bedded fine-grained conglomerate and coarse-grained sandstone, which are whitish to light-grey in colour. They are overlain by an about 100 m thick unit consisting of fine-grained conglomerate to coarse-grained sandstone layers with erosive base, separated by finer-grained, grey to black deposits dominated by carbonaceous sand- and siltstone. These deposits typically show fining-upward trends and frequently contain coal seams at the top. This unit is overlain by another 20 m of whitish, crossbedded conglomerate and sandstone, forming a prominent cliff in the middle part of the section (Fig. 3). The following 25 m show several well-developed fining-upward units from coarse-grained sand to fine-grained, carbonaceous sand and silt. The overlying deposits are dominated by light- to dark-grey and greenish-grey, medium- and fine-grained, carbonaceous and non-carbonaceous sandstone, which form a package of about 55 m thickness. Most abundant sedimentary textures are ripple cross-lamination and trough crossbedding. The uppermost, about 30 m thick unit is again dominated by whitish coarse-grained sandstone and fine-grained conglomerate. The top of the cliff is formed by a dolerite sill of the Jurassic Ferrar Group, which can be traced laterally over many kilometres along the Morozumi Range. Paleocurrent measurement carried out on sandstones of the Morozumi Range show an azimuthal range from 140° to 310° (mean flow towards NW).

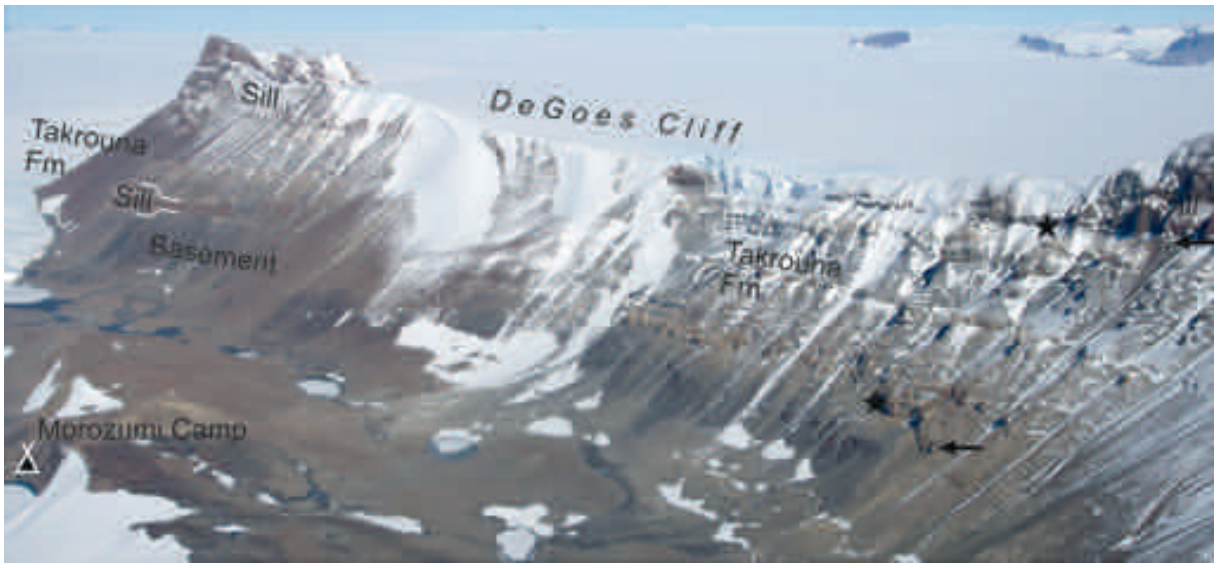

Fig. 4: DeGoes Cliff in the southern part of the Morozumi Range facing towards ENE. The measured section of the Takrouna Formation is indicated by the lower and upper asterix (section MR).

Abb. 4: In der nach ENE gewandten Steilwand (DeGoes Cliff) im Südteil der Morozumi Range wurde ein vollständiges Profil im aufgenommen (Profil MR, zwischen den beiden mit Stern markierten Punkten).

Plateau on the northwest side of DeGoes Cliff (section MT)

The approximately 55 m section MT (Fig. 2) above the sill consist of predominantly medium-grained sandstone showing cross-bedding and ripple cross-lamination, and locally comprise coalified plant axes. Some layers show white spots on weathering surfaces and tube-like vertical traces that are interpreted as bioturbation. The stratigraphic relationship to the section measured at DeGoes Cliff remains yet uncertain, because the sill is not strictly conformable.

Northern Freyberg Mountains

The Takrouna Formation is exposed in the eastern part of the Alamein Range, in particular along the western side of the Canham Glacier, and at the northern flank of an unnamed peak in the western Alamein Range (Collinson et al. 1986). The type section of the Takrouna Formation described by Dow & Neall (1974) is located 4 km NW of the actual Takrouna Bluff below a thick mafic dolerite sill (Collinson et al. 1986), comprising a 60 m thick succession of *Glossopteris*-bearing sandstone. A 280 m thick sequence has been mentioned north of Takrouna Bluff, but has not been investigated before.

The Alamein Range has been a key locality during this field campaign (Fig. 2). Fieldwork in this area could be carried out from January 16 until 21, 2010. We studied the sedimentary sequence on an E-facing slope about 10 km NW of Takrouna Bluff (section AL, Figs. 3 & 8, Tab. 1) and measured a cumulative thickness of approximately 300 m. The camp was located on the west side of Canham Glacier at a prominent NE-facing cliff, which represents the second outcrop investigated in detail (section AR).

Alamein Range – unnamed peak 10 km NW of Takrouna Bluff (section AL)

The basement at section AL consists of Granite Harbour Intrusives, which are unconformably overlain by a poorly exposed alternation of grey to greenish-grey silt- and fine-grained sandstone, and carbonate containing fine-grained clastic detritus. Some carbonate units show fibrous calcites and bioturbation; some nodular as well as some brecciated horizons have been observed. The overlying, approximately 10 to 15 m thick, poorly sorted conglomerate unit contains a range of metamorphic and igneous basement clasts. The following succession is dominated by coarse-grained and pebbly, cross-bedded sandstone, intercalated with medium-grained sandstone, carbonaceous fine-grained sand- and siltstone, and fine-grained conglomerate. Grain size trends and sedimentary textures allow a subdivision of the succession into several distinct packages. The top of the section is formed by a thick dolerite sill, which can be traced to the northernmost tip of the Alamein Range.

Northern Alamein Range cliff (section AR)

The upper part of the section has been investigated along the approximately 3 km-long NW-SE trending cliff close to the camp, which provides excellent 2-3D exposures (section AR, Fig. 5). The lowermost part at the southern end of the cliff (71°53.6 S, 163°07.6 E, 998 m) exposes a fining-up sequence at the glacier level, followed by a pebbly, coarse-grained sandstone unit of a more tabular and laterally extensive nature. The section continues with a 90 m thick succession of predominantly medium- to coarse-grained sandstone mainly consisting of large-scale channel bodies. The top of the sedimentary section, accessible at the northern end of the cliff, is distinct light-grey to white in colour and comprises evidence of bioturbation, paleosoil relics and *Skolithos*-like burrows. Measured paleocurrent data indicate a relatively constant direction towards the NW.

Fig. 5: Field camp at the NE-facing cliff (Takrouna Formation, section AR) in the northern Alamein Range (Freyberg Mountains). The slope visible in the background is part of the outcrop exposing the base of the section and the underlying igneous basement (section AL).

Abb. 5: Feldlager an der nach NE gewandten Steilwand (Takrouna Formation, Profil AR) im Nordteil der Alamein Range (Freyberg Mountains). Die im Hintergrund sichtbare Flanke gehört zu dem Aufschluss an dem die Basis der sedimentären Abfolge und die unterlagernden Magmatite aufgeschlossen sind (Profil AL).

Southern Freyberg Mountains

Outcrops in the southern part of the Freyberg Mountains were described at several localities by previous workers at Smiths Bench, Mt. Camelot, Mt. Baldwin, Mawhango Névé and Monte Cassino (DOW & NEALL 1974, WALKER 1983, COLLINSON & KEMP 1983, COLLINSON et al. 1986).

The planned camp at Monte Cassino had to be canceled due to logistical constraints and poor weather conditions. However, a complete section at the east facing slope south of Monte Cassino and parts of the section and at a south-east facing cliff at the southern tip of Mawhango Névé were investigated during two helicopter reconnaissance surveys (Tab. 1, Figs. 2 & 8).

Monte Cassino (section AC)

The lower part of the exposed section is dominated by alternations of cross-bedded sandstone and carbonaceous sand- and siltstone showing overall fining-upward trends. The upper part consists mainly of fining-up units beginning with pebbly, coarse-grained erosive sandstone bodies grading into ripple-laminated, medium-grained sandstone. Some concave-up surfaces with lateral extents at meter scale are filled by medium- to fine-grained sandstone and comprise coalified plant axes. The top of the sedimentary succession, underneath a mafic dolerite sill of the Ferrar Group, consists of a 10 m thick unit composed of several fine-grained conglomeratic to coarse-grained sandstone bodies with up to 80 cm thick cross-bedding sets.

Moawhango Névé (section AM)

The succession at this location is composed of predominantly medium- to coarse-grained, trough cross-bedded, ripple-laminated as well as planar cross-bedded sandstone, typically forming thin, lateral extensive bodies. Remains of plant axes on the bedding surfaces and patchy distributed, roundish weathering cavities with an average size of 1 cm occur within all units. The small cavities probably represent traces of bioturbation. Paleocurrent directions at both sections AC and AM point mainly towards the WSW.

Neall Massif

Outcrops of the Takrouna Formation and underlying heterogeneous diamictite deposits occur at several ridges and peaks in the Neall Massif area, east of Black Glacier. We studied the outcrops along the unnamed east-west-trending ridge south of Neall Massif, some of which were already described by COLLINSON et al. (1986). Additional to the outcrops mapped in the northern part of Neall Massif and at the Jago Nunataks (GANOVEX-Team 1987), rewarding sections of sedimentary rocks were observed from the helicopter at the western margin of Neall Massif, but could not be studied on the ground.

The campsite (January 21 to 28) was located in a central position directly north of the unnamed ridge, thus all parts of the ridge were accessible by foot within less than 5 km (Figs. 2 & 8, Tab. 1). The approximately 8 km long ridge south of Neall Massif consists of low-grade meta-sedimentary basement rocks in the eastern part, and roughly W-dipping (10-15°) sedimentary rocks and intrusive Ferrar dolerites in the central and western part.

East end of the ridge (section NM)

The base of the sedimentary succession is exposed at a peak near the east end of the ridge (Fig. 2, Tab. 1). The basal deposits consist of unsorted to poorly sorted, partly matrix-supported conglomerate, sandy greenish-grey to dark-grey pelites and locally carbonate beds; the latter two lithologies are poorly exposed. The conglomerate form the small peak at the GPS-position 72°08.8' S, 164°43.2' E, 2050 m. It contains a variety of clast types including granite, granodiorite, felsic to intermediate volcanic rocks, quartzite, fine-grained greenish metamorphic rocks, fine-grained dark-grey to black clasts, schists, clastic sedimentary rocks, quartz and feldspar. The largest boulders observed in-situ measure about 30 cm in diameter, but rounded boulders up to a size of 1.2 m occurring in the debris may also be derived from this unit. The adjacent peak about 1 km to the west is mainly formed by whitish to light-grey sandstone, but could not be investigated in more detail.

Central part of the ridge (section NJ)

At the central part of the ridge, an about 35-40 m thick sandstone unit is exposed in between two dolerite sills (section NJ, Fig. 2, Tab. 1). The stratigraphic position of these sedimentary rocks is yet unclear (Fig. 6). The contact of sedimentary rocks to the underlying sill is sharp and the lowermost 10 cm are strongly cemented and very solid. The upper contact zone of at least 3 m thickness contains brownish rocks with relics of sedimentary textures and many irregular fissures. The sedimentary section is dominated by light-grey and brownish-grey

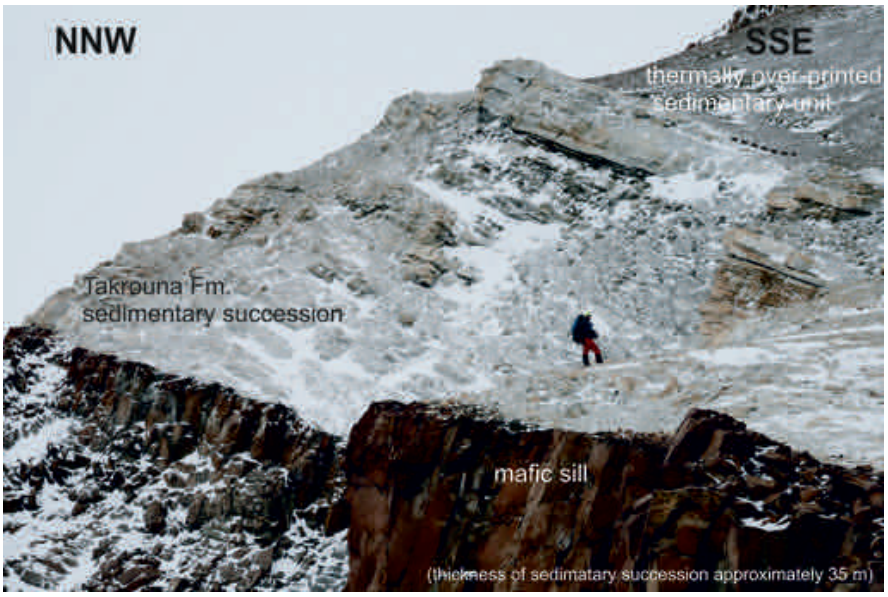

Fig. 6: Sedimentary succession (section NJ) about 500 m SE of the camp site at Neall Massif. The sedimentary rocks are enclosed by two dolerite sills of the Ferrar Group.

Abb. 6: Sedimentgesteine der Takrouna Formation (Profil NJ) etwa 500 m SE des Feldlagers im Neall Massif. Die Sedimentgesteine sind hier zwischen zwei Lagergängen der Ferrar Group aufgeschlossen.

sandstone and fine-grained conglomerate, interbedded with fine-grained sandstone and siltstone that contain coalified plant fragments. Most of the sandstone horizons show spotted whitish-grey weathering surfaces as well as roundish weathering cavities.

Further up the ridge, above a mafic intrusion (72°08.7' S, 164°39.9' E), a poorly to moderately sorted, mainly clast-supported, unstratified conglomerate is exposed. The dominant clast types are granitic and metamorphic basement rocks up to approximately 20 cm size. It is overlain by an about 25 m thick unit of compositionally similar coarse-grained, crudely stratified conglomerate, which is interbedded with brownish- to greenish-grey sandstone. The overlying deposits, which form the summit of the adjacent peak (72°08.8' S, 164°39.6' E, 2130 m), are made up of whitish to light-grey sandstone, minor conglomerate, and locally thin carbonaceous fine-grained sandstone to siltstone. Although the stratigraphic position of this section is not clear, we assume that it represents the transition from proximal alluvial-fluvial, or possibly fluvio-glacial deposits into the fluvial Takrouna Formation.

West end of the ridge (section NA)

The outcrop investigated appears as a prominent peak in the western part of the ridge (section NA, Tab. 1). At the base of the outcrop, north of the summit, an approximately 50 m thick succession of dark-grey to greenish-grey poorly sorted, matrix-supported conglomerate deposits is dominated by metamorphic and less abundant granitic clasts that are overlain by a Ferrar dolerite sill. These rocks are coarse-grained in the lower part, and predominantly finer-grained in the upper part, grading into grey to black sandy pelite. Interbedded with the fines are poorly sorted pebbly sandstones that are compositionally similar to the underlying deposits. The next unit is characterized by well-sorted whitish to light grey, trough cross-bedded sandstone. The following, approximately 145 m thick section was measured along the eastern ridge of the peak. The lowermost outcrop of the Takrouna Formation at this location shows clast-supported conglomerate with interbedded thin greenish to light-grey sandstone beds. These beds are predominantly coarse- to medium-grained and extend laterally only over a few meters. The conglomerate comprises frequently imbricated cobbles of granitic composition, milky quartz and metamorphic basement clasts. The conglomerate is overlain by pebbly, coarse-grained sandstone with up to 5 m thick cross-bedding sets and erosive base. The major part of the ridge consists of trough cross-bedded units ranging from fine- and medium-grained conglomerate to medium-grained sandstone. Individual units are typically coarse-grained at the base and partly show fining-upward trends on a 1-6 m scale. Locally, the conglomerate-sandstone units are separated by dark-grey, carbonaceous sandstone and minor siltstone, containing some thin coal seams in the lower part of the measured section. The uppermost 15-20 m are coarser-grained than the central and lower part of the section. The measured sections at the Neall Massif indicate relatively consistent mean flow directions towards the WSW.

Lanterman Range

Beacon deposits occur in many small outcrops along the western margin of the Lanterman Range. Although flat-lying sedimentary rocks on top of the basement have been described (COLLINSON et al. 1986), most of the thicker sections were affected by post-Permian folding and faulting. Therefore long continuous stratigraphic sections in this mountain range are rare.

Only one outcrop in the Lanterman Range could be investigated briefly during a helicopter survey. We selected the southern of two spurs with Beacon deposits north of the Orr Glacier, which exposes a relatively thick and easily accessible section of clastic deposits (Figs. 2 & 8, Tab. 1).

Spur north of the Orr glacier (section LO)

The sedimentary rocks form a slightly irregular syncline with a faulted contact to the basement. The sedimentary succes-

sion starts with a basal clast- to matrix-supported conglomerate that contains predominantly granitic components, and a variety of different clasts including meta-sedimentary clasts, quarzites, volcanic and sedimentary lithoclasts. Intercalated sandy units increase upwards in abundance. A coarse- to medium-grained sandy unit showing no stratification but spotted greyish-white weathering surfaces occurs on top of the conglomerate and alternates with units consisting of fine- to medium-grained sandstone. A coarse conglomerate separates the lower part of the outcrop from the upper that mainly consists of relatively homogeneous, whitish to light-grey, medium- to coarse-grained sandstone. Weathering faces typically show a spotted distribution of white and grey colours, and very rough surfaces. The sandstone contains large lens- to layer-shaped grey and brownish concretions, and are locally interbedded with brownish, poorly sorted layers of pebble- and cobble-bearing sandstone.

Retreat Hills

Beacon deposits at the Retreat Hills have been mapped (GANOVEX-Team 1987), but were never described in detail. An outcrop of the Takrouna Formation was observed at the southernmost nunatak of the Retreat Hills, and studied during a reconnaissance survey (Figs. 2 & 8, Tab.1).

Southern Peak (section RH)

Predominantly tilted blocks of sedimentary rock form an approximately 10 m thick outcrop. The sedimentary succession starts with coarse-grained pebbly sandstone. The base of the section is covered by snow, but metamorphic basement rocks are exposed at the nunatak north of this outcrop. Notable within this section is the intense bioturbation of all horizons that mainly show pipes of *Skolithos*-like burrows with maxi mum lengths up to 15 cm as well as patchy distributions of black irregular shaped concretions (Fig. 7).

Comparative investigations on Triassic deposits at Vulcan Hill and Timber Peak

Permian and Triassic deposits in northern Victoria Land have been distinguished by the occurrence of *Glossopteris*- and *Dicroidium*-bearing floras, respectively, as well as by the compositional differences of the sandstones (COLLINSON et al. 1986, TESSENSOHN & MÄDLER 1987). The sedimentological features of the sandstones, however, were described as comparatively similar (COLLINSON & KEMP 1983). The Triassic deposits in North Victoria Land were studied in detail during GANOVEX IX (SCHÖNER et al. 2011, BOMFLEUR et al. 2011). Two key outcrops at Timber Peak and Vulcan Hills were re-visited briefly during reconnaissance surveys for additional sampling, gathering of further paleocurrent data, and for re-investigation of sedimentological details in comparison with the Permian deposits (Tab. 1). Both sections are dominated by medium- to coarse-grained sandstones, which are partly whitish to light-grey and quartz-rich, and partly greenish-grey and rich in rock fragments. Fine-grained deposits interbedded with the sandstones at both sections contain *Dicroidium*-bearing macrofloras, which were already described by TESSENSOHN & MÄDLER (1987) and GAIR et al. (1965).

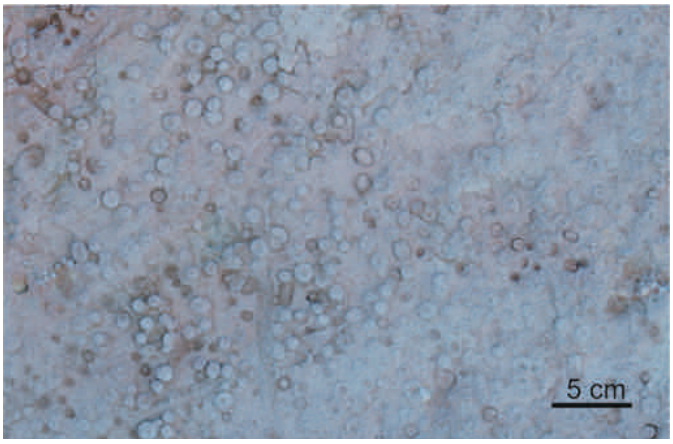

Fig. 7: Bedding plane of a sandstone at Retreat Hills (section RH) showing abundant *Skolithos*-like burrows.

Abb. 7: Schichtfläche eines Sandsteins in den Retreat Hills (Profil RH) mit häufigen *Skolithos*-ähnlichen Grabbauten.

DISCUSSION

The overall depositional setting of the Takrouna Formation has been described as low sinuosity braided streams (WALKER 1983, COLLINSON et al. 1986), draining towards the coast located in present-day Tasmania. Results of the present study confirm that the Takrouna Formation has been deposited in a large fluvial drainage system dominated by braided stream deposits. A large-scale, overall fining-upward grain size evolution is evident especially from the continuous section at the Morozumi Range. This general trend is interrupted by two smaller scale coarsening-up trends, terminating in sheet-like coarse-grained sandstone bodies in the central part and at the top of the studied succession. Compared to the section studied at DeGoes Cliff in the Morozumi Range, coarser-grained facies appear in the eastern part of the study area (Alamein Range, Neall Massif), whereas a generally finer-grained succession is present in the westernmost section (Helliwell Hills). Similar regional sedimentological variations have already been noted by COLLINSON et al. (1986) and WALKER (1983). Based on the facies distribution and the paleocurrent patterns the easternmost section was most likely deposited proximal to the eastern margin of the sedimentary basin, whereas the westernmost sections probably represent a position close to the basin axis. At the basin margin the river system appears to have remained highly energetic with a low potential to preserve fine-grained deposits such as fine- to medium-grained sandstones, siltstones, organic rich mudstones and occasionally coal. Towards the basin axis the depositional environment is more variable, showing a pronounced development of the units mentioned above.

The syn-Permian tectonic features described by WALKER (1983) at DeGoes Cliff in the Morozumi Range could be verified. No indications for syn-depositional faulting were observed at any of the investigated outcrops of the Takrouna Formation. Our field results suggest that at least the sections located in the central part of basin can be correlated lithostra-

tigraphically, but this has to be verified by further petrographic investigations.

CONCLUSIONS

During the expedition GANOVEX X four complete and several detailed sections could be logged within the six different mountain ranges in the northern part of northern Victoria Land (Fig. 8). This enables the recognition of the distribution of different lithofacies types that allows a distinction of more proximal and distal parts of the fluvial system of the Takrouna Formation. Coarse-grained successions that comprise minor variation in fluvial style were probably deposited close to the basin margin. Sedimentary successions showing a great variety of facies, grain size and fluvial architecture more likely represent locations close to the basin axis. Further conclusions regarding the depositional evolution of the fluvial system, the lithostratigraphic framework and possible tectonic as well as climatic controls on sedimentation will be drawn based on further petrographical and geochemical analysis of the sedimentary rocks. These investigations will focus on sediment provenance and diagenesis.

ACKNOWLEDGMENTS

We thank the Bundesanstalt für Geowissenschaften und Rohstoffe (BGR, Hannover) for inviting us to join the expedition GANOVEX X and for the logistical support during the expedition. We are grateful to Franz Tessensohn (BGR), Ricarda Hanemann (University Jena), Andreas Läufer (BGR) and Frank Lisker (University Bremen) for sharing their field experience from former GANOVEX expeditions, which helped us to prepare the field campaign and to select the most promising sedimentary sections. We are most thankful to Mike Atkinson (Christchurch), who was not only an excellent field guide but also helped us to collect many samples of the Permian *Glossopteris*-bearing horizons. We kindly acknowledge the work of the pilots Steve, Phil, Carl and Jamie and the engineer Jim of Helicopters New Zealand (Nelson), who safely transported us to all essential localities, and were patient with us when field work took longer and samples were heavier than originally planned. We thank Franz Tessensohn and Frank Lisker for their helpful review comments, which improved the manuscript. The research project is supported by the German Research Foundation (Deutsche Forschungsgemeinschaft, DFG), grant SCHO 1269/1-1, and is part of the DFG research program SPP 1158 (Antarctic research and comparative studies in Arctic sea ice areas).

References

Barrett, P.J. (1991): The Devonian to Jurassic Beacon Supergroup of the Transantarctic Mountains and correlatives in other parts of Antarctica.- In: R.J. Tingey (ed), The Geology of Antarctica, Oxford University Press, Oxford: 120-152.

Bomfleur, B., Schneider, J., Schöner, R., Viereck-Goette, L. & Kerp, H. (2011): Fossil sites in the continental Victoria and Ferrar groups (Triassic–Jurassic) of North Victoria Land, Antarctica.- Polarforschung 80: 88-99.

Collinson, J.W. & Kemp, N.R. (1983): Permian-Triassic sedimentary sequence in northern Victoria Land, Antarctica.- In: R.L. Oliver, P.R. James & J.B. Jago (eds), Antarctic Earth Science, Australian Academy of Science, Canberra: 221-225.

Collinson, J.W., Pennington, C.D. & Kemp, N.R. (1986): Stratigraphy and petrology of Permian and Triassic fluvial deposits in northern Victoria Land, Antarctica.- In: E. Stump (ed), Geological Investigations in Northern Victoria Land, Antarctic Research Series 46: 211-242.

Collinson, J.W., Isbell, J.L., Elliot, D.H., Miller, M.F., Miller, J.M.G. & Veevers, J.J. (1994): Permian-Triassic Transantarctic Basin.- In: J.J. Veevers & C.M. Powell (eds), Permian-Triassic Pangean basins and foldbelts along the Panthalassan margin of Gondwanaland, Geol. Soc. Amer. Mem. 184: 173-222.

Dow, J.A.S. & Neall, V.E. (1974): Geology of the lower Rennick Glacier, northern Victoria Land, Antarctica.- New Zealand J. Geol. Geophys. 17: 659-714.

Gair, H.S., Norris, G. & Ricker, J. (1965): Early Mesozoic microfloras from Antarctica.- New Zealand J. Geol. Geophys. 8: 231-235.

GANOVEX-Team (1987): Geological Map of North Victoria Land, Antarctica, 1:500 000 - Explanatory Notes.- Geol. Jb. B 66: 7-79.

Laird, M.G. & Bradshaw, J.D. (1981): Permian tillites of North Victoria Land, Antarctica.- In: M.J. Hambrey & W.B. Harland (eds), Earth's pre-Pleistocene glacial record, Cambridge Univ. Press, London: 237-240.

Tessensohn, F. & Mädler, K. (1987): Triassic plant fossils from North Victoria Land, Antarctica.- Geol. Jb. B 66: 187-201.

Schöner, R., Viereck-Götte, L., Schneider, J. & Bomfleur, B. (2007): Triassic-Jurassic sediments and multiple volcanic events in North Victoria Land, Antarctica: A revised stratigraphic model.- In: A.K. COOPER & C.R. RAYMOND (eds), Antarctica: A Keystone in a Changing World. Online Proceedings of the 10th ISAES, USGS Open-File Report 2007-1047, Short Res. Paper 102: 1-5.

Schöner, R., Bomfleur, B., Schneider, J. & Viereck-Götte, L. (2011): A systematic description of the Triassic to Lower Jurassic Section Peak Formation in North Victoria Land (Antarctica).- Polarforschung 80: 71-87.

Skinner, D.N.B. (1981): Possible Permian glaciation in north Victoria Land, Antarctica.- Geol. Jb. B 41: 261-266.

USGS-LIMA (2009): http://lima.usgs.gov. Publication date 04/2009.

Viereck-Goette, L., Schöner, R., Bomfleur, B. & Schneider, J. (2007): Multiple shallow level sill intrusions coupled with hydromagmatic explosive eruptions marked the initial phase of Ferrar Magmatism in north Victoria Land, Antarctica.- In: A.K. COOPER & C.R. RAYMOND (eds), Antarctica: A Keystone in a Changing World. Online Proceedings of the 10th ISAES, USGS Open-File Report 2007-1047, Short Res. Paper 104: 1-5.

Walker, B.C. (1983): The Beacon Supergroup of northern Victoria Land, Antarctica.- In: R.L. OLIVER, P.R. JAMES & J.B. JAGO (eds.), Antarctic Earth Science. Australian Acad. Scie., Canberra: 211-214.

Fig. 8: Simplified overview of the lithological columns of the investigated sections. AC = Monte Cassino, AL = unnamed peak 10 km northwest of Takrouna Bluff, AM = Moawhango Névé, AR = Northern Alamein Range cliff, BT = Plateau directly north of Boggs Valley, BV = Boggs Valley, LO = Spur north of the Orr glacier, MR = DeGoes Cliff, MT = Plateau northwest of DeGoes Cliff, NA = West end of Neall Massif ridge, NJ = Central part of Neall Massif ridge, NM = East end of Neall Massif ridge, RH = southern peak of Retreat Hills.

Abb. 8: Vereinfachte Übersicht über die lithologische Abfolge der untersuchten Profile. AC = Monte Cassino, AL = unbenannter Berg 10 km nordwestlich des Takrouna Bluff, AM = Moawhango Névé, AR = Nördliches Kliff der Alamein Range, BT = Plateau unmittelbar nördlich von Boggs Valley, BV = Boggs Valley, LO = Felsrücken nördlich des Orr Glacier, MR = DeGoes Cliff, MT = Plateau nordwestlich von DeGoes Cliff, NA = westliches Ende des Felsrückens im Neall Massif, NJ = zentraler Teil des Felsrückens im Neall Massif, NM = östliches Ende des Felsrückens im Neall Massif, RH = südlicher Felsgipfel der Retreat Hills.

Fig. 8 / Abb. 8 continued ►

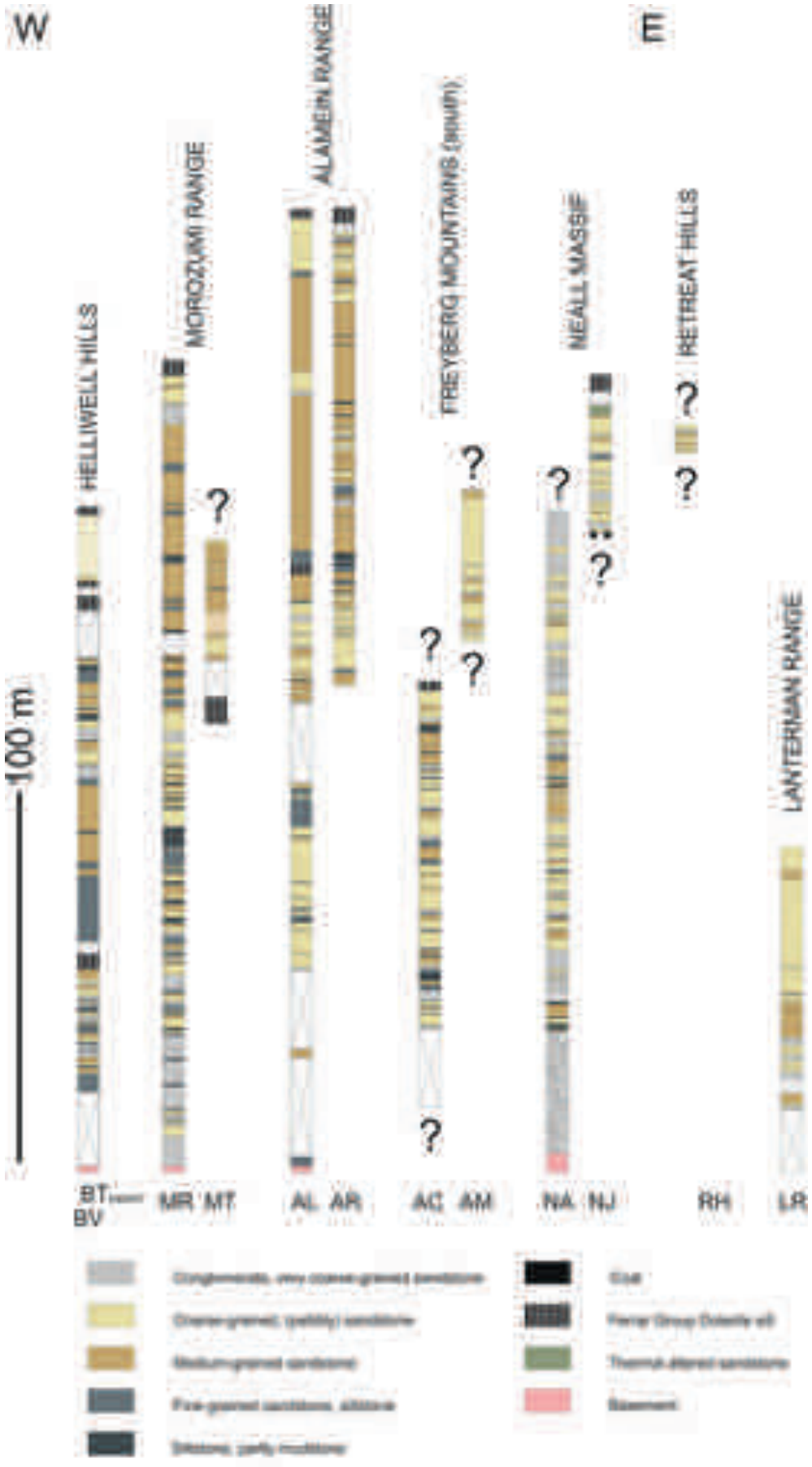
W
E
HELLIWELL HILLS
MOROZUMI RANGE
ALAMEIN RANGE
FREYBERG MOUNTAINS (groups)
NEALL MASSIF
RETREAT HILLS
LANTERMAN RANGE
100 m
BT
BV
MR
MT
AL
AR
AC
AM
NA
NJ
RH
LR

Fig. 8 / Abb. 8

Polarforschung 84 (1), 59–66, 2014

Recent Thermochronological Research in Northern Victoria Land, Antarctica

by Frank Lisker[1], Jannis Prenzel[1], Andreas L. Läufer[2] and Cornelia Spiegel[1]

Abstract: Northern Victoria Land forms a segment of the Transantarctic Mountains in the western Ross Sea that is characterized by extreme landscape contrasts. A high Alpine coastal morphology developed in immediate vicinity to high-elevated inland plateaus and deep, structurally defined glacial troughs. Recent thermochronological research during the last five years discovered that the whole region was occupied by a Mesozoic sedimentary basin. This recognition requires future thermochronological research to focus on five main objectives: (1) More and better data, new and complementary techniques, and quantitative modelling, (2) evolution of the Mesozoic Victoria Basin on the continental crust of SE Australia and the western Ross Sea, (3) Passive margin formation versus West Antarctic rifting, (4) timing and amount of the final exhumation and uplift of the Transantarctic Mountains since the Eocene/Oligocene, and (5) Landscape contrasts in northern Victoria Land resulting from the interplay between climate, tectonics and lithology. This paper also gives an overview of thermochronological field work during expedition GANOVEX X und reviews subsequent research in the Terra Nova Bay region, were up to 1.1 km thick post-Ferrar sediments were deposited between ~180 and ~35 Ma.

Zusammenfassung: Das nördliche Victoria Land bildet ein Segment des Transantarktischen Gebirges im westlichen Ross-Meer das durch extreme Landschaftskontraste gekennzeichnet ist. Einer hochalpinen Küstenmorphologie stehen landeinwärts in unmittelbarer Nähe tief eingeschnittene Hochlandplateaus mit tiefen, strukturell kontrollierten glazialen Trögen gegenüber. Thermochronologische Studien der letzten fünf Jahre belegen dass die gesamte Region von einem mesozoischen Sedimentbecken bedeckt war. Diese Erkenntnis erfordert weitere thermochronologische Untersuchungen mit besonderem Fokus auf fünf Schwerpunkten: (1) Mehr und bessere Daten, Einsatz neuer und komplementärer Techniken und quantitative Modellierungen, (2) Bildung des mesozoischen Victoriabeckens auf der kontinentalen Kruste SE Australiens und des westlichen Ross-Meers, (3) Entwicklung des passiven Kontinentalrands versus Rifting des Westantarktischen Riftsystems, (4) zeitlicher Verlauf und Betrag von finaler Exhumierung und Hebung des Transantarktischen Gebirges seit dem Eozän/Oligozän und (5) Landschaftskontraste im nördlichen Victoria Land resultierend aus der Wechselwirkung von Klima, Tektonik und Lithologie. Der Artikel gibt auch einen Überblick über die thermochronologische Feldarbeit während der Expedition GANOVEX X und die anschließende Erforschung der Terra Nova Bucht, in der zwischen ~180 und ~35 Ma bis zu 1.1 km mächtige post-Ferrar-Sedimente abgelagert wurden.

INTRODUCTION

Northern Victoria Land forms the northernmost segment of the Transantarctic Mountains in the Ross Sea sector of Antarctica (Fig. 1A). The region occupies a crucial position in the context of both the Gondwana breakup between Antarctica and Australia and the subsequent uplift of the Transantarctic Mountains since it is located at the intersection of two continental-scale crustal structures: the passive continental margin in the north and the Cenozoic West Antarctic Rift System in the east (Fig. 1A). Its basement comprises lithological units of different rheological and erosional competence (Wilson Terrane versus Bowers and Robertson Bay terranes). It exposes the transition between two contrasting landscape styles: high-standing plateaus towards the continental interior versus coastal Alpine geomorphology, and a broad spectrum of thermal indications has been recognized here (Fig. 2).

This constellation has placed the region in the focus of numerous uplift and exhumation studies during the last two decades. Since the post-Jurassic tectonic history of the Transantarctic Mountains is not recorded by petrological or stratigraphic evidence, this research chiefly relies on thermochronological, structural and geophysical data, geomorphological observation and on the sedimentary record of adjacent offshore basins and troughs. Two decades of thermochronological investigation produced large apatite fission track (FT) datasets obtained from vertical profiles and single samples from various parts of northern Victoria Land by Fitzgerald & Gleadow (1988), Balestrieri et al. (1994, 1997, 1999), Lisker (1996), Schäfer (1998), Balestrieri & Bigazzi (2001), Rossetti et al. (2003, 2006), Lisker et al. (2006), and Storti et al. (2008). The range of both apatite FT ages (~30 to ~250 Ma) and proxies (mean track lengths usually <14 μm, with standard deviations >1.5 μm) coincides with the general FT data pattern throughout the Transantarctic Mountains.

Accordingly, the established uplift concept of the Transantarctic Mountains (summarized by Fitzgerald 2002 and Lisker 2002) was also applied to northern Victoria Land. It comprises three cooling stages due to exhumation (denudation) and associated uplift during the Early Cretaceous, Late Cretaceous, and Cenozoic (Fig. 1B). The exhumation episodes have been related to regional rifting events: (I) the initial breakup between Australia and Antarctica, (II) the main extension phase between East and West Antarctica along low-angle extensional faults; and (III) southward propagation of seafloor spreading from the Adare Trough into continental crust underlying the western Ross Sea in the early Cenozoic (cf. Fitzgerald 2002). This traditional interpretation of regionally consistent stepwise exhumation since the Early Cretaceous appears well in agreement with present structural and geophysical data, and seems to be consistent for the majority of the sampled apatite FT locations when considered separately.

However, the paradigm fails to explain the substantial variation of timing and amount of exhumation between the different segments of the Transantarctic Mountains despite the uniform distribution of marker horizons (stratigraphic units,

[1] FB 5 – Geowissenschaften, Universität Bremen, PO Box 330440, D-28334 Bremen, Germany.
[2] Bundesanstalt für Geowissenschaften und Rohstoffe (BGR), Stilleweg 2, D-30655 Hannover, Germany.

Manuscript received 12 August 2014; accepted in revised form 04 December 2014.

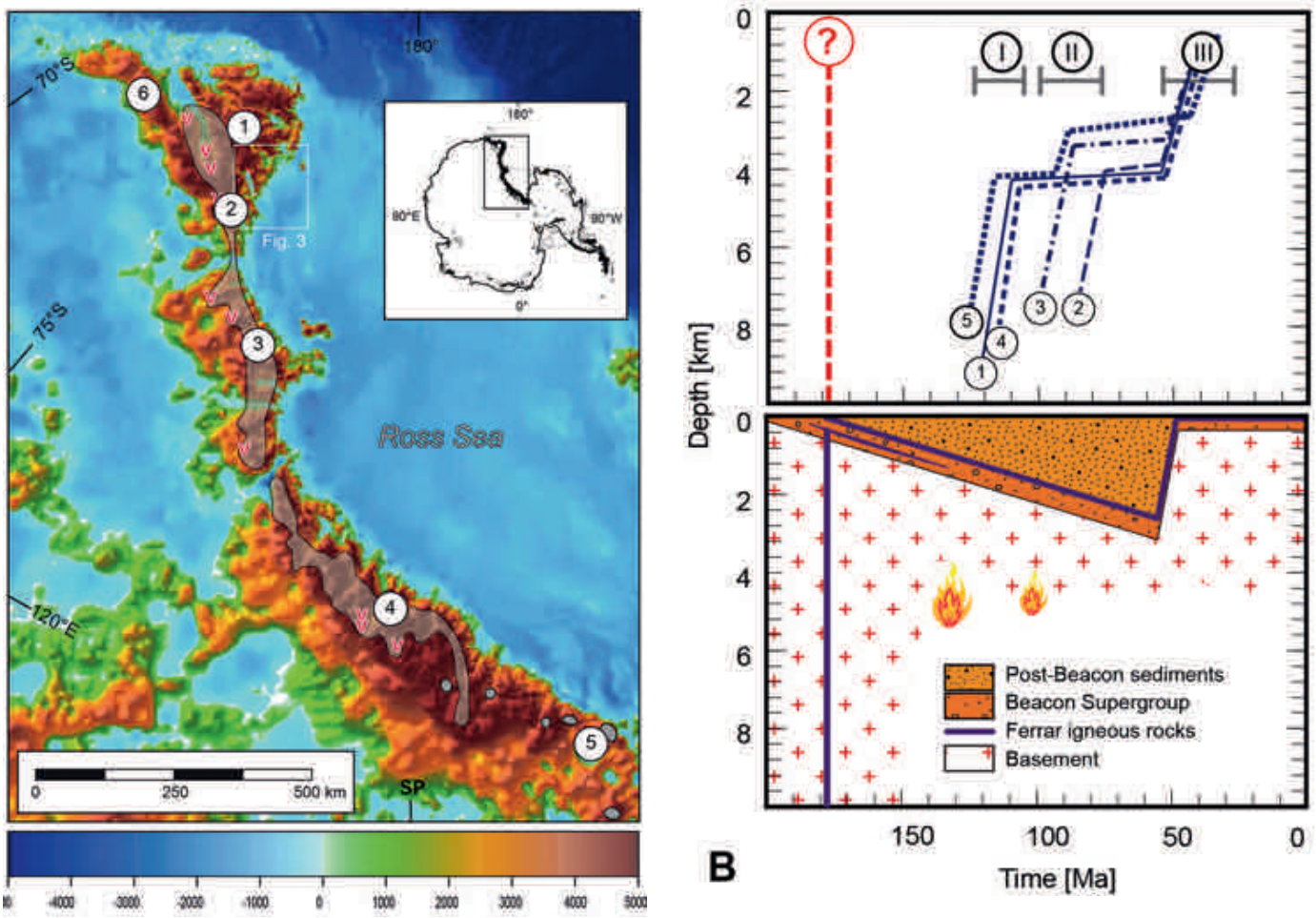

Fig. 1: A: Topographic and bathymetric map of part of Transantarctic Mountains and Ross Sea (from LISKER & LÄUFER 2013). The transparent grey overlay shows the distribution of Beacon Supergroup and Jurassic Ferrar igneous rocks, with the red symbol "v" indicating the occurrence of Ferrar lava flows and volcanoclastics (after ELLIOT & FLEMING 2008). Both Beacon sediments and volcanic rocks are crucial paleosurface indicators. Numbered circles mark the target areas of exhumation studies based on apatite fission track (FT) data: (1) FITZGERALD & GLEADOW (1988), (2) BALESTRIERI et al. (1994, 1997), (3) GLEADOW & FITZGERALD (1987), (4) FITZGERALD (1994), (5) FITZGERALD & STUMP (1997), (6) LISKER et al. (2006). The Inset shows the location of the region within Antarctica. **B:** Schematic diagram showing the contrasting burial and exhumation scenarios for the Transantarctic Mountains. Numbers in the figure refer to locations in map. Top = traditional scenario of monotonous cooling/exhumation in three episodes since the Jurassic (modified after FITZGERALD 2002). The question mark at 180 Ma indicates that this concept does not consider the age crossover between Ferrar emplacement and early Cenozoic cooling/exhumation. Note also the diachronous course and the missing structural trend of the "exhumation" paths. Bottom = formation of the Mesozoic Victoria Basin and Cenozoic cooling/exhumation based on the relationship between timing of Ferrar effusion (red stippled line) and apatite fission track data (LISKER & LÄUFER 2013). Maximum burial depth, heatflow, and timing of exhumation may vary along the Victoria Basin.

Abb. 1: A: Ausschnitt aus topographischer und bathymetrischer Karte von Transantarktischem Gebirge und Rossmeer (aus LISKER & LÄUFER 2013). Der transparent grau schattierte Bereich zeigt die Verteilung von Beacon Supergruppe und jurassichen Ferrar-Magmatiten, das rote „v"-Symbol steht für Ferrar-Laven und Vulkanoklastiten (nach ELLIOT & FLEMING 2008). Beacon-Sedimente und -Vulkanite sind nachdrückliche Beweise von Paläo-Oberflächen. Die nummerierten Kreise markieren die Untersuchungsgebiete früherer Exhumierungsstudien auf der Grundlage von Apatit-Spaltspurendaten (FT): (1) FITZGERALD & GLEADOW (1988), (2) BALESTRIERI et al. (1994, 1997), (3) GLEADOW & FITZGERALD (1987), (4) FITZGERALD (1994), (5) FITZGERALD & STUMP (1997), (6) LISKER et al. (2006). Das Inset zeigt die Lage der Region innerhalb der Antarktis. **B:** Übersichtsdiagramm der kontrastierenden Versenkungs- und Exhumierungsszenarien für das Transantarktische Gebirge. Die Ziffern in der Abbildung beziehen sich auf die Lokationen der nebenstehenden Karte. Oben = traditionelles Szenario monotoner Abkühlung/Exhumierung in drei Episoden seit dem Jura (modifiziert nach Fitzgerald 2002). Das Fragezeichen bei 180 Ma unterstreicht dass dieses Konzept die Altersüberschneidung von Ferrar-Vulkanismus und känozoischer Abkühlung/Exhumierung nicht berücksichtigt. Beachtung verdienen auch diachroner Verlauf und fehlender struktureller Trend der „Exhumierungs-Pfade". Unten = Ausbildung eines Mesozoischen Viktoriabeckens und känozoische Abkühlung/Exhumierung basierend auf Zeit der Ferrar-Effusion (rote gestrichelte Linie) und Apatit-Spaltspurendaten (Lisker & Läufer 2013). Maximale Versenkungstiefe, Wärmefluss und Exhumierungszeiten können innerhalb des Viktoriabeckens variieren.

erosion surfaces), and the lack of spatial correlation with the loci of tectonic activities (Fig. 1A). It also does not account for thermochronological age data from the Transantarctic Mountains front that are substantially younger than the latest of the postulated cooling/exhumation episodes (e.g., FITZGERALD & GLEADOW 1988, BALESTRIERI et al. 1994, 1997, FITZGERALD et al. 2006). Most importantly, the recent recognition of crossover age relationships between vertical apatite FT age profiles and the effusion age of Ferrar volcanic and volcanoclastic rocks reveals that the postulated uplift/exhumation history bases on a self-contradiction (LISKER & LÄUFER 2013). Instead, the regional compilation of thermochronological and stratigraphic data, the broad range of Late Jurassic-Cretaceous paleotemperatures between 60 and 340 °C derived from various geochronological, magnetic, mineralogical, and petrographic studies (Fig. 2 and references below), the diachronous timing of the thermal peaks (e.g., MOLZAHN & WÖRNER 1999), and the fit of the continental shelfs of Antarctica and Australia can only be explained by varying heat flow within a now vanished "Mesozoic Victoria Basin" during the Cretaceous. Qualitative

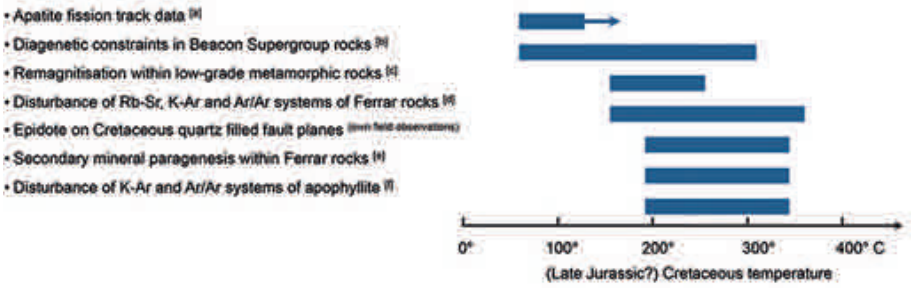

Fig. 2: Compilation of paleotemperatures derived from thermal indicators in Beacon and Ferrar rocks. (a) = Fitzgerald (2002) and Lisker (2002); (b) = Balance & Watters (2002), Bernet & Gaupp (2005); (c) = Faure & Mensing (1993), refs. in Molzahn et al. (1999); (e) = Hornig (1993); (f) = Molzahn et al. (1999).

Abb. 2 : Kompilation von Paläotemperaturen auf der Grundlage thermischer Indikatoren in Beacon- und Ferrar-Gesteinen. (a) = Fitzgerald (2002) und Lisker (2002); (b) = Balance & Waters (2002), Bernet & Gaupp (2005); (c) = Faure & Mensing (1993), refs. in Molzahn et al. (1999); (e) = Hornig (1993); (f) = Molzahn et al. (1999).

interpretation of these constraints suggests that regional exhumation due to the formation of the West Antarctic Rift System and uplift of the Transantarctic Mountains did not commence prior to the Paleocene.

Objectives of thermochronological research in northern Victoria Land

The Antarctic expedition GANOVEX X 2009/10 of the German Federal Institute of Geosciences and Natural Resources (BGR) provided the opportunity to have a fresh look to the regional geological evolution of northern Victoria Land in the context of the Mesozoic Victoria Basin. The evolution before, during and after the breakup of Gondwana needs to be studied in a composite approach of scientists from various disciplines: geophysics, structural geology, petrology, sedimentology, stratigraphy, paleontology, and thermochronology. Within this frame, thermochronological research there focuses on five main topics.

(1) More and better data, new and complementary techniques, and quantitative modelling. A large set of more than 500 apatite FT ages and associated proxies, most of them obtained from vertical profiles, has been compiled during the last two decades from the Pacific termination of the Transantarctic Mountains by various workers (compiled by Lisker & Läufer 2011). However, these data were only interpreted quantitatively in the past while Prenzel et al. (2013) demonstrated that reliable thermal histories depend on quantitative modelling. Unfortunately, the bulk of the available data is not suitable for modelling since they were either generated by population method or they lack information about the chemical composition (and therefore the annealing properties) of apatites (cf. Lisker & Läufer 2011, Prenzel et al. 2013). Moreover, some areas, especially in the morphologically diverse Robertson Bay Terrane, were not sampled and studied representatively. Consequently, most published apatite FT data need to be either supplemented with essential annealing proxies (e.g., Dpar) or substituted completely by new data obtained via external detector method, and should be complemented by new data from so far underexplored areas. Furthermore, the thermal sensitivity should be extended to temperatures as low as ~40 °C by application of (U-Th-Sm)/He analysis on apatites. Then, vertical sample profiles distributed representatively throughout the region will provide a general frame for thermal history modelling and should be connected via horizontal sample arrays. Eventually, numerical modelling of the extensive thermochronological dataset of northern Victoria Land using PECUBE may be applied to quantify rates of crustal heat transport, landscape evolution and tectonic processes (see below).

(2) Evolution of the Mesozoic Victoria Basin on the continental crust of SE Australia and the western Ross Sea. A main goal of the thermochronological work within the region is to reconstruct extension, depth and geometry of the Victoria Basin. The comparison of the brittle fabrics from basement, Beacon and Ferrar rocks provides information on the finite strain field during extension and the relative sequence of regional tectonic events. This work has to be complemented by further search for remnants and additional indirect evidence of Late Jurassic Cretaceous sediments on the continent and especially on shelf and Ross Sea sequences, for example in the context of Antarctic drilling campaigns (ANDRILL). The according dataset will be correlated with existing data from northern Victoria Land and Australia since a consistent basin formation model has to take into account the common early rifting history of Antarctica and Australia. Current breakup models largely ignore the discrepancy between the extensive shelf of Australia that contains up to 15 km of post-mid Jurassic sediments, and the short shelf in front of northern Victoria Land with only a thin sedimentary cover.

(3) Passive margin formation versus West Antarctic rifting. Isotherm patterns derived from thermal history modelling of apatite FT and (U-Th-Sm)/He analyses may be used to determine basic parameters for the understanding of continental rifting and margin evolution. This includes timing, distribution and depth of exhumation, geometry and segmentation of the passive/sheared margin, the isostatic compensation of exhumation, and the classification of the margin type. The topic also comprises a quantification of potential denudational interferences between Gondwana margin evolution and Cenozoic Ross Sea rifting. The lithospheric rigidity (variable already along the continental margin alone), and the flexural wavelengths of passive continental margin and West Antarctic Rift System may divert considerably, and flexural warping and denudational rebound of the crust will likely show maximum interference at the locus of the NE Robertson Bay Terrane. Alternatively, the maximum overlap could be located at the Rennick Graben that forms the continuation of the Victoria Land Basin of the West Antarctic Rift System into Terra Nova Bay and northern Victoria Land (Cooper et al. 1987). Our understanding of the regional landscape evolution can be improved, and a respective long-term model established

only by evaluation, quantification and modelling of amounts and rates of exhumation of the diachronous continental and rift margins, the distances between the two eroding escarpment fronts, the age difference between both escarpments, and the initial pre-rift shape of the land surface for each of the rifted margins evolved. Eventually, these constraints need to be linked quantitatively with the respective morphological parameters, with special consideration of the decreasing topographic altitude of the Transantarctic Mountains and their increasing asymmetry towards the north.

(4) Timing and amount of final exhumation and surface uplift of the Transantarctic Mountains. The thermochronological research of the last decades usually referred – mainly due to the limited resolution of apatite FT data – to the Cretaceous to Paleocene cooling/exhumation history of the Transantarctic Mountains. However, recent thermochronological data from the Rennick Graben and southern Victoria Land (Balestrieri et al. 1994, Rossetti et al. 2003, Fitzgerald et al. 2006, Storti et al. 2008, Lisker unpubl. data) and dating of tectonic events in the Terra Nova Bay region (Di Vicenzo et al. 2004) indicate a significant Eocene/Oligocene exhumation stage that is also supported by the sedimentary record of the adjacent Ross Sea troughs (e.g., Florindo et al. 2005). Though, post-Oligocene cooling is only detected qualitatively by apatite FT data, not resolved. (U-Th-Sm)/He analysis on apatites from the rapidly uplifted/eroded massifs at the Transantarctic Mountains front will provide insight in timing and amount of exhumation since the Oligocene: (a) Did exhumation occur in response to a single major uplift stage at the Eocene-Oligocene boundary; (b) are there several discrete uplift/exhumation stages, or (c) are the Transantarctic Mountains the result of a more gradual uplift process? The variation of low-temperature isotherms in time and space in the context of the geological record will allow to conclude on the influence of lithology of the now vanished rock column and of climate change and permanent glaciation on uplift and exhumation of the Transantarctic Mountains. A high-resolution exhumation pattern will also contribute to test existing uplift models of the Transantarctic Mountains, which are still discussed controversially by either a simple shear model (Fitzgerald et al. 1986, modified by Salvini et al. 1997), a flexural uplift model (Stern & ten Brink 1989), or a delayed phase changing model (Smith & Drewry 1984). Other models, such as the plateau collapse model of Bialas et al. (2007) are ruled out by the crossover relationships shown by Lisker & Läufer (2013).

(5) Landscape contrasts and climatic implications resulting from the interplay between climate, tectonics and lithology. Perhaps the most unique feature of northern Victoria Land is the distinctive landscape contrast across the termination of the Transantarctic Mountains. Although described repeatedly by geologists and geomorphologists (e.g., Tessensohn 1994, Van der Wateren et al. 1994, Baroni et al. 2005), contrasting uplift and exhumation in northern Victoria Land could not be quantified and profoundly interpreted yet since apatite FT ages of usually >30 Ma did not allow to dating the onset of the youngest exhumation phase(s). A few Neogene thermochronological age data have been reported only by Fitzgerald & Gleadow (1988) and Balestrieri et al. (1997) so far. The low resolution of existing cooling/exhumation data hampered tight constraints on time, temperature and spatial patterns. Moreover, earlier workers often ignored the intimate link between geological and geomorphological indications. A compilation of topographic and thermochronological data reveals that lithological differences between igneous and high-grade metamorphic basement units on the one side and low-grade metasedimentary terranes on the other side produce profound differences in both geomorphology and intensity of exhumation. Moreover, this relationship is superimposed by tight interaction between erosion behaviour and climate change. For example, hypothetical Cretaceous uplift of the Transantarctic Mountains had the potential to trigger long-term glaciation of polar Gondwana, while global cooling since the Eocene/Oligocene has produced different glacial systems (wet, dry) of extremely varying erosion efficiency. Recognition and quantification of these relationships will provide a deeper insight in the long-term climate evolution on the margin of the East Antarctic Craton.

Thermochronological field work during GANOVEX X

Field work during GANOVEX X focussed on mapping, measurements and sampling of the brittle kinematic inventory, and sample collection of horizontal and vertical profiles for FT and (U-Th-Sm)/He analyses. Particular attention was paid to morphologically exposed outcrops (escarpments, glacial valleys, erosion surfaces), unconformities, Phanerozoic deposits (Beacon Supergroup), superficial or shallow igneous bodies (Black Prince volcanics, Ferrar sills and volcanoclastics, Meander intrusives), regional faults, and dyke occurrences. We observed and sampled thermal features associated with tectonic structures, such as fault coatings and mineralization (e.g., epidote), secondarily grown white mica, bleaching horizons and aureols, pseudotachilytes, dykes and veins, secondary zeolithes within volcanic rocks etc.

Thermochronological fieldwork and sampling was carried out in two general areas: in the vicinity of Mariner Glacier and in the Terra Nova Bay region (Fig. 3). This separation was related to the logistic division of the expedition into two legs, but also follows the rheological and geomorphological properties of the basement units building up northern Victoria Land. Here, the Alpine topography cut in the meta-sedimentary rocks of the Bowers and Robertson Bay Terranes (Mariner Glacier area: Admiralty Block of Tessensohn 1994) contrasts with the plateau landscape dominating the Wilson Terrane (Terra Nova Bay region: Outback Shoulder of Tessensohn 1994).

Fieldwork during the first leg of GANOVEX X in the vicinity of Mariner Glacier was performed via helicopter support (Helicopters New Zealand) from the vessel MS “Italica” on 29 outcrops (Tab. 1 & Fig. 3) in three target areas, with varying sampling rationale. Sampling in front and at the flanks of the Mariner Glacier (17 outcrops/samples) and in the southern Victory Mountains (vertical profile of 5 samples) concentrated on the lithological contrast between Wilson metamorphics or Admiralty Intrusives and Robertson Bay/Leap Year/Sledgers groups, and on the control of erosion levels by volcanics and near-surface intrusions. A different approach was chosen for Mount Murchison where a vertical profile of seven specimens was sampled to complete an existing profile of very young apatite FT age (Fitzgerald & Gleadow 1988: 25-36 Ma), and to complement it with (U-Th-Sm)/He data to conclude

Sample	Location	Latitude South	Longitude East	Elevation (m a.s.l.)	Lithology
		Leg I Mariner Glacier area			
4001	No Ridge	73°29.863	167°01.709	928	Granite (Meander Intrusives)
4002	Apostrophe Island	73°31.140	167°26.038	38	Gabbro (Granite Harbour Intrusives)
4003	Spatulate Ridge	73°29.176	167°15.461	530	Gabbro (Granite Harbour Intrusives)
4004	Eagles Bluff	73°15.631	167°10.096	391	Granite (Meander Intrusives)
4005	W Cape Crossfire	73°09.072	168°10.353	199	Granite (Admiralty Intrusives)
4006	Cloudy Ridge	73°20.210	168°43.911	4	Graywacke (Robertson Bay Group)
4007	Mt. Murchison	73°23.073	166°53.551	1300	Granite (Granite Harbour Intrusives)
4008	Mt. Murchison	73°25.492	166°18.721	3200	Granite (Granite Harbour Intrusives)
4009	Mt. Murchison	73°25.152	166°18.406	3414	Gneiss (Wilson Metamorphics)
4010	Mt. Murchison	73°24.851	166°25.015	2176	Gneiss (Wilson Metamorphics)
4011	Mt. Murchison	73°26.733	166°29.609	1577	Gneiss (Wilson Metamorphics)
4012	Mt. Murchison	73°20.739	166°00.112	661	Gneiss (Wilson Metamorphics)
4013	Cape King	73°36.000	166°33.470	74	Granite (Admiralty Intrusives)
4014	Emerging Island	73°23.117	168°01.838	76	Granite (Admiralty Intrusives)
4015	Retreat Hills	72°55.644	165°09.543	2694	Amphibolite (Wilson Metamorphics)
4017	Between Navigator Nunatak and Deception Plateau	73°12.261	164°26.763	2322	Granite (Granite Harbour Intrusives)
4018	Mt Kinet	73°17.437	165°52.361	1740	Granite (Granite Harbour Intrusives)
4019	Nunatak N Husky Ridge	73°18.326	166°02.757	1140	Mica schist (Wilson Metamorphics)
4020	Frank's Point	73°16.221	166°18.428	385	Descent Unit
4021	Cape Crossfire	73°05.149	168°16.665	985	Rhyolithe (Hallet Volcanics)
4023	S Victory Mts	72°50.637	167°57103	2494	Graywacke (Robertson Bay Group)
4024	S Victory Mts	72°49.018	167°55.512	3089	Graywacke (Robertson Bay Group)
4025	S Victory Mts	72°49.872	167°58.957	2164	Graywacke (Robertson Bay Group)
4026	S Victory Mts	72°50.041	168°00.424	1824	Graywacke (Robertson Bay Group)
4027	S Victory Mts	72°43.279	167°52.283	2559	Granite (Admiralty Intrusives)
4028	Husky Ridge	73°18.757	166°20.478	409	Granite (Granite Harbour Intrusives)
4029	Husky Ridge	73°24.448	166°25.957	2196	Granite (Granite Harbour Intrusives)
		Leg II Terra Nova Bay			
4030	Mount Frustrum	73°21.244	162°56.807	2465	Kirkpatrick Basalt
4031	Mount Frustrum	73°31.851	162°40.790	2500	Kirkpatrick Basalt
4032	Lichen Hills N	73°15.984	162°00.858	2285	Granite (Granite Harbour Intrusives)
4033	Lichen Hills S	73°20.885	162.16.848	2161	Granite (Granite Harbour Intrusives)
4034	Mount Frustrum	73°22.863	162°55.631	3096	Kirkpatrick Basalt
4035	Mount Frustrum	73°22.235	162°51.741	2139	Kirkpatrick Basalt
4036	Mount Baxter	73°22.256	162°51.817	2442	Granite (Granite Harbour Intrusives)
4039	Mount Crummer	75°03.152	162°38.532	485	Granite (Granite Harbour Intrusives)
4040	Mount Crummer	75°03.085	162°39.340	370	Granite (Granite Harbour Intrusives)
4041	Mount Crummer	75°02.506	162°40.363	32	Granite (Granite Harbour Intrusives)
4042	Ridge N Bier Point	74°08.167	164°07.985	1466	Granite (Granite Harbour Intrusives)
4043	Inexpressible Island	74°56.056	163°42.940	25	Granite (Granite Harbour Intrusives)
4044	Cape Phillipi	75°13.955	162°32.708	363	Granite (Granite Harbour Intrusives)
4045	Starr Nunatak	75°53.908	162°35.605	109	Granite (Granite Harbour Intrusives)
4046	McDaniel Nunatak	75°48.302	161°46.895	854	Granite (Granite Harbour Intrusives)
4047	Evans Height	75°05.674	161°32.418	739	Granite (Granite Harbour Intrusives)
4048	Mount Larson	74°50.874	162°12.395	1520	Granite (Granite Harbour Intrusives)
4049	Mount Monteagle	73°45.594	165°22.762	2091	Granite (Granite Harbour Intrusives)
4050	Mount Monteagle	73°43.597	166°00.597	1200	Granite (Granite Harbour Intrusives)
4051	Mount Monteagle	73°41.502	165°56.573	1415	Granite (Granite Harbour Intrusives)
4052	Mount Monteagle	73°41.478	166°03.870	1042	Granite (Granite Harbour Intrusives)
4053	Mount Monteagle	73°39.709	166°07.975	367	Granite (Granite Harbour Intrusives)
4054	Harrow Peak	74°04.730	164°51.711	37	Granite (Granite Harbour Intrusives)
4055	Mount Crummer Top	75°02.992	162°34.597	881	Granite (Granite Harbour Intrusives)
4056	Mount Gaberlein	75°03.450	162°04.051	1154	Granite (Granite Harbour Intrusives)
4057	Mount Stierer	75°05.072	162°08.174	900	Granite (Granite Harbour Intrusives)
4058	Mount Bellinghausen	75°06.778	162°06.617	1222	Granite (Granite Harbour Intrusives)
4059	Mount Bellinghausen	75°06.433	162°06.954	1065	Granite (Granite Harbour Intrusives)
4060	SE Mt. Bellinghausen	75°09.076	162°14.049	736	Granite (Granite Harbour Intrusives)
4061	Fleming Head	75°09.531	162°38.655	213	Conglomerate (Bowers Group)
4062	Fleming Head	75°13.396	162°36.216	1	Granite (Granite Harbour Intrusives)
4063	E Mount Stierer	75°04.819	162°20.486	508	Granite (Granite Harbour Intrusives)

Tab. 1: List of samples collected during GANOVEX X. **Tab. 1:** Verzeichnis der während GANOVEX X genommenen Proben.

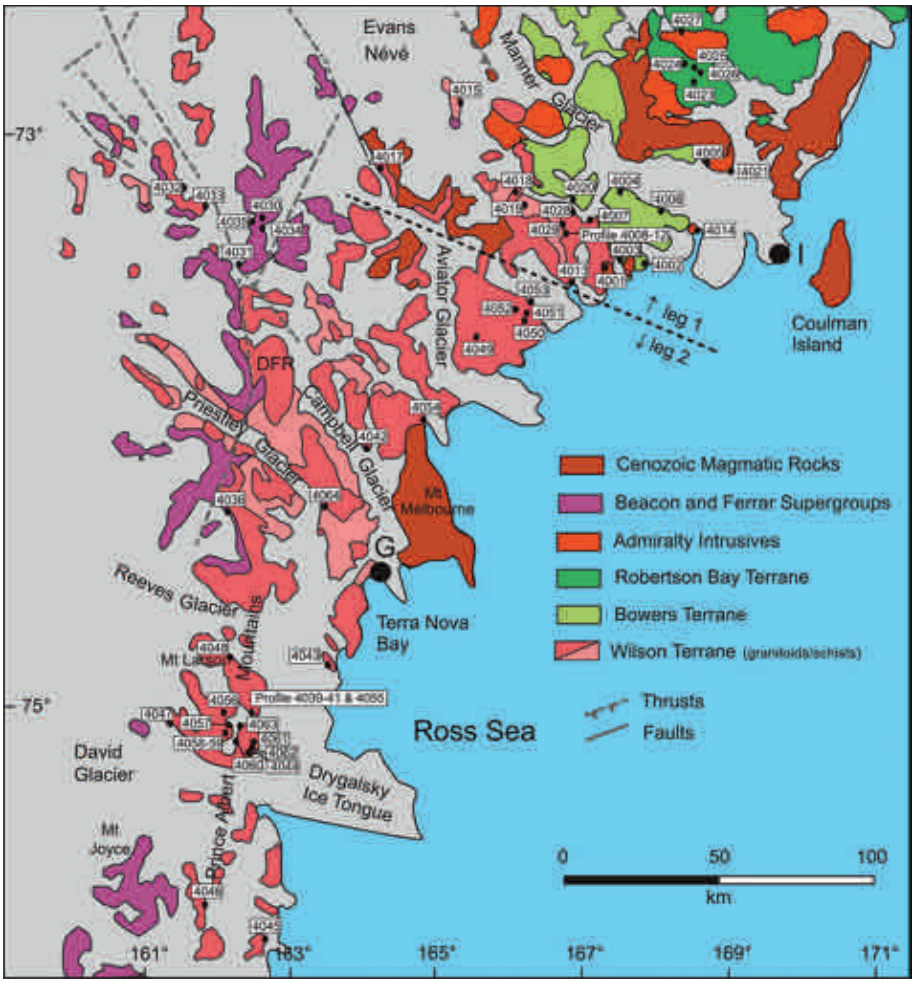

Fig. 3: Sample locations for thermochronological studies of the GANOVEX X campaign in the vicinity of Mariner Glacier (leg 1) and in the Terra Nova Bay region (leg 2). DFR = Deep Freeze Range, EHR = Eisenhower Range, I = position of expedition vessel "Italica" (base for leg 1), G = Gondwana Station (base for leg 2).

Abb. 3: Probenlokationen thermochronologischer Studien der GANOVEX X-Kampagne im Umfeld von Mariner Glacier (Leg 1) und Terra Nova Bay (Leg 2). DFR = Deep Freeze Range, EHR = Eisenhower Range, I = Position des Expeditionsschiffs „Italica" (Basis für Leg 1), G = Gondwana Station (Basis für Leg 2).

on the youngest exhumation phase(s) in coastal northern Victoria Land. Sampled rock types include granitoids (Granite Harbour, Admiralty, and Meander Intrusives: eight locations/samples), mafic rocks (Tiger Gabbro: 2), volcanic rocks (2), high-grade metamorphic rocks (Wilson metamorphics: 11), and low-grade metasedimentary rocks (Robertson Bay, Leap Year, and Sledgers groups: 6).

Fieldwork during the second leg of GANOVEX X in the Terra Nova Bay region was based on helicopter operations from the German Gondwana Station on 33 outcrops (Tab. 1 & Fig. 3). Main target area was the region of the Southern Prince Albert Mountains where 12 outcrops/samples and a vertical profile of four specimens at Mount Crummer were sampled. To the northeast of Gondwana Station, a vertical profile of five specimens was sampled at Mount Monteagle beneath an elevation of 1500 m to complete an existing profile of apatite FT ages above the mentioned altitude (Balestrieri et al. 1997). Furthermore, a vertical profile of four specimens at Mount Frustrum at the GANOVEX X geophysics base camp in the Mesa Range, two samples at Lichen Hills located east of this camp and six samples in an area in the vicinity of Gondwana Station, e.g., Black Ridge, were collected. Sampled rock types include mainly Granite Harbour Intrusives (28 locations/samples) and subordinately volcanic rocks (Kirkpatrick Basalt: 4) and low-grade metasedimentary rocks (Bowers: 1).

New thermochronological research in the Terra Nova Bay area

Some of the general questions listed above were initially addressed during the last couple of years, mainly in the Eisenhower Range/Terra Nova Bay area. The Eisenhower Range constitutes a ~70 km long and up to 3000 m high plateau forming an escarpment along the Priestley Glacier (Fig. 3). The basement consists of Wilson Terrane – late Proterozoic and Early Paleozoic Ross orogenic, low- to medium-grade metamorphic and granitic rocks (e.g., Borg et al. 1987). Post-Ross orogenic erosion formed a low-relief erosion surface overlain by the clastic Triassic to Jurassic Beacon Supergroup deposits. Triassic to Jurassic Beacon sediments with a thickness varying between ~30 m and ~50 m are preserved (e.g., Schöner et al. 2011). Beacon deposition was followed by intrusion and extrusion of magmatic rocks in/on basement and sediments during the Ferrar event at ~180 Ma (e.g., Elliot & Fleming 2008). Two recent thermochronogical studies of Prenzel et al. (2013, 2014) compiled new apatite FT data and apatite (U-Th-Sm)/He (AHe) from vertical profiles in the Eisenhower Range, and merged them with published apatite FT data. These data, supplemented by paleotemperature and pressure estimates derived from Beacon sandstones, provide new quantitative results on regional burial evolution and first regional constraints on basin inversion and exhumation processes.

Thirty-four apatite FT ages between 32 ±2 and 259 ±18 Ma and AHe ages from 21 samples between 37 ±3 and 173 ±16 Ma correlate positively with sample elevations between ~200 and ~2600 m. Thermal history modelling of these data and complementary thermal indications detect heating of the paleosurface on the Eisenhower Range to temperatures ≥80 °C subsequent to Ferrar magmatism, and constrain Late Eocene rapid cooling. Regression of modeled paleotemperatures against sample elevations refers to a high Jurassic (~45 °C/km) and a moderate Cretaceous – Eocene (28 ±8 °C/km) geothermal gradient. The texture of Beacon sandstones supports strong mechanical compaction that requires a higher overburden than preserved in the stratigraphic record. Model–led paleotemperatures and pressures suggest basement burial that increases from Late Jurassic (0.7-1.1 km) to Eocene (1.8-2.1 km). The overburden comprises 0.7-1.1 km cumulative Beacon/Ferrar rocks and 0.7-1.4 km of post-Ferrar sediments. Rapid cooling of the whole sample suite between ~35 and 30 Ma implies fast erosion of the post-Ferrar sediments and (re) exposure of underlying magmatic rocks. Subsequent differential sample cooling to present-day surface temperature infers ongoing exhumation by glacial incision enhanced by isostatic response to basin inversion. Decreasing amounts of exhumation from the coast (>3 km) towards the interior (1.5-2.2 km) point to backstepping incision along the fault controlled Priestley Glacier. Substantial exhumation of the Eisenhower Range since the Late Eocene is hence triggered by both tectonic and climatic factors, superimposed by considerable lithological influence during the initial exhumation stage.

The new findings from the Eisenhower Range and their interpretation are supported by new data from adjacent areas, the Deep Freeze Range and the northern Prince Albert Mountains. New thermochronological ages (28 ±3 to 274 ±17 Ma) from Deep Freeze Range positively correlate with elevations (1060-3120 m) with AHe ages being usually 10-20 Ma younger than corresponding apatite FT ages (Prenzel et al. submitted). For the Terra Nova Bay region, thermal history modelling detects common Mesozoic to Eocene heating/burial of the Jurassic surface and constrains rapid Late Eocene cooling/exhumation. The correlation of sample paleotemperatures versus elevation indicates an increased Jurassic (44 ±15 °C/km) and a moderate Cretaceous to Eocene (24 ±7 °C/km) geothermal gradient. Paleotemperatures and gradients used in tandem infer basement burial varying from ~2 km in Deep Freeze and Eisenhower Ranges to ~3.4 km in the Prince Albert Mountains. This vanished rock column consisted of Beacon and Ferrar rocks and 0.6-1 km of post-Ferrar deposits. Burial variation is apparently attributed to a higher thickness of Beacon and Ferrar rocks in the southern Terra Nova Bay and may represent the pre-Ferrar topography. The relative homogeneous post-Ferrar sediment thickness throughout the entire region indicates a continuous, uniform Mesozoic to Eocene sedimentary basin. Mid-Jurassic basin formation and subsequent sediment accumulation until the Late Eocene is explained by initiation of extension within the West Antarctic Rift System at ~180 Ma with a continuous stable stress field of low E-W extension during Ross Sea opening until ~35 Ma. Late Eocene/Early Oligocene basin inversion is linked with right lateral strike-slip and transtensional faulting attributed to major Eocene tectonic reorganization in the Ross Sea region from Cretaceous orthogonal to Cenozoic oblique rifting. Subsequent final exhumation with deepest incision at the coast is explained by a change of exhumation style from downwearing to backstepping incision from the coast towards the interior obviously caused by a combination of glacial incision, climate cooling, and isostatic surface rebound in response to sediment removal at ~30 Ma.

CONCLUSIONS

Recent thermochronological research in northern Victoria Land demonstrated that the region occupied a central position in a long-lasting Mesozoic Victoria Basin between Antarctica and Australia, and opened new perspectives for the formation of the Transantarctic Mountains and the Gondwana breakup. It also concluded that the bulk of published thermochronological data from the region is not suitable for reliable thermal history modelling, and therefore new, better and more data obtained with different thermochronological methods are required. A particular obvious gap in the sample record has been closed during the field campaign GANOVEX X in the Mariner Glacier area, NE Robertson Bay Terrane and in the Terra Nova Bay region.

Thermal history modelling of new thermochronological data from the Eisenhower Range and adjacent areas postdated exhumation and uplift of the high-standing plateaus of the Transantarctic Mountains in the northern Ross Sea to the Eocene/Oligocene boundary and reconstructed pre-Oligocene basin deposits in the order of 0.6-1.1 km for the Terra Nova Bay region. No qualitative constraints were obtained yet from Alpine ranges of the Robertson Bay Terrane. Depth, geometry and timing of basin evolution in this part of the Mesozoic Victoria Basin as well as the origin of the landscape contrast across northern Victoria Land and the influence of climate, tectonics and lithology on geomorphology need to be studied in the future.

ACKNOWLEDGMENTS

The research described here was funded by the German Research Foundation (DFG grants LI 745/12 to F.L. and LA 1080/7 to A.L.). F.L. and J.P. are very indebted to Bundesanstalt für Geowissenschaften und Rohstoffe (BGR), Hannover, for invitation to participate in GANOVEX X. The authors wish to thank the crews of MS “Italica” and Helicopters New Zealand – especially Steve Spooner – for logistic support and the members of the GANOVEX X team for cooperative field work and stimulating discussions. Special thanks go to Brian Staite, Friedhelm Henjes-Kunst, Glen Phillips, and Karsten Piepjohn. The manuscript benefitted from two constructive reviews of U. Glasmacher and F. Tessensohn.

References

Balestrieri, M.L. & Bigazzi, G. (2001): First record of the Late Cretaceous denudation phase in the Admiralty Block (Transantarctic Mountains, northern Victoria Land, Antarctica).- Rad. Meas. 34: 445-448.

Balestrieri, M.L., Bigazzi, G., Ghezzo, C. & Lombardo, B. (1994): Fission track dating of apatites from the Granite Harbour Intrusive Suite and uplift-denudation history of the Transantarctic Mountains in the area between the Mariner and David Glaciers (northern Victoria Land, Antarctica).- Terra Antartica 1: 82-87.

Balestrieri, M.L., Bigazzi, G. & Ghezzo, C. (1997): Uplift-denudation of the Transantarctic Mountains between the David and the Mariner glaciers,

northern Victoria Land (Antarctica); constraints by apatite fission-track analysis.- In: C.A. RICCI (ed), The Antarctic region; geological evolution and processes; proceedings of the VII international symposium on Antarctic Earth sciences, Terra Antarctica Publication, Siena, 547-554.

Balestrieri, M.L., Bigazzi, G. & Ghezzo, C. (1999): The Transantarctic Mountains: a natural laboratory for apatite fission-track analysis. Result from Italian Antarctic expeditions.- Rad. Meas. 31: 621-626.

Ballance, P.F. & Watters, W.A. (2002): Hydrothermal alteration, contact metamorphism, and authigenesis in Ferrar Supergroup and Beacon Supergroup rocks, Carapace Nunatak, Allan Hills, and Coombs Hills, Victoria Land, Antarctica.- New Zealand J. Geol. Geophys. 45: 71-84.

Baroni, C.N., Ciccacci, V., Righini, S., Salvatore, G. & Cristina, M. (2005): Fluvial origin of the valley system in northern Victoria Land (Antarctica) from quantitative geomorphic analysis.- Geol. Soc. Amer. Bull. 117: 212-228.

Bernet, M. & Gaupp, R. (2005): Diagenetic history of Triassic sandstone from the Beacon Supergroup in central Victoria Land, Antarctica.- New Zealand J. Geol. Geophys. 48: 447-458.

Bialas, R.W., Buck, W.R., Studinger, M. & Fitzgerald, P.G. (2007): Plateau collapse model for the Transantarctic Mountains-West Antarctic Rift System: Insights from numerical experiments.- Geology 35: 687-690.

Borg, S.G., Stump, E., Chappell, B.W., McCulloch, M.T., Wyborn, D., Armstrong, R.L. & Holloway, J.R. (1987): Granotoids of northern Victoria Land, Antarctica: Implications of chemical and isotopic variations to regional crustal structure and tectonics.- Amer. J. Sci. 287: 127-169.

Cooper, A.K., Davey, F.J. & Behrendt, J.C. (1987): Seismic stratigraphy and structure of the Victoria Land Basin, western Ross Sea, Antarctica. In: A.K. COOPER & F.J. DAVEY (eds), The Antarctic continental margin: Geology and geophysics of the of the western Ross Sea, Earth Sci. Ser., 5B. Amer. Assoc. Pet. Geol., Houston, 27-76.

Delisle, G. & Fromm, K. (1984): Results of paleomagnetic investigations of Ferrar Supergroup Rocks, North Victoria Land.- Geol. Jb. B41: 41-55.

Delisle, G. & Fromm, K. (1989): Further evidence for a Cretaceous thermal event in North Victoria Land.- In: D. DAMASKE & H.J. DUERBAUM (eds), German Antarctic North Victoria Land Expedition 1984/85; GANOVEX IV. Geol. Jb. Reihe E: Geophysik. Schweizerbart, Stuttgart, 143-151.

Di Vincenzo, G., Rocchi, S., Rossetti, F. & Storti, F. (2004): 40Ar-39Ar dating of pseudotachylytes: the effect of clast-hosted extraneous argon in Cenozoic fault-generated friction melts from the West Antarctic Rift System.- Earth Planet. Sci. Letters 223: 349-364.

Elliot, D.H. & Fleming, T.H. (2008): Physical volcanology and geological relationships of the Jurassic Ferrar Large Igneous Province, Antarctica.-J. Volcanol. Geotherm. Res. 172: 20-37.

Faure, G. & Mensing, T.M. (1993): K-Ar dates and paleomagnetic evidence for Cretaceous alteration of Mesozoic basaltic lava flows, Mesa Range, northern Victoria Land, Antarctica.- Chem. Geol. 109: 305-315.

Fitzgerald, P.G. (1994): Thermochronologic constraints on post-Paleozoic tectonic evolution of the central Transantarctic Mountains, Antarctica. - Tectonics 13(4): 818-836.

Fitzgerald, P.G. (2002): Tectonics and landscape evolution of the Antarctic plate since the breakup of Gondwana, with an emphasis on the West Antarctic Rift System and the Transantarctic Mountains.- Royal Soc. New Zealand Bull. 35: 453-469.

Fitzgerald, P.G., Baldwin, S.L., Webb, L.E. & O'Sullivan, P.B. (2006): Interpretation of (U-Th)/He single grain ages from slowly cooled crustal terranes: A case study from the Transantarctic Mountains of southern Victoria Land.- Chem. Geol. 225: 91-120.

Fitzgerald, P.G. & Gleadow, A.J.W. (1988): Fission-track geochronology, tectonics and structure of the Transantarctic Mountains in northern Victoria Land, Antarctica.- Chem. Geol. 73: 169-198.

Fitzgerald, P.G., Sandiford, M. & Gleadow, A.J.W. (1986): Asymmetric extension associated with uplift and subsidence in the Transantarctic Mountains and Ross Embayment.- Earth Planet. Sci. Lett. 81: 67-78.

Fitzgerald, P.G. & Stump, E. (1997): Cretaceous and Cenozoic episodic denudation of the Transantarctic Mountains, Antarctica: new constraints from apatite fission track thermochronology in the Scott Glacier region.- J. Geophys. Res. B, Solid Earth and Planets 102(B4): 7747-7765.

Fleming, T.H., Elliot, D.H., Jones, L.M., Bowman, J.R. & Siders, A.M. (1992): Chemical and isotopic variations in an iron-rich lava-flow from the Kirkpatrick Basalt, north Victoria Land, Antarctica: Implications for low-temperature alteration.- Contrib. Mineral. Petrol. 111: 440-457.

Fleming, T.H., Elliot, D.H., Foland, K.A., Jones, L.M. & Bowman, J.R. (1993): Disturbance of Rb-Sr and K-Ar isotopic systems in the Kirkpatrick Basalt, north Victoria Land, Antarctica: implications for middle Cretaceous tectonism.- In: R.H. FINDLAY, R. UNRUG, M.R. BANKS & J.J. VEEVERS (eds), Gondwana Eight: assembly, evolution and dispersal. Balkema, Hobart, 411-424.

Fleming, T.H., Foland, K.A. & Elliot, D.H. (1999): Apophyllite 40Ar/39Ar and Rb-Sr geochronology; potential utility and application to the timing of secondary mineralization of the Kirkpatrick Basalt, Antarctica.- J. Geophys. Res. B, Solid Earth and Planets 104(B9): 20,081-20,122.

Florindo, F., Wilson, G.S., Roberts, A.P., Sagnottia, L. & Verosub, K.L. (2005): Magnetostratigraphic chronology of a late Eocene to early Miocene glacimarine succession from the Victoria Land Basin, Ross Sea, Antarctica.- Global Planet. Change 45: 207-236.

Gleadow, A.J.W. & Fitzgerald, P.G. (1987): Uplift history and structure of the Transantarctic Mountains: New evidence from fission track dating of basement apatites in the Dry Valleys area, southern Victoria Land.- Earth Planet. Sci. Lett. 82: 1-14.

Hornig, I. (1993): High-Ti and Low-Ti Tholeiites in the Jurassic Ferrar Group, Antarctica.- Geol. Jb. E47: 335-369.

Lisker, F. (1996): Geodynamik des Westantarktischen Riftsystems basierend auf Apatit-Spaltspuranalysen.- Ber. Polarf. 198: 1-108.

Lisker, F. (2002): Review of fission track studies in northern Victoria Land - Passive margin evolution versus uplift of the Transantarctic Mountains.- Tectonophysics 349: 57-73.

Lisker, F., Läufer, A., Rossetti, F., Olesch, M. & Schäfer, T. (2006): The Transantarctic Beacon Basin: New insights from fission track data and structural data from the USARP Mountains and adjacent areas (northern Victoria Land, Antarctica).- Basin Res. 18: 315-340.

Lisker, F. & Läufer, A. (2011): Thermochronological research in northern Victoria Land (Antarctica): the key to the final disintegration of Gondwana.- Polarforschung 80: 100-110.

Lisker, F. & Läufer, A. (2013): The Victoria Basin: vanished link between Antarctica and Australia.- Geology 41: 1044-1046.

Mensing, T.M. & Faure, G. (1996): Cretaceous alteration of Jurassic volcanic rocks, Pain Mesa, northern Victoria Land, Antarctica.- Chem. Geol. 129: 153-161.

Molzahn, M., Wörner, G., Henjes-Kunst, F. & Rocholl, A. (1999): Constraints on the Cretaceous thermal event in the Transantarctic Mountains from alteration processes in Ferrar flood basalts Glob. Planet. Change 23: 45-60.

Prenzel, J., Lisker, F., Balestrieri, M.L., Läufer, A. & Spiegel, C. (2013): The Eisenhower Range, Transantarctic Mountains: A natural laboratory to evaluate qualitative interpretation concepts of thermochronological data.- Chem. Geol. 352: 176-187.

Prenzel, J., Lisker, F., Elsner, M.R.S., Balestrieri, M.L., Läufer, A. & Spiegel, C. (2014): Burial and exhumation of the Eisenhower Range, Transantarctic Mountains, based on thermochronological, maturity and sediment petrographic constraints.- Tectonophysics 630: 113-130.

Prenzel, J., Lisker, F., Balestrieri, M.L., Läufer, A. & Spiegel, C. (submitted): The evolution of the Mesozoic Victoria Basin between Antarctica and Australia – New insights from thermochronological studies in the Terra Nova Bay region, Transantarctic Mountains, Antarctica.- Gondwana Research.

Rossetti, F., Lisker, F., Storti, F. & Läufer, A. (2003): Tectonic and denudational history of the Rennick Graben (northern Victoria Land): Implications for the evolution of rifting between East and West Antarctica. Tectonics, 22(2): 1016, doi:10.1029/2002TC001416.

Rossetti, F., Storti, F., Busetti, M., Lisker, F., Di Vincenzo, G., Läufer, A.L., Rocchi, S. & Salvini, F. (2006): Eocene initiation of Ross Sea dextral faulting and implications for East Antarctic neotectonics.- J. Geol. Soc. 163: 119-126.

Salvini, F., Brancolini, G., Busetti, M., Storti, F., Mazzarini, F. & Coren, F. (1997): Cenozoic geodynamics of the Ross Sea Region, Antarctica: Crustal extension, intraplate strike-slip faulting and tectonic inheritance.- J. Geoph. Res. 102: 24,669-24,696.

Schäfer, T. (1998): Thermo-tektonische Entwicklung von Oates Land und der Shackleton Range (Antarktis) basierend auf Apatit-Spaltspuranalysen.- Ber. Polarforsch. 263: 1-107.

Schöner, R., Bomfleur, B., Schneider, J. & Viereck-Götte, L. (2011): A systematic description of the Triassic to Lower Jurassic Section Peak Formation in North Victoria Land (Antarctica).- Polarforschung 80: 71-87.

Smith, A.G. & Drewry, D.J. (1984): Delayed phase change due to hot asthenosphere causes Transantarctic uplift?- Nature 309: 536-538.

Stern, T.A. & Ten Brink, U.S. (1989): Flexural Uplift of the Transantarctic Mountains.- J. Geophys. Res. 94: 10315-10330.

Storti, F., Balestrieri, M.L., Balsamo, F. & Rossetti, F. (2008): Structural and thermochronological constraints to the evolution of the West Antarctic Rift System in central Victoria Land.- Tectonics,27(TC4012).

Studinger, M., Bell, R.E., Fitzgerald, P.G. & Buck, W.R. (2006): Crustal architecture of the Transantarctic Mountains between the Scott and Reedy Glacier region and South Pole from aerogeophysical data.- Earth Planet. Sci. Letters 250: 182-199.

Tessensohn, F. (1994): The Ross Sea region, Antarctica: structural interpretation in relation to the evolution of the southern ocean.- Terra Antartica, 1: 553-558.

Van der Wateren, F.M., Luyendyk, B.P., Verbers, A.L.L.M. & Smith, C.H. (1994): Landscape evolution model of the West Antarctic Rift System relating tectonic and climatic evolutions of the rift margins.- Terra Antartica 1: 453-456.

Deutsche Gesellschaft für Polarforschung e. V.
Konto: Postbank Hannover, IBAN DE15250100300001494306, BIC PBNKDEFF
Bank transfer from abroad: IBAN DE15250100300001494306 BIC PBNKDEFF

POLARFORSCHUNG
Organ der Deutschen Gesellschaft für Polarforschung e. V.
Journal of the German Society of Polar Research

Mitteilungen für die Autoren: Die Zeitschrift POLARFORSCHUNG, herausgegeben von der Deutschen Gesellschaft für Polarforschung e.V. (DGP) und dem Alfred-Wegener-Institut Helmholtz-Zentrum für Polar- und Meeresforschung (AWI) dient der Publikation von Originalbeiträgen aus allen Bereichen der Polar- und Gletscherforschung in Arktis und Antarktis wie in alpinen Regionen mit polarem Klima. Manuskripte können in englischer (bevorzugt) und deutscher Sprache eingereicht werden und sind zu richten an: Deutsche Gesellschaft für Polarforschung, Schriftleitung Polarforschung, c/o Alfred-Wegener-Institut Helmholtz-Zentrum für Polar- und Meeresforschung, Postfach 12 01 61, D-27515 Bremerhaven, E-mail: <Dieter.Fuetterer@awi.de>. Eingesandt Manuskripte werden Fachvertretern zur Begutachtung vorgelegt und gelten erst nach ausdrücklicher Bestätigung durch die Schriftleitung als zur Veröffentlichung angenommen. Für detaillierte Angaben zur Manuskripterstellung siehe die Web-Seite der DGP: <http://www.dgp-ev.de>

Erscheinungsweise: POLARFORSCHUNG erscheint ab Jahrgang 2011, Band 81 mit jährlich zwei Heften
Open access: Alle Artikel sind in elektronischer Form im Internet verfügbar <http://www.polarforschung.de.>. Polarforschung ist im Directory of Open Access Journals (DOAJ <http://www.doaj.org> geführt.
Bezugsbedingungen: Für Mitglieder der Deutschen Gesellschaft für Polarforschung e.V. (DGP) ist der Bezugspreis für die Zeitschrift im Mitgliedsbeitrag enthalten. Für Nichtmitglieder beträgt der Bezugspreis eines Heftes € 30,00; Bezug über den Buchhandel oder über die Geschäftsstelle.

Information for contributors: *POLARFORSCHUNG – published by the Deutsche Gesellschaft für Polarforschung (DGP) and the Alfred Wegener Institute Helmholtz Centre for Polar Polar and Marine Research (AWI) – is a peer-reviewed, multidisciplinary research journal that publishes the results of scientific research related to the Arctic and Antarctic realm, as well as to mountain regions associated with polar climate. The POLARFORSCHUNG editors welcome original papers and scientific review articles from all disciplines of natural as well as from social and historical sciences dealing with polar and subpolar regions.*
Manuscripts may be submitted in English (preferred) or German. In addition POLARFORSCHUNG publishes Notes (mostly in German), which include book reviews, general commentaries, reports as well as communications broadly associated with DGP issues. Manuscripts and all related correspondence should be sent to: Deutsche Gesellschaft für Polarforschung e.V., Editorial Office POLARFORSCHUNG, c/o Alfred Wegener Institute Helmholtz Centre for Polar Polar and Marine Research, PO Box 12 01 61, D-27515 Bremerhaven, e-mail <Dieter.Fuetterer@awi.de>. Manuscripts can be considered as definitely accepted only after written confirmation from the Editor. – For a detailed guidance of authors please visit the DGP web page at: <http://www.dgp-ev.de>

Publication: *POLARFORSCHUNG will be published efective of volume 81, 2011 two times a year.*
Open access: *PDF versions of all POLARFORSCHUNG articles are freely available from <http://www.polarforschung.de>. POLARFORSCHUNG is listed in the Directory of Open Access Journals (DOAJ) <http://www.doaj.org>*
Subscription rates: *For members of the German Society for Polar Research (DGP), subscription to POLARFORSCHUNG is included in the membership dues. For non-Members the price for a single issue is € 30.00.*

Deutsche Gesellschaft für Polarforschung

26. Internationale Polartagung

6. – 11. September 2015 in München

German Society of Polar Research

26th International Polar Symposium

September 6 – 11. 2015 Munich, Germany

Information:

E-mail: http://www.DGP-EV.de

post@keg.badw.de